

Optimal Abort Policy for Mission-Critical Systems under Imperfect Condition Monitoring

Qiuzhuang Sun,¹ Jiawen Hu,² and Zhi-Sheng Ye³

¹School of Mathematics and Statistics, University of Sydney, Australia

²School of Aeronautics and Astronautics, University of Electronic Science and Technology of China, China

³Department of Industrial Systems Engineering and Management, National University of Singapore, Singapore
Emails: qiuzhuang.sun@sydney.edu.au; hdl@sjtu.edu.cn; yez@nus.edu.sg

While most on-demand mission-critical systems are engineered to be reliable to support critical tasks, occasional failures may still occur during missions. To increase system survivability, a common practice is to abort the mission before an imminent failure. We consider optimal mission abort for a system whose deterioration follows a general three-state (normal, defective, failed) semi-Markov chain. The failure is assumed self-revealed, while the healthy and defective states have to be inferred from imperfect condition monitoring data. Due to the non-Markovian process dynamics, optimal mission abort for this partially observable system is an intractable stopping problem. For a tractable solution, we introduce a novel tool of Erlang mixtures to approximate non-exponential sojourn times in the semi-Markov chain. This allows us to approximate the original process by a surrogate continuous-time Markov chain whose optimal control policy can be solved through a partially observable Markov decision process (POMDP). We show that the POMDP optimal policies converge almost surely to the optimal abort decision rules when the Erlang rate parameter diverges. This implies that the expected cost by adopting the POMDP solution converges to the optimal expected cost. Next, we provide comprehensive structural results on the optimal policy of the surrogate POMDP. Based on the results, we develop a modified point-based value iteration algorithm to numerically solve the surrogate POMDP. We further consider mission abort in a multi-task setting where a system executes several tasks consecutively before a thorough inspection. Through a case study on an unmanned aerial vehicle, we demonstrate the capability of real-time implementation of our model, even when the condition-monitoring signals are generated with high frequency.

Key words: Semi-Markov chain; partially observable Markov decision process; control-limit policy; mixture of Erlang distribution, optimal stopping.

1. Introduction

An on-demand mission-critical system is required to operate continuously for a period of time to complete a mission (Kim et al. 2010). Classical examples include commercial jetliner serving routes between cities, emergency response vehicles like ambulance and fire engines, and medical devices like a cardiopulmonary bypass machine used in cardiac surgery. Some recent examples include autonomous underwater vehicles for underwater inspection and maintenance in offshore infrastructure, automated waste collection systems for marine debris removal, and unmanned aerial vehicles (UAVs) used for such tasks as wildfire monitoring, product delivery, combat, and power grids inspection. While these systems are engineered to be reliable to support critical tasks, occasional failures may still occur during missions. As evidence, a record number of 20 large Air Force drones crashed in major accidents in 2015 according to the Washington Post (Whitlock 2016); electrical failure of the cardiopulmonary bypass device is estimated to be 1 per 1,000 cases (Durukan et al. 2016); and the helicopter emergency medical services in the US reported an average 4.5 accidents per 100,000 flying hours, out of which around one third were fatal (Bryan 2014). The system failure causes not only a mission failure, but also a huge system failure cost including possible threaten to human lives. To increase system survivability, a common practice is to abort the mission before an imminent failure. For instance, an autonomous vehicle or crewed aircraft diagnosed to be defective could abort its mission and return to the base for crash prevention (Yang et al. 2020); a malfunctioning ambulance might pull over at a location convenient for the next ambulance to take over the patient, rather than continuing to travel and risking a breakdown on the road; in the event of an abnormal heart-lung machine, a perfusionist can manage a patient's venous return during weaning from cardiopulmonary bypass and subsequently employ less effective/reliable hand-cranking for systemic perfusion (Durukan et al. 2016).

Several distinctive features of emergent mission abort can be discerned from the above examples. Each on-demand mission typically has a short duration when compared to the service life of the system. Throughout the mission, advanced sensors monitor system health in real time and trigger alarms when a potentially suspicious defect is detected. Abort, as an option to respond to alarms, has a non-negligible duration compared with the mission duration. During abort, a system failure is possible, and thus abort may be unnecessary if it takes longer time than completing the mission. Intuitively, an abort decision balances the system failure risk and the zero-one yield from mission success over a short-term horizon when the system is deemed defective. These features make abort fundamentally different from condition-based maintenance (CBM), which monitors system ageing and preventively replaces the system when it reaches wear-out with unacceptably high risk of breakdown. CBM trades off uptime against system failure costs over an infinite horizon or a

horizon significantly longer than a system's service life. Because of *the linear yield in uptime, the long planning horizon, and the commonly assumed negligible maintenance time*, the optimal CBM policy typically has a simple control limit or a simple control-limit function. See [Elwany et al. \(2011\)](#), [Chen et al. \(2015\)](#), [Drent et al. \(2023\)](#) when system degradation follows a continuous-state stochastic process with random effects, [Kim \(2016\)](#) and [Zhu et al. \(2023\)](#) when system deterioration follows a multi-state Markov chain with model misspecification, and [Khaleghei and Kim \(2021\)](#) when system failure follows a three-state semi-Markov process. In contrast, *the zero-one yield, the short planning horizon, and the non-negligible abort duration* rule out a simple control-limit policy for mission abort decisions when the state evolution is non-Markovian. This is evidenced by Theorem 4 ahead, where we show that the optimal policy is defined by lower and upper control-limit functions under a spherical coordinate system, when the system deterioration follows a partially observable three-state (normal, defective, failed) semi-Markov chain with phase-type sojourn times.

For a partially observable three-state system whose health status is inferred from condition-monitoring data and whose failure is self-revealed, existing solutions base the abort decision on a charting statistic that monitors its latent state. The mission is aborted once the charting statistic triggers an alarm. This is a two-step procedure where the decision rule in the second step is predicated on the alarm generated from the first step. Some studies considered a more complicated decision rule for mission abort. For example, [Qiu and Cui \(2019\)](#) classify a system as defective upon receiving a defect signal, leading to a mission abort if the remaining time to complete the mission exceeds an optimized threshold. [Cha et al. \(2018\)](#) confirm the defective status once \bar{m} warning signals are received in total, and abort the mission if the remaining mission duration is longer than a time threshold $\bar{\xi}$. Both \bar{m} and $\bar{\xi}$ can be optimized. [Zhao et al. \(2021\)](#) compute the expected time for the system to reach a certain degradation level. The mission is aborted if this time is smaller than a threshold. These rule-based methods, albeit easy to implement, fall short in optimizing the trade-off between system failure and mission success.

Optimality guarantee of an abort policy is possible if the underlying system dynamics governing the system state transition and condition-monitoring data generation are known, but this direction remains unexplored. For a three-state Markovian deteriorating system with condition-monitoring data, its optimal mission abort control can be attained through a partially observable Markov decision process (POMDP), and our Corollary 2 ahead shows that the optimal policy enjoys a relatively simple structure. Given that the mission duration is typically much shorter than the system service life, it is reasonable to posit an exponential sojourn time from the healthy state to either the defective or failure state. However, assuming an exponential sojourn time from defective to failure states may be questionable, as this distribution is contingent on the endogenous physical mechanisms governing the progression from a defect to the ultimate collapse. This argument is well

supported by real-world lifetime datasets from physical systems (Mittman et al. 2019, Meeker et al. 2022). Violation of the Markovian assumption can severely invalidate solutions from a POMDP. As an illustration, Section 9 considers a bimodal sojourn time from defect to failure. Approximating such a system by a simple Markov process loses critical information about the sojourn time in the defective state, leading to inferior decisions. Our numerical results show that the cost increment from this simple approximation can be near 20% compared to the proposed method.

This study considers a general three-state semi-Markov deteriorating system in which we allow general distributions for both transition times from healthy to defective and from defective to failure. The associated mission abort unfolds as an optimal stopping problem, as formulated in Problem (1) ahead. Directly solving this problem is intractable due to the non-Markovian process dynamics. For a tractable solution, we introduce a novel tool of Erlang mixtures to approximate non-exponential sojourn times therein. The original three-state semi-Markov system can then be approximated with a surrogate continuous-time Markov chain (CTMC) whose number of states is larger than three in the original semi-Markov system and is determined by the number of components in the two Erlang mixture distributions. By properly linking the surrogate CTMC to condition-monitoring data, a surrogate POMDP can be constructed. The optimal mission abort policy derived from this surrogate POMDP serves as an approximation to optimal stopping of the original problem (1). Consolidating the above idea is not a simple task for reasons as follows.

- In principle, an infinite array of CTMCs can be devised, each with absorbing time conforming to the same Erlang mixture distribution. However, an arbitrary selection of two CTMCs for the two Erlang mixture distributions may make the concatenated CTMC complicated, posing challenges in theoretical analysis and numerical computations of the resulting surrogate POMDP. Therefore, the first crucial question to address is the initial design of the two CTMCs.
- The surrogate POMDP approximates the original semi-Markov dynamics and retains the same mission abort cost structure. When its solution is used to approximate the optimal solution of the original mission abort problem, i.e., the stopping time problem (1) ahead, it is not immediately clear how the approximation works and what is the quality of the approximation since the two problems are defined in different probability spaces.
- If the optimal policy of the surrogate POMDP well approximates that of Problem (1), analyzing its structure would provide deeper insights into the abort problem. For example, one may inquire: (a) What is the structure of the optimal policy, and how does it differ from that of a standard CBM when the underlying system dynamics are as simple as a CTMC? (b) Does a similar structure persist when the sojourn times become non-exponential? (c) If not, can we characterize it? The first question aids in understanding the fundamental disparity between mission abort and CBM, while the last two offer insights into the influence of non-exponential sojourn times on the

optimal policy. However, POMDPs with more than two states are notoriously challenging to analyze (Zhang and Zhang 2023), while our surrogate POMDP is anticipated to have many states for an accurate approximation of the original system.

- With numerous states in the surrogate POMDP, directly employing standard point-based value iteration (PBVI) algorithms (Pineau et al. 2003) for a numerical solution of the optimal policy proves to be exceedingly inefficient. By leveraging structural properties of the optimal policy, it might be possible to tailor an effective algorithm for our mission abort setting.

This study aims to address the challenges outlined above. The contributions of this work can be summarized as follows.

Our first contribution lies in the development of a general modeling and solution framework for optimal mission abort with imperfect condition-monitoring data, an imperative consideration for a multitude of on-demand mission-critical systems. We consider a general three-state semi-Markov deterioration process, resulting in an intractable optimal stopping problem in (1). We address this intricacy by introducing an innovative Erlang mixture recipe to approximate the two non-exponential sojourn times of the semi-Markov process, leading to an CTMC approximation of the original semi-Markov process. The surrogate CTMC is subsequently correlated to surrogate condition-monitoring signals, which are generated by mirroring the signal generation process of the original system. This leads to a surrogate POMDP for approximating (1), with the surrogate CTMC as system dynamics, mission abort decisions as actions, and surrogate condition-monitoring signals as observations. We craft a construction for the CTMC approximation in Section 4.1 that endows this surrogate POMDP with favorable theoretical properties.

Our second contribution stems from asymptotic analysis on the efficacy of the POMDP solution in approximating the optimal mission abort decision rules defined in Problem (1). To comprehend the approximation, we conceptualize the surrogate POMDP as a model defined in a probability space distinct from that of the original abort problem, while the surrogate signals retain the same sample space as the original signals. As such, the POMDP optimal policy, akin to the optimal abort decision rules from solving the original problem (1), is a map from the sample space for the condition-monitoring signals to the binary action space. Our Theorem 1 shows that the POMDP optimal policies, indexed by a sequence of Erlang rate parameters and treated as measurable functions in the original probability space, converge almost surely to the optimal abort decision rules defined by (1) as the Erlang rate parameter goes to infinity. This result implies asymptotic optimality of the POMDP solution for the abort decision in that the expected cost by adopting the POMDP solution converges to the optimal expected cost in (1) almost surely.

Our third contribution is to provide comprehensive structural results on the optimal policy of the surrogate POMDPs. Under a general surrogate POMDP, we demonstrate in Theorem 3 that

there exists a threshold on the cumulative mission time, beyond which mission abort is always unnecessary. This finding offers solid support for the prevailing abort heuristic (Cha et al. 2018, Qiu and Cui 2019). Nevertheless, even when the system dynamics follow the simplest CTMC, our upcoming Corollary 2 reveals that before reaching the time threshold, abort is optimal if and only if the belief state for defect falls in an interval whose upper endpoint is *smaller than one*. This clearly reveals why the existing rule-based methods, which abort upon confirmation of a defect, cannot be optimal. Moreover, the result is highly indicative of the distinction from CBM where a system is replaced upon confirmation of severe ageing. We further show in Theorem 4 that the optimal abort policy can be delineated by an interval for the distance from the current belief state vector to the belief vector with unit mass on the worst state right before failure, with the two endpoints dependent on the angle of the current vector in an appropriately designed spherical coordinate system. In this coordinate system, the region with abort as the optimal action can be shown to be convex. This important property helps us to develop a modified PBVI algorithm. As demonstrated in Section 9, the runtime of our modified algorithm is less than 10% of the standard PBVI algorithm, while maintaining the same numerical error.

The remainder of the paper is organized as follows. Section 2 reviews related literature. Section 3 illustrates the mission abort problem. Section 4 introduces Erlang mixture distributions to approximate the system failure process as a CTMC and then formulates a POMDP framework. Section 5 derives structural properties of our model and shows the optimal abort policy follows a control-limit structure. To deal with the curse of dimensionality, Section 6 develops an algorithm that approximately solves the optimization problem. Section 7 further investigates two special cases of our model which can be exactly solved after discretizing the state space. Section 8 extends to a multi-task setting. Section 9 conducts a case study on a UAV, which have become increasingly prevalent in various domains, including asset management, healthcare and supply chain. Section 10 concludes this study and discusses future research. All technical proofs are provided in Appendix A.

2. Literature Review

Myers (2009) pioneers the mission abort problem by basing the abort decision on the number of failed components, which oversimplifies the system dynamics. Similar to this work, condition-monitoring signals are not considered in the early literature. Some subsequent studies base the abort decision on the number of shocks observed during the mission (Levitin et al. 2021). In practice, however, shocks are hard to define and quantify, and magnitude of shocks often matters. Both Qiu and Cui (2019) and Yang et al. (2020) use condition-monitoring signals to design the mission abort policy, but their models ignore the false and missed alarms. This leads to suboptimal performances as condition-monitoring data are generally imperfect. We are not aware of an analytically

optimal policy for mission abort under condition monitoring, even assuming Markovian system deterioration.

Condition-based mission abort shares similarities to CBM, both of which use imperfect signals to predict system failure and make decisions. In the literature of CBM, Markov decision processes (MDPs) and POMDPs are frequently used. [Elwany et al. \(2011\)](#) and [Drent et al. \(2023\)](#) assume observable system degradation and use an MDP to integrate Bayesian learning and maintenance decision-making. Control-limit policies with simple threshold functions are shown to be optimal in both studies. When the system health state is unobservable, [Kim and Makis \(2013\)](#) use a POMDP to show the optimality of a two-level control-limit policy for inspection and replacement of a three-state system. [Kim \(2016\)](#) considers parameter uncertainty and uses a robust POMDP to show the optimality of a control-limit policy for replacement of a two-state system. Recently, [Zhang and Zhang \(2023\)](#) develop a dual framework for POMDPs based on [Zhang \(2010\)](#) to analytically derive the optimal inspection and replacement policy of a three-state system. The model introduces a novel perspective for maintenance problems by representing the optimal maintenance policy through six graphs. As discussed in Section 1, most existing maintenance models assume a negligible maintenance time compared to the long planning horizon with linear yield in uptime. In contrast, a distinctive aspect of mission abort problems is that aborting a mission incurs a non-negligible rescue time (see Section 3.3) and a zero-one mission failure cost. Hence, existing analysis for maintenance models cannot be directly applied to our problem.

Most existing studies on reliability assume a Markovian deterioration system for tractability, which can be challenged in many applications as discussed in Section 1. Departing from this norm, [Krishnamurthy \(2011\)](#) addresses a change point detection problem where the change time follows a phase-type distribution. [Wang and Lee \(2015\)](#) propose a Bayesian control chart that includes a phase-type distributed transition time from in-control to out-of-control states as a special case. Both studies justify the use of phase-type distributions by highlighting their denseness property within the space of all positive-valued distributions, making them well-suited for approximating non-Markovian systems. [Khaleghei and Kim \(2021\)](#) further explicitly construct a phase-type distribution to approximate a given semi-Markov process. Based on the corresponding approximating Markov processes, a sequence of POMDPs is formulated for maintenance optimization. Their main approximation result, c.f. Proposition 2 therein, states that the optimal objective values of the surrogate POMDPs converge to that of the original system. Their Theorem 3 establishes a control-limit structure for the optimal control policy of the POMDP, and their Figure 3 numerically shows that the control limits of the surrogate POMDPs, represented as a sequence of real numbers, converge to some limit which they regard as the optimal control limit for the original problem.

In contrast to [Khaleghei and Kim \(2021\)](#), the optimal policy for our original mission abort problem under a partially observed semi-Markov system can be highly unstructured. We approximate the optimal policy, which is a set of functions from the signal space to the binary action space, using the POMDP optimal policy. Convergence for this functional approximation necessitates a meticulous definition of probability spaces for various stochastic systems and is technically challenging. In comparison, [Khaleghei and Kim \(2021\)](#) do not prove convergence of optimal POMDP control limits to that of the original problem, which is convergence of a sequence of real numbers. Furthermore, they only accommodate a general distribution for the transition time from the defective to failure state. Our proposed model is more general by allowing the transition time from the healthy to defective state to be general distributed as well. This generalization leads to a non-trivial and interesting construction of CTMCs as shown in Section 4.1 ahead.

To solve a POMDP for optimal stopping, standard methods such as value iteration ([Piri et al. 2022](#)) or continuation-value iteration ([Zhang 2010](#)) are effective when the state space is small. Due to the curse of dimensionality, however, it is computationally infeasible to exactly solve a general large-scale POMDP. Acceleration algorithms can be devised for solving a POMDP when the optimal policy exhibits certain structural properties. For example, [Khaleghei and Kim \(2021\)](#) show that the optimal policy of their surrogate POMDP is defined by a simple control limit on the system reliability; solving this POMDP thus simplifies to a one-dimensional search for the optimal control limit. In contrast, the optimal policy of our surrogate POMDP for mission abort lacks such a simple structure. Popular methods to tackle a general POMDP include online planning methods ([Silver and Veness 2010](#)) and offline iterative methods such as grid-based methods ([Sandıkçı et al. 2013](#)) and PBVI algorithms ([Pineau et al. 2003](#)). These general-purpose algorithms do not effectively scale to POMDPs with many states. To attain an accurate solution within a reasonable timeframe, it is desirable to expedite the numerical procedure by capitalizing on structural insights derived from the mission abort problems.

3. Problem Statement

Consider a mission-critical system that is required to operate continuously for a constant mission time $H > 0$. This section formulates the mission abort decision problem given in-situ signals indicating the health condition of the system. Section 3.1 models the system failure process. Section 3.2 introduces the observable signals used to infer the system health state. Section 3.3 describes the decision-making problem.

3.1. System Failure Process

During a mission, suppose the system failure process can be modeled by a stochastic process $\{X(t), t \geq 0\}$ with a state space $\mathbb{S} = \{1, 2, 3\}$ defined on a probability space $(\Omega, \mathcal{F}, \mathbb{P})$, where $X(t) =$

1, 2, and 3 indicate healthy, defective, and failure system states at time t , respectively. The failure state is self-announcing, but we cannot exactly tell whether the system is healthy ($X(t) = 1$) or defective ($X(t) = 2$) given that it is working at t . Such a three-state model is commonly used in the existing literature to model failure processes (Panagiotidou and Tagaras 2010, Abbou and Makis 2019) and has been widely validated by real diagnostic data (Makis et al. 2006). We stipulate $X(0) = 1$, meaning a healthy state at the onset. Based on degradation physics, we require $X(t)$ to be nondecreasing in t (Panagiotidou and Tagaras 2010). As such, the system can either fail directly from a healthy state or go through a two-phase failure process, namely, from healthy to defective and then to the failure state. Notationally, let T_{1j} be the underlying time to transition directly from state 1 to state $j \in \{2, 3\}$. If $T_{12} \geq T_{13}$, the system fails at time T_{13} ; otherwise, the system enters the defective state 2 at time T_{12} , and the sojourn time at this state before transitioning to failure is T_{23} . Based on the above assumptions, the system failure time $\xi \triangleq \inf\{t \geq 0 : X(t) = 3\}$ is

$$\xi = \begin{cases} T_{13}, & T_{13} \leq T_{12}, \\ T_{12} + T_{23}, & \text{otherwise.} \end{cases}$$

We model T_{13} as an exponential random variable with rate ζ , while T_{12}, T_{23} follow a general continuous distribution with probability density functions (PDFs) $g(\cdot), f(\cdot)$ and cumulative distribution functions (CDFs) $G(\cdot), F(\cdot)$, respectively. Furthermore, we model T_{12}, T_{13}, T_{23} as independent random variables. The exponential assumption on T_{13} is a reasonable premise given that the mission time H is typically substantially shorter than the system lifetime. The failure rate of T_{13} approximates the failure rate of the system at its present age, a value that remains relatively constant over a short mission duration for a long-lived system (Khojandi et al. 2018, Abbou and Makis 2019, Tian et al. 2021). Similarly, an exponential T_{12} is also appropriate, and the manifestation of the defect over the short mission duration should be non-informative on the progression of the defect to eventual failure. Here, we opt for a general distribution for T_{12} as it does not introduce fundamental complexity into the methodology developed subsequently. In contrast, a generic distribution for the duration T_{23} from defective to failure states is based on the consideration that T_{23} is usually short and exhibits increasing failure rate when the system is defective. An increasing failure rate is a common assumption in reliability modeling, e.g., for production systems (Iravani and Duenyas 2002) and commercial modular aero-propulsion systems (Zhu et al. 2023), and has been validated by many real-world datasets (Meeker et al. 2022). Letting $h(\cdot)$ be the hazard rate of T_{23} , this assumption is formally stated as follows.

ASSUMPTION 1. *The hazard rate $t \mapsto h(t)$ for T_{23} is nondecreasing, and the failure rate at the defective state is larger than that at the healthy state, i.e., $h(0) > \zeta$.*

Section 5 analyzes the optimal abort policies with and without Assumption 1.

3.2. Observed Signals

If the system is functioning at time t , it can be either healthy ($X(t) = 1$) or defective ($X(t) = 2$) for $t < \xi$. To infer the underlying health state, we consider condition-monitoring signals collected with an inter-sampling interval δ . The interval δ is exogenously determined by sensor properties and is typically short in practice that entails real-time abort decision-making. The condition-monitoring signal Y_n at time $n\delta$ takes values in $[K] \triangleq \{1, \dots, K\}$ for $n \in [N] \triangleq \{1, \dots, N\}$, where we assume $N \triangleq H/\delta$ is an integer. This assumption is not restrictive because if the condition-monitoring data are multi-dimensional, many state-of-the-art prognostic algorithms have been developed to fuse them into a discrete categorical signal (Hong et al. 2018, Liu et al. 2022). For completeness, we let $Y_n = 0$ with probability one if the system has failed at time $n\delta$ for $n \in [N]$.

Letting $X_n \triangleq X(n\delta)$, we model its stochastic dependence with Y_n as $\mathbb{P}(Y_n = k \mid X_n = i) = d_{ik}$ for $i \in \{1, 2\}$ and $k \in [K]$. The state-observation matrix is then denoted by $\mathbf{D} = (d_{ik})_{2 \times K}$. In practice, this matrix can be estimated based on historical experimental data (Piri et al. 2022). The following assumption is needed when we establish the monotonicity of value functions in Section 5.

ASSUMPTION 2. *The matrix \mathbf{D} is totally positive of order 2 (TP2), i.e., $d_{ik}d_{i'k'} \geq d_{ik'}d_{i'k}$ for all $i \leq i'$ and $k \leq k'$.*

In words, Assumption 2 requires that a larger Y_n indicates the system is more likely to be at the defective state. Similar assumptions are commonly imposed on the state-observation matrix on disease severity in the healthcare literature (Sandıkçı et al. 2013).

3.3. Mission Abort Decision Making

Upon receiving a new signal Y_n at time $n\delta$, our available data are $Y_{1:n} \triangleq (Y_1, \dots, Y_n)$, and we have two action choices: (i) to abort the mission and initiate a rescue procedure, or (ii) to continue the mission until observing Y_{n+1} . The system can fail during either rescue or mission, incurring a *system* failure cost C_s . Moreover, a *mission* failure cost C_m is incurred if the mission is not completed. When the mission is aborted at time $n\delta$, we let w_n , $n = 0, \dots, N-1$, be the rescue time with $w_0 = 0$. When the mission is finished at time $H \triangleq N\delta$, we assume there is an additional time $w_N \geq 0$ to stop the system. For example, a UAV takes time w_N to fly back to the base upon finishing an inspection mission. The following assumptions on the rescue procedure are in force.

ASSUMPTION 3. (i) *The rescue time w_n is nondecreasing with n .* (ii) *The rescue procedure does not affect the failure process $X(t)$.*

Assumption 3 is common in literature (Yang et al. 2020, Levitin et al. 2021). We illustrate it using the UAV example again. Consider a UAV that leaves the ground base to conduct a mission at a

certain altitude. During the mission, the altitude of the UAV increases over time before it reaches the required altitude. The monotone assumption on w_n is valid since a UAV at a higher altitude needs more time to land on the ground base. Moreover, the rescue procedure does not change the system failure rate so the failure process $X(t)$ is not affected. As a consequence of Assumption 3(i), we have $w_n \leq H - n\delta + w_N$ for all $n = 0, \dots, N - 1$. This inequality indicates that the rescue time at time $n\delta$ is shorter than the time to complete the mission and to stop the system; otherwise, there is no need to abort the mission.

Based on the above setting, our objective is to find the optimal mission abort policy during the mission time $[0, H]$ that minimizes the expected total loss for a mission.

4. POMDP Formulation

Our decision-making problem is to determine a set of decision rules $a_n : \{0, \dots, K\}^n \mapsto \{0, 1\}$ for $n \in [N - 1]$, such that given $Y_{1:n} = y_{1:n} \in [K]^n$, the action $a_n(y_{1:n}) = 1$ means aborting the mission at time $n\delta$ and $a_n(y_{1:n}) = 0$ means doing nothing until the next decision epoch. On the other hand, $Y_n = 0$ indicates the system has failed at time $n\delta$, and we let $a_n(Y_{1:n}) = 1$ if $Y_n = 0$ for completeness. Given $(a_n)_{n \in [N-1]}$, we denote $\mathfrak{T} \triangleq \min\{n\delta : a_n(Y_{1:n}) = 1, n \in [N - 1]\} \cup \{N\delta\}$ as the random time when the mission is aborted ($\mathfrak{T} < H$) or finished ($\mathfrak{T} = H$). Let $C(X(\mathfrak{T} + w_{\mathfrak{T}/\delta}), \mathfrak{T})$ be the total operational cost for the mission, which is a function of the random time \mathfrak{T} and the state $X(\mathfrak{T} + w_{\mathfrak{T}/\delta})$ when the system is fully stopped. Then $C(X(\mathfrak{T} + w_{\mathfrak{T}/\delta}), \mathfrak{T})$ is given by

$$C(X(\mathfrak{T} + w_{\mathfrak{T}/\delta}), \mathfrak{T}) = (C_m + C_s)\mathbb{1}\{X(\mathfrak{T} + w_{\mathfrak{T}/\delta}) = 3\} + C_m\mathbb{1}\{X(\mathfrak{T} + w_{\mathfrak{T}/\delta}) < 3, \mathfrak{T} < H\},$$

where $\mathbb{1}\{\cdot\}$ is the indicator function. Our abort decision-making problem can be written as:

$$\begin{aligned} \min_{\{a_n : n \in [N-1]\}} & \mathbb{E}[C(X(\mathfrak{T} + w_{\mathfrak{T}/\delta}), \mathfrak{T})] \\ \text{s.t.} & \quad \mathfrak{T} = \min\{n\delta : a_n(Y_{1:n}) = 1, n \in [N - 1]\} \cup \{N\delta\}; \\ & \quad a_n(y_{1:n}) = 1 \text{ if } y_n = 0, n \in [N - 1], \end{aligned} \tag{1}$$

where the expectation \mathbb{E} is taken with respect to the stochastic process $\{X(t), 0 \leq t \leq H + w_N\}$ and condition-monitoring signals $Y_{1:N}$. Let $\{a_n^* : n \in [N - 1]\}$ be the set of optimal actions, and $\mathfrak{T}^* \triangleq \min\{n\delta : a_n^*(Y_{1:n}) = 1, n \in [N - 1]\} \cup \{N\delta\}$ be the optimal stopping time. We assume the set of optimal actions is unique. In case there are multiple sets of optimal actions, we stipulate the set with the smallest \mathfrak{T}^* as the optimal solution.

4.1. Erlang Approximation

Compared with most existing optimal stopping problems with Markovian system dynamics (Abbou and Makis 2019, Tian et al. 2021), the non-exponential sojourn times T_{12} from healthy to

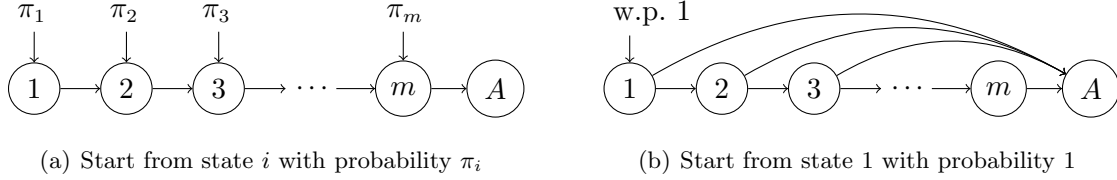


Figure 1 Two CTMC schemes with m transient states and an absorbing state A . With proper choice of the initial probabilities $(\pi_i)_{i \in [m]}$ and the transition rates, their absorbing times can follow the same distribution. The two schemes are used to approximate the transitions from \mathcal{X}_1 to \mathcal{X}_2 and from \mathcal{X}_2 to \mathcal{X}_3 , respectively.

defect and T_{23} from defect to failure make Problem (1) challenging to solve. We approximate them using two sequences of Erlang mixture distributions. This approximation will induce a sequence of surrogate POMDPs whose optimal policies approximate that for Problem (1).

We start with approximating the distribution of the nonnegative T_{23} by an Erlang mixture (also known as the hyper-Erlang distribution). Let $E_m^{(\lambda)}(\cdot)$ be the CDF of an Erlang distribution with rate $\lambda > 0$ and shape $m \in \mathbb{N}_+$. Corollary 4.1 of Wiens (1979) shows that for any integer-valued function $m_2 \triangleq m_2(\lambda)$ of λ satisfying $\lim_{\lambda \rightarrow \infty} m_2/\lambda \rightarrow \infty$, the random variable $T_{23}^{(\lambda)} \geq 0$ with CDF

$$F^{(\lambda)}(t) = \sum_{i=1}^{m_2-1} \left[F\left(\frac{i}{\lambda}\right) - F\left(\frac{i-1}{\lambda}\right) \right] E_i^{(\lambda)}(t) + \left[1 - F\left(\frac{m_2-1}{\lambda}\right) \right] E_{m_2}^{(\lambda)}(t), \quad t \geq 0, \quad (2)$$

converges weakly to T_{23} as $\lambda \rightarrow \infty$. In view of this property, we approximate the distribution of T_{23} by that of $T_{23}^{(\lambda)}$ for some fixed $\lambda > 0$ and $m_2 \triangleq m_2(\lambda) > 0$. We choose $\lambda > \zeta$ and let

$$G^{(\lambda)}(t) = \sum_{i=1}^{m_1-1} \left[G\left(\frac{i}{\lambda-\zeta}\right) - G\left(\frac{i-1}{\lambda-\zeta}\right) \right] E_i^{(\lambda-\zeta)}(t) + \left[1 - G\left(\frac{m_1-1}{\lambda-\zeta}\right) \right] E_{m_1}^{(\lambda-\zeta)}(t), \quad t \geq 0, \quad (3)$$

for some $m_1 \triangleq m_1(\lambda)$ satisfying $\lim_{\lambda \rightarrow \infty} m_1/\lambda \rightarrow \infty$. Then $T_{12}^{(\lambda)} \sim G^{(\lambda)}$ converges weakly to T_{12} as $\lambda \rightarrow \infty$ and is used to approximate T_{12} . The choice of $\lambda - \zeta$ in (3) is a pivotal maneuver. It allows us to construct a surrogate CTMC with identical transition rates out of any transient state, and the resulting surrogate POMDP has nice structural properties, as shown in Section 5.

After the Erlang mixture approximations, two CTMCs with m_1 and m_2 transient states can be constructed with absorbing times following $G^{(\lambda)}$ and $F^{(\lambda)}$, respectively. Concatenation of the two CTMCs yields a surrogate CTMC with $m_1 + m_2$ transient states and one absorbing state (labeled as $m_1 + m_2 + 1$) that approximates the original non-Markovian dynamics $X(\cdot)$. However, the CTMC construction is non-unique (Buchholz et al. 2014). For illustration, Figure 1 shows two simple schemes to construct a CTMC based on an Erlang mixture distribution with m components. In Figure 1(a), the CTMC can start from any transient state, after which the state transition sequence is deterministic. In Figure 1(b), the CTMC starts from the first state. In each transition,

it moves either to the next transient state or directly to the absorbing state. In both CTMCs, we can select appropriate initial probabilities or transition rates to make their absorbing times follow a given m -component mixture of Erlang distribution. In principle, there are infinitely many CTMC schemes for $G^{(\lambda)}$ and $F^{(\lambda)}$ in (2) and (3). It is extremely difficult, if not unattainable, to establish structural results for the resulting surrogate model if we casually choose two CTMCs.

After thorough experimentation, we find that using the scheme in Figure 1(a) for $G^{(\lambda)}$ and that in Figure 1(b) for $F^{(\lambda)}$ notably simplifies the ensuing theoretical analysis. The rationale behind this choice is as follows. In Figure 1(a) for $G^{(\lambda)}$, we obtain a simple CTMC with deterministic transitions at a cost of a random start captured by an initial distribution. Its absorbing state A corresponds to the collection of states $m_1 + 1, m_2 + 2, \dots, m_1 + m_2$ in the concatenated surrogate CTMC. This explains the importance of starting the second chain, i.e., Figure 1(b) for $F^{(\lambda)}$, at the first state that corresponds to state $m_1 + 1$ in the surrogate CTMC after concatenation. As such, state m_1 transitions to state $m_1 + 1$ with probability one in the surrogate CTMC. Initiating the second CTMC deterministically comes with a cost of a complicated transition rate matrix. Nonetheless, this complexity does not pose an obstacle for our mission abort problem, because the absorbing state in Figure 1(b) for $F^{(\lambda)}$ corresponds to the self-revealed failure state $m_1 + m_2 + 1$ in the concatenated surrogate CTMC. The acquisition of condition-monitoring data signifies the system's operational status, conditional on which we can logically exclude any transition from states $i \in [m_1 + m_2]$ to the failure state $m_1 + m_2 + 1$ in the CTMC analysis. With the above construction, any transient state in our constructed surrogate CTMC can only transition to the next state when condition-monitoring data are received. This greatly simplifies the Kolmogorov backward equation for the surrogate CTMC.

With Figure 1(a) for $G^{(\lambda)}$ and Figure 1(b) for $F^{(\lambda)}$, we construct a surrogate CTMC $\{X^{(\lambda)}(t) : t \geq 0\}$ and the associated condition-monitoring signals $\{Y_n^{(\lambda)} : n \in [N]\}$ on some probability space $(\Omega^{(\lambda)}, \mathcal{F}^{(\lambda)}, P^{(\lambda)})$, which is different from $(\Omega, \mathcal{F}, \mathbb{P})$ for $\{X(t), t \geq 0\}$ and $Y_{1:N}$. Let the state space of $X^{(\lambda)}(t)$ be $\mathcal{X} \triangleq \{1, \dots, m_1 + m_2 + 1\}$ with state $m_1 + m_2 + 1$ absorbing and others transient. The states in $\mathcal{X}_1 \triangleq \{1, \dots, m_1\}$ correspond to the healthy state $X(t) = 1$, states in $\mathcal{X}_2 \triangleq \{m_1 + 1, \dots, m_1 + m_2\}$ correspond to the defective state $X(t) = 2$, and the state in $\mathcal{X}_3 \triangleq \{m_1 + m_2 + 1\}$ corresponds to the failure state $X(t) = 3$. We let $P^{(\lambda)}(X^{(\lambda)}(0) = i) = \pi_{0i}^{(\lambda)}$, where

$$\pi_{0i}^{(\lambda)} = \begin{cases} 1 - G((m_1 - 1)/(\lambda - \zeta)), & i = 1, \\ G((m_1 + 1 - i)/(\lambda - \zeta)) - G((m_1 - i)/(\lambda - \zeta)), & i = 2, \dots, m_1, \\ 0, & i = m_1 + 1, \dots, m_1 + m_2 + 1. \end{cases} \quad (4)$$

Denote $q_{ij} \triangleq \lim_{\epsilon \downarrow 0} \frac{1}{\epsilon} P^{(\lambda)}(X^{(\lambda)}(t + \epsilon) = j \mid X^{(\lambda)}(t) = i)$, $i \neq j$, as the instantaneous transition rate from state $i \in \mathcal{X}$ to state $j \in \mathcal{X}$. We construct the CTMC $X^{(\lambda)}(t)$ such that its instantaneous transition rate matrix $\mathbf{Q} = (q_{ij})_{i,j \in \mathcal{X}}$ satisfies

$$q_{ij} = \begin{cases} \lambda - \zeta, & j = i + 1, i \in \mathcal{X}_1, \\ \zeta, & i \in \mathcal{X}_1, j = m_1 + m_2 + 1, \\ \lambda[1 - p_{i-m_1}(\lambda)], & j = i + 1, i, j \in \mathcal{X}_2, \\ \lambda p_{i-m_1}(\lambda), & i \in \mathcal{X}_2 \setminus \{m_1 + m_2\}, j = m_1 + m_2 + 1, \\ \lambda, & i = m_1 + m_2, j = m_1 + m_2 + 1, \end{cases} \quad (5)$$

$q_{ij} = 0$ for other $i \neq j$, and $q_{ii} = -\sum_{j \in \mathcal{X}: j \neq i} q_{ij}$, where

$$p_i(\lambda) \triangleq \frac{F(i/\lambda) - F((i-1)/\lambda)}{1 - F((i-1)/\lambda)}, \quad i \in [m_2 - 1]. \quad (6)$$

The above construction leads to $q_{ii} = -\lambda$ for all $i \in [m_1 + m_2]$, facilitating the subsequent analysis in Section 5. Consistent with $X(t)$, the states in \mathcal{X}_1 and \mathcal{X}_2 are unobservable, but the failure state $m_1 + m_2 + 1$ of $X^{(\lambda)}(t)$ is observable. We associate the surrogate signal $Y_n^{(\lambda)}$ with $X^{(\lambda)}(n\delta)$ as $P^{(\lambda)}(Y_n^{(\lambda)} = k \mid X^{(\lambda)}(n\delta) \in \mathcal{X}_i) = d_{ik}$ for $i = 1, 2$ and $k \in [K]$. When $X^{(\lambda)}(n\delta) = m_1 + m_2 + 1$, we let $Y_n^{(\lambda)} = 0$ with $P^{(\lambda)}$ -probability one.

With the above construction, the surrogate CTMC $X^{(\lambda)}(\cdot)$ can be linked to the independent random variables $T_{12}^{(\lambda)}$, T_{13} , and $T_{23}^{(\lambda)}$ as follows.

PROPOSITION 1. *Consider the CTMC $X^{(\lambda)}(\cdot)$ with initial probabilities in (4) and transition rate matrix \mathbf{Q} in (5). Then the first hitting time of $X^{(\lambda)}(\cdot)$ to the states in \mathcal{X}_2 has the same distribution as $T_{12}^{(\lambda)}$, and the absorption time of $X^{(\lambda)}(\cdot)$ has the same distribution as $T_{13} \mathbb{1}\{T_{13} \leq T_{12}^{(\lambda)}\} + (T_{12}^{(\lambda)} + T_{23}^{(\lambda)}) \mathbb{1}\{T_{13} > T_{12}^{(\lambda)}\}$, where $T_{12}^{(\lambda)}$, $T_{23}^{(\lambda)}$ and T_{13} are independent random variables.*

Recall the absorption time of $\{X(t) : t \geq 0\}$ is $\xi \triangleq T_{13} \mathbb{1}\{T_{13} \leq T_{12}\} + (T_{12} + T_{23}) \mathbb{1}\{T_{13} > T_{12}\}$. Since $(T_{12}^{(\lambda)}, T_{23}^{(\lambda)}) \rightsquigarrow (T_{12}, T_{23})$ as $\lambda \rightarrow \infty$, the above proposition, together with the continuous mapping theorem, implies that the absorption time of $\{X^{(\lambda)}(t) : t \geq 0\}$ converges weakly to the absorption time of $\{X(t) : t \geq 0\}$.

In the original problem, the decision at time $n\delta$ is based on the observed signal $Y_{1:n}$ with $Y_{1:n} \triangleq (Y_1, \dots, Y_n)$, and the decision rule is a map $a_n : \{0, 1, \dots, K\}^n \mapsto \{0, 1\}$. We are interested in the sequence of the optimal decision rules $(a_n^*)_{n \in [N-1]}$ determined by Problem (1), which is hard to solve. In view of the distributional similarity in Proposition 1, we can consider a surrogate problem where the state-signal process $\{X(\cdot), Y_{1:N}\}$ in the original problem is replaced by $\{X^{(\lambda)}(\cdot), Y_{1:N}^{(\lambda)}\}$, while the cost structure remain unchanged. The optimal decision rule $a_{\lambda,n}^* : \{0, 1, \dots, K\}^n \mapsto \{0, 1\}$

for this surrogate problem is expected to be a good approximation of the map a_n^* , $n \in [N-1]$. To consolidate this intuition, we can obtain $a_{\lambda,n}^*$ from solving the following surrogate problem:

$$\begin{aligned} \min_{\{a_{\lambda,n} : n \in [N-1]\}} & \mathbb{E}^{(\lambda)}[C(X^{(\lambda)}(\mathfrak{T} + w_{\mathfrak{T}/\delta}), \mathfrak{T})] \\ \text{s.t.} \quad & \mathfrak{T} = \min\{n\delta : a_{\lambda,n}(Y_{1:n}^{(\lambda)}) = 1, n \in [N]\} \cup \{N\delta\}, \\ & a_{\lambda,n}(y_{1:n}) = 1, \quad \text{if } y_n = 0, n \in [N-1], \end{aligned} \quad (7)$$

where the expectation $\mathbb{E}^{(\lambda)}$ is taken with respect to $\{X^{(\lambda)}(t), 0 \leq t \leq H + w_N\}$ and $Y_{1:N}^{(\lambda)}$. Let $\mathfrak{T}^{(\lambda*)} \triangleq \min\{n\delta : a_{\lambda,n}^*(Y_{1:n}^{(\lambda)}) = 1, n \in [N-1]\} \cup \{N\delta\}$ be the optimal stopping time of the surrogate problem. Again, if there are multiple sets of optimal actions $\{a_{\lambda,n}^* : n \in [N-1]\}$, we stipulate the set with the smallest $\mathfrak{T}^{(\lambda*)}$ as the optimal solution. This optimal solution is solved under the $P^{(\lambda)}$ -law, which is used to approximate $\{a_n^* : n \in [N-1]\}$ obtained under the \mathbb{P} -law. To assess its performance in the original problem, we define $\mathfrak{T}^{(\lambda)} \triangleq \min\{n\delta : a_{\lambda,n}^*(Y_{1:n}) = 1, n \in [N-1]\} \cup \{N\delta\}$ as the stopping time using the approximate solution in the original problem. The following theorem shows the accuracy of the approximation under the \mathbb{P} -law.

THEOREM 1. *Consider the sequence of optimal actions $\{a_{\lambda,n}^* : n \in [N-1]\}$ defined in the surrogate problem (7), and $\{a_n^* : n \in [N-1]\}$ defined in the original problem (1). For any $n \in [N-1]$, we have $a_{\lambda,n}^*(Y_{1:n}) \rightarrow a_n^*(Y_{1:n})$ \mathbb{P} -almost surely as $\lambda \rightarrow \infty$. As a result, $C(X(\mathfrak{T}^{(\lambda)} + w_{\mathfrak{T}^{(\lambda)}/\delta}), \mathfrak{T}^{(\lambda)}) \rightarrow C(X(\mathfrak{T}^* + w_{\mathfrak{T}^*}/\delta), \mathfrak{T}^*)$ \mathbb{P} -almost surely as $\lambda \rightarrow \infty$, and*

$$\begin{aligned} \mathbb{E}[C(X(\mathfrak{T}^* + w_{\mathfrak{T}^*}/\delta), \mathfrak{T}^*)] &= \lim_{\lambda \rightarrow \infty} \mathbb{E}[C(X(\mathfrak{T}^{(\lambda)} + w_{\mathfrak{T}^{(\lambda)}/\delta}), \mathfrak{T}^{(\lambda)})] \\ &= \lim_{\lambda \rightarrow \infty} \mathbb{E}^{(\lambda)}[C(X^{(\lambda)}(\mathfrak{T}^{(\lambda*)} + w_{\mathfrak{T}^{(\lambda*)}/\delta}), \mathfrak{T}^{(\lambda*)})]. \end{aligned} \quad (8)$$

The first part of Theorem 1 indicates that we can solve the surrogate problem (7) with sufficiently large λ and use the resulting sequence of decision rules $(a_{\lambda,n}^*)_{n \in [N-1]}$ for online decision-making in the original problem. The first equality of (8) reveals that this sequence of decision rules is asymptotically optimal in that the expected costs of the original mission abort problem, when applying these approximate policies, converge to the optimal expected costs of Problem (1). In comparison, Proposition 2 of Khaleghei and Kim (2021) shows that the optimal objective values of their surrogate problems converge to that of the original semi-Markov maintenance problem, which corresponds to the second equality in (8). Such convergence result might not be interesting enough, as the two objective values are obtained from two different stochastic systems. In contrast, our convergence results in Theorem 1, except the second equality in (8), are under the \mathbb{P} -law for the original non-Markovian system. The result directly shows the expected cost of applying the actions obtained from the surrogate problem to the original problem. Comparing this cost with the optimal cost provides a straightforward assessment of solution quality.

The above theorem is an asymptotic result. To gain some insight on an appropriate choice of the λ value, we look at the system failure rate when the CTMC $X^{(\lambda)}(\cdot)$ starts from the defective state, i.e., $h^{(\lambda)}(t) \triangleq \lim_{\Delta t \downarrow 0} P^{(\lambda)}(X^{(\lambda)}(t + \Delta t) = m_1 + m_2 + 1 \mid X^{(\lambda)}(0) = m_1 + 1, X^{(\lambda)}(t) \neq m_1 + m_2 + 1) / \Delta t$. Under Assumption 1, the time T_{23} from defective to failure has a nondecreasing hazard rate $h(\cdot)$, and $h(0) > \zeta$. If $T_{23}^{(\lambda)}$ well approximates T_{23} in distribution, $h^{(\lambda)}(t)$ should also have this property. We formalize these statements as follows.

LEMMA 1. *Under Assumptions 1, there exists a constant $\bar{\lambda} > 0$ such that $h^{(\lambda)}(0) > \zeta$ and $h^{(\lambda)}(t)$ is nondecreasing in $t > 0$ for any $\lambda > \bar{\lambda}$.*

In view of the above lemma, a necessary condition for good approximation of the surrogate problem is that $h^{(\lambda)}(t)$ is nondecreasing in $t \geq 0$ and $h^{(\lambda)}(0) > \zeta$ when Assumption 1 holds. As such, we need to carefully monitor this property when selecting λ . The properties in Lemma 1 will also be useful in Section 5 when we establish structural properties and derive the optimal abort policy for the surrogate problem under Assumption 1. When Assumption 1 does not hold, λ can be chosen through a visual comparison of the CDFs $F^{(\lambda)}, G^{(\lambda)}$ and the original F, G , as illustrated in Appendix C.1.

4.2. Bellman Recursion

For fixed $\lambda > 0$, $m_1 \triangleq m_1(\lambda)$, and $m_2 \triangleq m_2(\lambda)$, we now formulate the surrogate problem (7) as a POMDP where $\mathcal{X}_1 \cup \mathcal{X}_2$ are treated as hidden states. Let $p_{ij}(\delta) \triangleq P^{(\lambda)}(X^{(\lambda)}(t + \delta) = j \mid X^{(\lambda)}(t) = i)$, $i, j \in \mathcal{X}$, be the transition probability from state i to state j during a sampling interval δ , which can be computed by solving the Kolmogorov backward equations (Liu et al. 2021). Then $\mathbf{P}(\delta) = (p_{ij}(\delta))_{i,j \in \mathcal{X}}$ is the one-step transition probability matrix. For $n \in [N]$ and $i \in \mathcal{X}_1 \cup \mathcal{X}_2$, define $\Pi_{ni} \triangleq P^{(\lambda)}(X^{(\lambda)}(n\delta) = i \mid Y_{1:n}^{(\lambda)})$ as the conditional probability that the CTMC $X^{(\lambda)}(\cdot)$ is at hidden state i at time $n\delta$ given the signals $Y_{1:n}^{(\lambda)}$. After the value of $Y_{1:n}^{(\lambda)}$ is observed, the system *belief state* at time $n\delta$ is $\boldsymbol{\pi}_n \triangleq [\pi_{n1}, \dots, \pi_{n, m_1 + m_2}]'$, where π_{ni} is a realization of Π_{ni} . The belief state space is then given by the probability simplex $\mathcal{S} \triangleq \{\boldsymbol{\pi} = (\pi_i)_{i \in [m_1 + m_2]} \in \mathbb{R}_+^{m_1 + m_2} : \sum_{i=1}^{m_1 + m_2} \pi_i = 1\}$. As with the existing POMDP literature (e.g., Liu et al. 2021, Wang 2022), we introduce a value function $V^{(\lambda)}(n, \boldsymbol{\pi}_n)$, $n = 0, \dots, N$, that denotes the minimum cost-to-go at time $n\delta$ when the corresponding belief state is $\boldsymbol{\pi}_n \in \mathcal{S}$. The Bellman equations are given by

$$V^{(\lambda)}(n, \boldsymbol{\pi}_n) = \min\{V_{\text{ab}}(n, \boldsymbol{\pi}_n), V_{\text{c}}(n, \boldsymbol{\pi}_n)\}, \quad n = 0, \dots, N - 1, \quad (9)$$

where $V_{\text{ab}}(n, \boldsymbol{\pi}_n)$ and $V_{\text{c}}(n, \boldsymbol{\pi}_n)$ are the respective minimum cost-to-go when the action at time $n\delta$ is to *abort* and to *continue* the mission (we omit their dependence on λ for notational simplicity).

We first derive the explicit expression of $V_{\text{ab}}(n, \boldsymbol{\pi}_n)$. Assume that the system is working with a belief state $\boldsymbol{\pi}$. Let $\kappa(t, \boldsymbol{\pi})$ be the probability that the system's remaining useful life (RUL) is less than t , which is given by

$$\kappa(t, \boldsymbol{\pi}) = \boldsymbol{\pi}' \mathbf{p}_{\cdot, m_1+m_2+1}(t) \quad (10)$$

with $\mathbf{p}_{\cdot, m_1+m_2+1}(t) \triangleq [p_{1, m_1+m_2+1}(t), \dots, p_{m_1+m_2, m_1+m_2+1}(t)]'$. The expected cost of aborting the mission and initiating a rescue procedure at time $n\delta$ can then be expressed as

$$V_{\text{ab}}(n, \boldsymbol{\pi}_n) = C_{\text{m}} + C_{\text{s}} \kappa(w_n, \boldsymbol{\pi}_n), \quad n = 0, \dots, N, \quad (11)$$

where the first term is the mission failure cost due to abort and the second term is the expected cost of system failure during the rescue procedure.

Next, we compute the expected cost $V_{\text{c}}(n, \boldsymbol{\pi}_n)$, which is given by

$$V_{\text{c}}(n, \boldsymbol{\pi}_n) = (C_{\text{s}} + C_{\text{m}}) \kappa(\delta, \boldsymbol{\pi}_n) + \mathbb{E}^{(\lambda)} [V^{(\lambda)}(n+1, \boldsymbol{\Pi}_{n+1}) \mid \boldsymbol{\Pi}_n = \boldsymbol{\pi}_n], \quad n = 0, \dots, N-1, \quad (12)$$

with $\boldsymbol{\Pi}_n \triangleq (\Pi_{ni})_{i \in [m_1+m_2]}$. The first term in (12) is the expected cost for system and mission failure before the next decision epoch $(n+1)\delta$. The second term is the cost-to-go at the $(n+1)$ th decision epoch and can be evaluated as

$$\mathbb{E}^{(\lambda)} [V^{(\lambda)}(n+1, \boldsymbol{\Pi}_{n+1}) \mid \boldsymbol{\Pi}_n = \boldsymbol{\pi}_n] = \sum_{k=1}^K P^{(\lambda)}(Y_{n+1} = k \mid \boldsymbol{\Pi}_n = \boldsymbol{\pi}_n) V^{(\lambda)}(n+1, \boldsymbol{\pi}_{n+1}(\boldsymbol{\pi}_n, k)),$$

where $\boldsymbol{\pi}_{n+1}(\boldsymbol{\pi}_n, k)$ denotes the belief state at time $(n+1)\delta$ if the belief state at time $n\delta$ is $\boldsymbol{\pi}_n \in \mathcal{S}$ and the observed signal at time $(n+1)\delta$ is $Y_{n+1} = k \in [K]$. By Bayes' theorem, $\boldsymbol{\pi}_{n+1}(\boldsymbol{\pi}_n, k)$ is given by

$$\boldsymbol{\pi}'_{n+1}(\boldsymbol{\pi}_n, k) = \frac{\boldsymbol{\pi}'_n \tilde{\mathbf{P}}(\delta) \text{diag}(\tilde{\mathbf{d}}_k)}{\boldsymbol{\pi}'_n \tilde{\mathbf{P}}(\delta) \tilde{\mathbf{d}}_k}, \quad (13)$$

where $\tilde{\mathbf{P}}(\delta)$ is the square submatrix of $\mathbf{P}(\delta)$ containing the first $m_1 + m_2$ rows and columns of $\mathbf{P}(\delta)$, $\tilde{\mathbf{d}}_k \triangleq [d_{1k} \mathbf{1}'_{m_1}, d_{2k} \mathbf{1}'_{m_2}]'$, and $\mathbf{1}_r$ is the r -dimensional column vector of ones. Moreover, we have $P^{(\lambda)}(Y_{n+1} = k \mid \boldsymbol{\Pi}_n = \boldsymbol{\pi}_n) = \sum_{i=1}^{m_1+m_2} \sum_{j=1}^{m_1+m_2} \pi_{ni} p_{ij}(\delta) \tilde{d}_{jk}$.

Finally, the terminal cost of the Bellman equation is given by

$$V^{(\lambda)}(N, \boldsymbol{\pi}_N) \triangleq V_{\text{c}}(N, \boldsymbol{\pi}_N) = (C_{\text{s}} + C_{\text{m}}) \kappa(w_N, \boldsymbol{\pi}_N), \quad (14)$$

which is the expected loss for stopping the system (e.g., let the UAV fly back to the base) immediately after it completes the mission at time H .

Due to our CTMC construction, the system starts from state i with $P^{(\lambda)}$ -probability $\pi_{0i}^{(\lambda)}$. The belief state at time 0 is $\boldsymbol{\pi}_0^{(\lambda)} = (\pi_{0i}^{(\lambda)})_{i \in [m_1+m_2]}$. Based on the above finite-horizon POMDP framework, Problem (7) is equivalent to finding the optimal mission abort policy that minimizes

$V^{(\lambda)}(0, \pi_0^{(\lambda)})$, where the policy at time $n\delta$ maps any belief state $\pi_n \in \mathcal{S}$ to an action, i.e., to abort or continue the mission. Since π_n encapsulates all historical information from $Y_{1:n}$ (Bertsekas 2012, Wang 2022), basing abort on π_n is more reliable than on a single signal Y_n . When the system is healthy, an unusual Y_n signal cannot significantly change π_n . On the other hand, successive alarms would change the belief state towards \mathcal{X}_2 and trigger mission abort. Our structural results in the next section formalize the above reasoning.

5. Structural Properties

For notational simplicity, we drop the superscript in $V^{(\lambda)}(n, \pi)$ and write it as $V(n, \pi)$ hereafter. Different from most existing literature on POMDPs that assumes all the state are unobservable (e.g., Smallwood and Sondik 1973), the POMDP in Section 4 is based on a CTMC with both unobservable ($X^{(\lambda)}(t) \in \mathcal{X}_1 \cup \mathcal{X}_2$) and observable ($X^{(\lambda)}(t) = m_1 + m_2 + 1$) states. Nevertheless, we can still show that the value functions of our POMDP exhibit the same piecewise linearity and concavity as those in POMDPs where all states are unobservable.

LEMMA 2. *The value function $V(n, \pi)$ is piecewise linear and concave in π for all $n = 0, \dots, N$. Moreover, both $V_{\text{ab}}(n, \pi)$ and $V_c(n, \pi)$ are concave in π for all $n = 0, \dots, N - 1$.*

To fully characterize the optimal abort policy, we need structural properties in addition to the convexity in Lemma 2. We first study the optimal abort policy when Assumption 1 holds. In this case, we derive an upper bound of $V_c(n, \pi_n)$ and compare it with $V_{\text{ab}}(n, \pi_n)$ to obtain a sufficient condition under which to continue is the optimal action. Let

$$\bar{V}_c(n, \pi_n) \triangleq (C_s + C_m)\kappa((N - n)\delta + w_N, \pi_n), \quad n = 0, \dots, N, \quad (15)$$

be the cost-to-go of continuing the mission until the end of the mission, while $V_c(n, \pi_n)$ is the optimal cost-to-go if we continue the mission at the current decision epoch but use the optimal actions in the sequel. The cost-to-go of the latter case is obviously lower.

We want to compare the functions $\bar{V}_c(n, \pi)$ and $V_{\text{ab}}(n, \pi)$. For any two vectors $\pi^{(1)}, \pi^{(2)} \in \mathcal{S}$, let $\pi_j^{(i)}$ be the j th entry of $\pi^{(i)}$, $i = 1, 2$. Then $\pi^{(1)}$ is greater than $\pi^{(2)}$ with respect to the monotone likelihood ratio (MLR) ordering, denoted by $\pi^{(1)} \succeq_{\text{LR}} \pi^{(2)}$, if $\pi_i^{(1)}/\pi_j^{(1)} \geq \pi_i^{(2)}/\pi_j^{(2)}$ for all $i > j$ (Shaked and Shanthikumar 2007). A function $f : \mathcal{S} \mapsto \mathbb{R}$ is MLR nondecreasing (resp. nonincreasing) in $\pi \in \mathcal{S}$ if $f(\pi^{(1)}) \geq f(\pi^{(2)})$ (resp. $f(\pi^{(1)}) \leq f(\pi^{(2)})$) for any $\pi^{(1)} \succeq_{\text{LR}} \pi^{(2)}$. We then show the monotonicity of $V_{\text{ab}}(n, \pi)$ and the upper bound $\bar{V}_c(n, \pi)$.

LEMMA 3. *Suppose that Assumptions 1 and 3 hold and $\lambda > \bar{\lambda}$ for the $\bar{\lambda}$ in Lemma 1. We have $p_{i, m_1 + m_2 + 1}(t)$ is nondecreasing in $i \in [m_1 + m_2 + 1]$ for any $t > 0$. Moreover, the cost-to-go $V_{\text{ab}}(n, \pi)$ for the abort decision is MLR nondecreasing in $\pi \in \mathcal{S}$ and nondecreasing in n , and $\bar{V}_c(n, \pi)$ is MLR nondecreasing in $\pi \in \mathcal{S}$ and nonincreasing in n .*

Based on Lemma 3, we can derive the following results.

THEOREM 2. *Suppose that Assumptions 1 and 3 hold and $\lambda > \bar{\lambda}$, and consider the surrogate problem (7). The optimal actions satisfy $a_{\lambda,n}^*(y_{1:n}) = 0$ for all $y_{1:n} \in [K]^n$ and $n = 0, \dots, N-1$ if*

$$\frac{C_m}{C_s} \geq \exp[\lambda(H + w_N)] - 1. \quad (16)$$

Intuitively, Theorem 2 indicates that aborting a mission is never optimal during the planning horizon $[0, T]$ if the mission failure cost C_m is significantly larger than the system failure cost C_s . In this case, the priority of completing a mission is much higher than avoiding a system failure. On the other hand, we derive the following result when (16) is violated.

THEOREM 3. *Suppose that Assumptions 1 and 3 hold and $\lambda > \bar{\lambda}$ for the $\bar{\lambda}$ in Lemma 1. If the condition in (16) does not hold, let*

$$\hat{n} \triangleq \min \left\{ n = 0, \dots, N : \max_{\pi \in \mathcal{S}} (\bar{V}_c(n, \pi) - V_{ab}(n, \pi)) \leq 0 \right\}. \quad (17)$$

If $\hat{n} < N$, then the optimal actions satisfy $a_{\lambda,n}^(y_{1:n}) = 0$ for any $y_{1:n} \in [K]^n$ and $n = \hat{n}, \dots, N-1$. Moreover, the value function satisfies $V(n, \pi) = \bar{V}_c(n, \pi)$ for $n = \hat{n}, \dots, N-1$.*

Theorem 3 suggests that continuing the mission is the optimal action after a time threshold $\hat{n}\delta$, intuitively because the mission is nearly finished after this time. Yang et al. (2020) show a similar result when the state $X(t)$ is observable, under which the abort decision is straightforward. In comparison, the unobservable $X(t)$ makes it difficult to characterize the optimal abort policy for $n = 0, \dots, \hat{n} - 1$. To help with the analysis, we provide the following structural properties of the value function $V(n, \pi)$ in (9) and the belief state vector $\pi_{n+1}(\pi, k)$ in (13).

LEMMA 4. *Under Assumptions 1 and 2, the vector $\pi_{n+1}(\pi, k)$ satisfies the following properties for all $n = 0, \dots, N-1$ if $\lambda > \bar{\lambda}$.*

- *For any $\pi^{(1)}, \pi^{(2)} \in \mathcal{S}$ such that $\pi^{(1)} \succeq_{LR} \pi^{(2)}$, we have $\pi_{n+1}(\pi^{(1)}, k) \succeq_{LR} \pi_{n+1}(\pi^{(2)}, k)$ for all $k \in [K]$.*
- *For any $k_1, k_2 \in [K]$ such that $k_1 \geq k_2$, we have $\pi_{n+1}(\pi, k_1) \succeq_{LR} \pi_{n+1}(\pi, k_2)$ for all $\pi \in \mathcal{S}$.*

LEMMA 5. *Under Assumptions 1 and 2, the value function $V(n, \pi)$ is MLR nondecreasing in $\pi \in \mathcal{S}$ for any fixed $n = 1, \dots, N$ if $\lambda > \bar{\lambda}$.*

Lemma 4 orders the belief states at the next decision epoch based on the current belief $\pi \in \mathcal{S}$ and observed signal $k \in [K]$. It is established by showing that the matrix $\tilde{\mathbf{P}}(\delta)$ is TP2, c.f. Lemma EC.1 in Appendix A.8. Lemma 5 indicates that the cost-to-go is lower when the system is in a “healthier” state (in the sense of the MLR ordering). Let \mathbf{e}_i denotes the unit vector with 1 in the i th component. We need an additional structural property to fully characterize the optimal abort policy.

LEMMA 6. Assume Assumption 3 holds. If the program $\max\{n = 0, 1, \dots, N - 1 : V_c(n, \mathbf{e}_{m_1+m_2}) > V_{ab}(n, \mathbf{e}_{m_1+m_2})\}$ has an optimal feasible solution denoted as \tilde{n} , then $V_c(n, \mathbf{e}_{m_1+m_2}) > V_{ab}(n, \mathbf{e}_{m_1+m_2})$ for all $n \leq \tilde{n}$.

In the sense of MLR ordering, the smallest and largest vectors in \mathcal{S} are \mathbf{e}_1 and $\mathbf{e}_{m_1+m_2}$, respectively. Lemma 6 then specifies a range of periods where aborting the mission is optimal when the system is in the most “unhealthy” state $\mathbf{e}_{m_1+m_2}$. Theorem 4 ahead shows that the optimal mission abort policies before and after time $\tilde{n}\delta$ exhibit different structures.

The above analysis, together with the two thresholds \hat{n} in Theorem 3 and \tilde{n} in Lemma 6, sets the basis to derive the optimal abort policy. The main challenge in the analysis is the multivariate belief state $\boldsymbol{\pi}_n$ in an $(m_1 + m_2)$ -dimensional probability simplex \mathcal{S} , under which it is difficult to order an arbitrary pair of vectors $\boldsymbol{\pi}^{(1)}, \boldsymbol{\pi}^{(2)} \in \mathcal{S}$. To circumvent this difficulty, we follow Wang and Lee (2015) and transform $\boldsymbol{\pi}$ from a Cartesian coordinate system to a spherical coordinate system with the vertex $\mathbf{e}_{m_1+m_2}$ as the origin. Specifically, a vector $\boldsymbol{\pi} \in \mathcal{S} \setminus \{\mathbf{e}_{m_1+m_2}\}$ can be represented by $(r, \boldsymbol{\Phi}) \triangleq (r(\boldsymbol{\pi}), \boldsymbol{\Phi}(\boldsymbol{\pi}))$ in this spherical coordinate system by the transformation in Table 1. Here, r is the spherical radius and $\boldsymbol{\Phi} \triangleq [\phi_1, \dots, \phi_{m_1+m_2-1}]'$ is the angle vector. The transformations in Table 1 ensure $\phi_j \in [0, \pi/2]$ for all $j \in [m_1 + m_2 - 2]$ and $\phi_{m_1+m_2-1} \in (\pi/2, \pi]$. Under the spherical coordinate system, we can easily order two vectors with the same angle vector $\boldsymbol{\Phi}$ as shown below.

PROPOSITION 2. Consider the original space $\mathcal{S} = \{\boldsymbol{\pi} = (\pi_i)_{i \in [m_1+m_2]} \in \mathbb{R}_+^{m_1+m_2} : \sum_{i=1}^{m_1+m_2} \pi_i = 1\}$ and the corresponding spherical coordinate system using the transformation in Table 1. For any two vectors in \mathcal{S} with spherical coordinates $(r_1, \boldsymbol{\Phi})$ and $(r_2, \boldsymbol{\Phi})$, their Cartesian coordinates $\boldsymbol{\pi}^{(1)} \triangleq \boldsymbol{\pi}^{(1)}(r_1, \boldsymbol{\Phi})$ and $\boldsymbol{\pi}^{(2)} \triangleq \boldsymbol{\pi}^{(2)}(r_2, \boldsymbol{\Phi})$ satisfy $\boldsymbol{\pi}^{(1)} \succeq_{\text{LR}} \boldsymbol{\pi}^{(2)}$ if $r_1 < r_2$.

For a fixed angle vector $\boldsymbol{\Phi}$, the radius r can be understood as the distance of the belief state $(r, \boldsymbol{\Phi})$ to the most “unhealthy” state $\mathbf{e}_{m_1+m_2}$. Proposition 2 then implies that the system failure risk decreases in r . Based on this observation, we show that when the angle vector is fixed, the optimal abort policy is defined by a lower and an upper control limit with respect to the radius r .

THEOREM 4. Suppose that Assumptions 1–3 hold and $\lambda > \bar{\lambda}$ for the $\bar{\lambda}$ in Lemma 1. Let $(r_n, \boldsymbol{\Phi}_n)$ be the system belief state at time $n\delta$ under the spherical coordinate system in Table 1. When the condition in (16) does not hold, the optimal mission abort policy has the following structure.

- (i) For $n = 0, \dots, \tilde{n}$, there exists an upper control-limit function $\bar{r}_n(\boldsymbol{\Phi}_n) : [0, \pi/2]^{m_1+m_2-2} \times (\pi/2, \pi] \mapsto \mathbb{R}_+$ such that it is optimal to abort the mission if and only if $r_n < \bar{r}_n(\boldsymbol{\Phi}_n)$.
- (ii) For $n = \tilde{n} + 1, \dots, \hat{n} - 1$, there exist lower and upper functions $\underline{r}_n, \bar{r}_n : [0, \pi/2]^{m_1+m_2-2} \times (\pi/2, \pi] \mapsto \mathbb{R}_+$ such that mission abort is the optimal action if and only if $r_n \in [\underline{r}_n(\boldsymbol{\Phi}_n), \bar{r}_n(\boldsymbol{\Phi}_n)]$, where the interval is allowed to be empty.

Table 1 The spherical transform and inverse transform of the Cartesian belief vector ($\pi \neq e_{m_1+m_2}$).

Cartesian π to spherical $(r, \Phi) \triangleq (r(\pi), \Phi(\pi))$	Spherical (r, Φ) to Cartesian $\pi \triangleq \pi(r, \Phi)$
$r = \sqrt{\sum_{i=1}^{m_1+m_2-1} \pi_i^2 + (\pi_{m_1+m_2} - 1)^2}$	$\pi_2 = r \cos \phi_1$
$\phi_j = \arccos \frac{\pi_{j+1}}{\sqrt{\pi_{j+1}^2 + \dots + (\pi_{m_1+m_2-1})^2 + \pi_1^2}},$ $j \in [m_1 + m_2 - 2]$	$\pi_j = r \cos \phi_{j-1} \prod_{k=1}^{j-2} \sin \phi_k,$ $j = 3, \dots, m_1 + m_2 - 1$
$\phi_{m_1+m_2-1} = \arccos \frac{\pi_{m_1+m_2-1}}{\sqrt{\pi_1^2 + (\pi_{m_1+m_2-1})^2}}$	$\pi_{m_1+m_2} = 1 + r \cos \phi_{m_1+m_2-1} \prod_{k=1}^{m_1+m_2-2} \sin \phi_k$
	$\pi_1 = -r \left(\cos \phi_1 + \sum_{j=2}^{m_1+m_2-1} \cos \phi_j \prod_{k=1}^{j-1} \sin \phi_k \right)$

(iii) The set of states $\{\pi \in \mathcal{S} : V_{\text{ab}}(n, \pi) \leq V_c(n, \pi)\}$ is convex for all $n = 0, \dots, N - 1$.

The above theorem naturally divides the mission into three stages. By Proposition 2, a smaller r_n indicates that the system is more likely in a defective state when Φ_n is fixed. Intuitively, Theorem 4(i) indicates that the mission should be aborted when it is very likely to be defective at the initial stage of the mission. Nevertheless, Theorem 4(ii) presents a somewhat counter-intuitive result: during the middle stage of the mission, mission termination is optimal only if the system is in certain intermediate states. During such stages, it is optimal to continue the mission if the system is healthy. Interestingly, the existence of the lower control limit $\underline{r}_n(\Phi_n)$ implies that continuation is also optimal if the system is close to failure. This lower bound results from the rescue time w_n , which is assumed nondecreasing in n . If the system is very “unhealthy” upon abort at the middle stage, it is still highly likely to fail during the rescue procedure. Consequently, mission abort cannot effectively mitigate the failure risk, and it is worth continuing the mission even though the failure probability is large. Leveraging the piecewise-linear concavity of $V(n, \pi)$ in Lemma 2, the existence of the threshold \tilde{n} in Lemma 6, and the convexity of the set of belief states wherein an abort is optimal in Theorem 4(iii), Section 6 develops an efficient algorithm to solve the POMDP.

The following proposition provides two sufficient conditions under which $\{\tilde{n} + 1, \dots, \hat{n} - 1\}$ is an empty set, rendering the middle stage in Theorem 4(ii) nonexistent. In this case, we need only the upper bound $\bar{r}_n(\Phi_n)$ to characterize the mission abort region for each $n = 0, \dots, \hat{n} - 1$.

PROPOSITION 3. Suppose that Assumptions 1 and 3 hold and $\lambda > \bar{\lambda}$. We have $\tilde{n} \geq \hat{n} - 1$ if either conditions below is met:

(i) The optimal solution to the maximization problem:

$$\max_{i \in [m_1+m_2]} \left(1 + \frac{C_m}{C_s} \right) p_{i, m_1+m_2+1}((N - \hat{n} + 1)\delta + w_N) - p_{i, m_1+m_2+1}(w_{\hat{n}-1}) \quad (18)$$

is $i^* = m_1 + m_2$.

(ii) The rescue time satisfies $w_n = 0$ for all $n = 0, \dots, N$.

To understand condition (i) in Proposition 3, recall that $p_{i, m_1+m_2+1}((N - \hat{n} + 1)\delta + w_N)$ and $p_{i, m_1+m_2+1}(w_{\hat{n}-1})$ are the system failure probabilities of never terminating since time $(\hat{n} - 1)\delta$ and

terminating at $(\hat{n} - 1)\delta$, respectively. The objective function in (18) can then be understood as the gain of aborting the mission instead of continuing till the end, weighted by the costs C_m and C_s . If the gain attains its maximum when the system is in the most “unhealthy” state $e_{m_1+m_2}$, we only need the upper control-limit function \bar{r}_n in each period to make the abort decision. Moreover, when the rescue time keeps zero during the mission, we also have $\tilde{n} \geq \hat{n} - 1$. This scenario could happen for paper mills, where we can halt the system in a negligible time to prevent imminent failures such as the breaking of bolts (Ranjan et al. 2018). Interestingly, when w_n remains zero throughout the mission, our mission abort problem resembles a CBM problem, which typically assumes negligible maintenance time as discussed in Section 1. A potential violation of condition (ii) in Proposition 3 underscores a distinction between mission abort and CBM problems.

When Assumption 1 does not hold, Theorem 3 may not hold, i.e., we cannot guarantee the existence of a time threshold $\hat{n}\delta$ after which the mission is never aborted. Nevertheless, the structure of the optimal mission abort policy described in Theorem 4 keeps largely the same. We only need to replace \hat{n} in Theorem 4(ii) with N as detailed below.

COROLLARY 1. *Under Assumptions 2 and 3, the optimal mission abort policy for $n = 0, \dots, \tilde{n}$ has the same structure as that in Theorem 4(i), and the optimal policy for $n = \tilde{n} + 1, \dots, N - 1$ has the same structure as that in Theorem 4(ii). Moreover, Theorem 4(iii) still holds.*

6. Computational Solution Approach

The belief state space is an $(m_1 + m_2)$ -dimensional probability simplex \mathcal{S} . Due to the curse of dimensionality, it is computationally intractable to solve the Bellman equations (9) and (14) to optimality when m_1 or m_2 is large (Bertsekas 2012). Nevertheless, we can significantly reduce the computational burden of our problem by using the structural properties derived in Section 5.

First, Theorem 3 indicates the existence of a time threshold \hat{n} under Assumption 1, such that it is optimal to continue the mission for $n = \hat{n}, \dots, N$ no matter of the observed signal. To find \hat{n} , we need to solve the maximization problem: $\max_{\pi \in \mathcal{S}} \{\bar{V}_c(n, \pi) - V_{ab}(n, \pi)\}$ as shown in (17) for $n = 0, \dots, N$. Since \mathcal{S} is a probability simplex, the above maximization problem is a linear program, and the optimal solution is one of the vertices of \mathcal{S} (Bertsekas 2012), i.e., one of $e_1, \dots, e_{m_1+m_2}$. For fixed n , we only need to enumerate $\pi \in \{e_1, \dots, e_{m_1+m_2}\}$ to check if $\max_{\pi \in \mathcal{S}} \{\bar{V}_c(n, \pi) - V_{ab}(n, \pi)\} \leq 0$, based on which we can know whether $\hat{n} \leq n$ or $\hat{n} > n$. Then a binary search can be adopted to find \hat{n} , as detailed in Algorithm EC.1 in Appendix B. The binary search takes $\mathcal{O}(\log(N))$ steps to find the time threshold \hat{n} , where each step enumerates $\pi \in \{e_1, \dots, e_{m_1+m_2}\}$ to solve the linear program $\max_{\pi \in \mathcal{S}} \{\bar{V}_c(n, \pi) - V_{ab}(n, \pi)\}$.

For $n < \hat{n}$, exactly computing the value function $V(n, \pi)$ is computationally intractable. We approximate $V(n, \pi)$ by using the structural properties derived in Section 5. Specifically, Lemma 2

shows that $\boldsymbol{\pi} \mapsto V(n, \boldsymbol{\pi})$ is piecewise linear and concave for all $n = 0, \dots, N$. This means that for each n , there exists a finite set $\mathcal{A}_n \subseteq \mathbb{R}^{m_1+m_2}$ such that $V(n, \boldsymbol{\pi})$ can be written as

$$V(n, \boldsymbol{\pi}) = \min_{\boldsymbol{\alpha}_n \in \mathcal{A}_n} \boldsymbol{\alpha}'_n \boldsymbol{\pi}, \quad n = 0, \dots, N. \quad (19)$$

Solving the Bellman equations in (9) and (14) amounts to obtaining the finite sets \mathcal{A}_n , $n = 0, \dots, N$. This motivates us to approximate \mathcal{A}_n by a sequence of sets $\{\hat{\mathcal{A}}_n^{(\tau)}, \tau \in \mathbb{N}_+\}$ for $n = 0, \dots, N$, where each $\hat{\mathcal{A}}_n^{(\tau)}$ is a subset of \mathcal{A}_n . With $\hat{\mathcal{A}}_n^{(\tau)}$, we can approximate the value function $V(n, \boldsymbol{\pi})$ as

$$\hat{V}^{(\tau)}(n, \boldsymbol{\pi}) = \min_{\boldsymbol{\alpha}_n \in \hat{\mathcal{A}}_n^{(\tau)}} \boldsymbol{\alpha}'_n \boldsymbol{\pi}, \quad n = 0, \dots, N,$$

where $V(n, \boldsymbol{\pi}) \leq \hat{V}^{(\tau)}(n, \boldsymbol{\pi})$ for all $n = 0, \dots, N$, $\boldsymbol{\pi} \in \mathcal{S}$, and $\tau \in \mathbb{N}_+$ because $\hat{\mathcal{A}}_n^{(\tau)} \subseteq \mathcal{A}_n$. To obtain $\{\hat{\mathcal{A}}_n^{(\tau)}, \tau \in \mathbb{N}_+\}$, we propose a modified PBVI algorithm to iteratively construct $\hat{\mathcal{A}}_n^{(\tau)}$.

The classical PBVI algorithm (Pineau et al. 2003) iterates between a backup step and an expansion step. The backup step uses a finite set of belief states $\{\boldsymbol{\pi}_n^{(1)}, \dots, \boldsymbol{\pi}_n^{(L_\tau)}\}$ to construct $\hat{\mathcal{A}}_n^{(\tau)}$ for $n \in [\hat{n} - 1]$, where L_τ is the size of such a set at the τ th PBVI iteration. The construction of $\hat{\mathcal{A}}_n^{(\tau)}$ is done by approximating the cost-to-go for continuing the mission $V_c(n, \boldsymbol{\pi}_n)$ in (9) as $\hat{V}_c^{(\tau)}(n, \boldsymbol{\pi}_n)$, where $V_c^{(\tau)}(\cdot, \cdot)$ is defined analogously to (12) but with $\hat{V}^{(\tau)}(\cdot, \cdot)$ replacing $V(\cdot, \cdot)$ therein. This approximation enables us to approximately solve the Bellman equation to obtain $\hat{\mathcal{A}}_n^{(\tau)}$ for each $n \in [\hat{n} - 1]$ in a backward manner (c.f. Line 8 of Algorithm 1). Then the expansion step augments $\{\boldsymbol{\pi}_n^{(l)}\}_{l \in [L_\tau]}$ by sampling new elements $\boldsymbol{\pi}_n^{(l)}$, $l = L_\tau + 1, \dots, L_{\tau+1}$, for each $n \in [\hat{n} - 1]$ for constructing $\hat{\mathcal{A}}_n^{(\tau+1)}$ in the next iteration. We initialize the algorithm with a finite set of belief states $\{\boldsymbol{\pi}_n^{(1)}, \dots, \boldsymbol{\pi}_n^{(L_1)}\}$ for each $n \in [\hat{n} - 1]$ by simulation, as detailed in Algorithm 1 ahead. The algorithm terminates if the approximate value functions between two consecutive iterations are close enough or after a predetermined number of iterations.

Generally, the classical PBVI algorithm does not use any structural properties of $V(n, \boldsymbol{\pi})$ in the iteration. We develop a modified PBVI algorithm by using the structural properties of the optimal mission abort policy to further reduce the computational cost. Specifically, Theorem 4 indicates that the region $\{\boldsymbol{\pi} \in \mathcal{S} : V_{\text{ab}}(n, \boldsymbol{\pi}) \leq V_c(n, \boldsymbol{\pi})\}$ with mission abort as the optimal action is convex for all $n = 0, \dots, N - 1$. For a fixed n and a large τ , the above set can be well approximated by the convex hull

$$\text{conv} \left\{ \boldsymbol{\pi}_n^{(l)}, l \in [L_\tau] : V_{\text{ab}}(n, \boldsymbol{\pi}_n^{(l)}) \leq \hat{V}_c^{(\tau)}(n, \boldsymbol{\pi}_n^{(l)}) \right\}. \quad (20)$$

In words, mission abort is very likely to be the optimal action for the belief states in the convex hull in (20). If aborting the mission is optimal for any belief states $\boldsymbol{\pi}$ in period n , then $V(n, \boldsymbol{\pi}) = V_{\text{ab}}(n, \boldsymbol{\pi})$ is linear in $\boldsymbol{\pi}$ as shown in (11), which satisfies $V(n, \boldsymbol{\pi}) = \boldsymbol{\alpha}'_n \boldsymbol{\pi}$ for some $\boldsymbol{\alpha}_n \in \hat{\mathcal{A}}_n^{(\tau)}$. As such, all such belief states share the same coefficient $\boldsymbol{\alpha}_n$. To gain more information in later iterations, a

Algorithm 1 The modified PBVI algorithm to approximately calculate the value function.

Input: Transition rate matrix \mathbf{Q} , state-observation matrix \mathbf{D} , costs C_m, C_s , inspection interval δ , number of periods N , the set of α -vectors $(\mathcal{A}_n)_{n=\hat{n}}^N$, numbers of iterations Z_1, Z_2 , initial number of states L_1 , error ε , number of samples to simulate W

Output: The approximate value function

- 1: Init $\hat{\mathcal{A}}_n^{(\tau)} \leftarrow \mathcal{A}_n$ for all $n = \hat{n}, \dots, N$ and $\tau \geq 0$, and init $\hat{\mathcal{A}}_n^{(0)} \leftarrow \emptyset$ for all $n \in [\hat{n} - 1]$
 - 2: Running L_1 sets of simulations from state π_0 to the end of the decision horizon
 - 3: Compute the sets of belief states $\{\pi_n^{(l)}\}_{l \in L_1}$, $n \in [\hat{n} - 1]$, by Equation (13) based on the L_1 trajectories of simulated signals
 - 4: **for** $\tau \leftarrow 1, \dots, Z_1$ **do**
 - 5: **for** $n \leftarrow \hat{n} - 1, \dots, 1$ **do**
 - 6: **for** $l \leftarrow 1, \dots, L_\tau$ **do**
 - 7: Compute $V_{ab}(n, \pi_n^{(l)})$ by (11) and $\hat{V}_c^{(\tau)}(n, \pi_n^{(l)})$ as
$$\kappa(\pi_n^{(l)}, \delta)(C_s + C_m) + \sum_{k=1}^K \min_{\alpha_{n+1} \in \hat{\mathcal{A}}_{n+1}^{(\tau)}} \sum_{i=1}^{m_1+m_2} \sum_{j=1}^{m_1+m_2} \alpha_{n+1,j} \pi_{ni}^{(l)} p_{ij}(\delta) \tilde{d}_{jk}$$
 - 8: Set $\hat{\mathcal{A}}_n^{(\tau)}$ be the collection of coefficients corresponding to the belief vector $\pi_n^{(l)}$ in the function $\min\{V_{ab}(n, \pi_n^{(l)}), \hat{V}_c^{(\tau)}(n, \pi_n^{(l)})\}$
 - 9: Sample W underlying states from $\pi_n^{(l)}$ and simulate a signal for each sampled state to compute the belief state at time $(n+1)\delta$
 - 10: **if** $\tau > Z_2$ **then**
 - 11: Discard all belief states at time $(n+1)\delta$ in the convex hull in (20)
 - 12: **end if**
 - 13: Compute the minimum Euclidean distance between each of the above (kept) belief states and each state in $\{\pi_{n+1}^{(l)}\}_{l \in [L_\tau]}$
 - 14: Set $\pi_{n+1}^{(L_\tau+1)}$ to be the belief state that has the largest distance
 - 15: **end for**
 - 16: **end for**
 - 17: **if** $\max_{\pi \in \mathcal{S}, n=0, \dots, N} |\hat{V}_n^{(\tau)}(\pi) - \hat{V}_n^{(\tau-1)}(\pi)| < \varepsilon$ **then**
 - 18: Break the for-loop
 - 19: **end if**
 - 20: **end for**
-

sampled state inside (20) is discarded during the expansion step when τ is large. Moreover, in view of Lemma 6, if $V_{ab}(\tilde{n}, \mathbf{e}_{m_1+m_2}) \leq \hat{V}_c^{(\tau)}(\tilde{n}, \mathbf{e}_{m_1+m_2})$ for a large τ , it is likely that $V_{ab}(n, \mathbf{e}_{m_1+m_2}) \leq \hat{V}_c^{(\tau)}(n, \mathbf{e}_{m_1+m_2})$ for all $n \leq \tilde{n}$. When we find such \tilde{n} during the expansion step, we can include the state $\mathbf{e}_{m_1+m_2}$ to (20) and update the convex hull for all $n \leq \tilde{n}$. Other steps remain the same as the classical PBVI algorithm. This modified PBVI algorithm is summarized in Algorithm 1, and details on the backup and expansion steps are elaborated in Appendix B. With the approximate value function obtained by the PBVI algorithm, the optimal action at each belief state can be readily obtained. Numerical experiments in Section 9 show that the modified PBVI algorithm achieves a significant reduction in computational time compared with the classical PBVI algorithm.

Recall that the value function $V(n, \pi)$ is MLR nondecreasing in π by Lemma 4 when Assumption 1 holds. According to Tian et al. (2022), approximate dynamic programming (ADP) algo-

rithms using a finite set of sampled states, such as the PBVI algorithms, typically yield accurate approximations of $V(n, \pi)$ for π not visited by the algorithm ($\pi \notin \{\pi_n^{(i)} : i = 1, 2, \dots\}$), provided that the approximation maintains monotonicity of the value function. The following proposition illustrates that our PBVI algorithm can preserve such structural properties of $V(n, \pi)$.

PROPOSITION 4. *Suppose that Assumptions 1–3 hold and $\lambda > \bar{\lambda}$ for the $\bar{\lambda}$ in Lemma 1. The approximate value function $\hat{V}^{(\tau)}(n, \pi)$ is piecewise linear, concave, and MLR nondecreasing in $\pi \in \mathcal{S}$ for all $n = 0, \dots, N$ and $\tau \in \mathbb{N}_+$.*

In view of the preservation of the structural properties of $V(n, \pi)$, our PBVI algorithm is more appealing than other ADP methods, e.g., using a neural network to approximate $V(n, \pi)$, that generally do not have the preservation property in Proposition 4. Moreover, the PBVI algorithm is an offline method as it optimizes a policy before realization of observed signals. After optimization, the optimal policy can be implemented online to yield the optimal action in real time. In contrast, online planning methods such as Monte Carlo tree search (Silver and Veness 2010) may not be suitable for real-time abort decision-making when the inter-sampling interval δ is very small.

7. Insights into Specialized Models

This section derives some additional structural results for two special cases of our model. The first case in Section 7.1 investigates the decision problem when all T_{12} , T_{13} , and T_{23} are exponential. The second case in Section 7.2 assumes an exponential distribution for T_{23} while T_{12} remains non-exponential. In both cases, the POMDP can be exactly solved after discretizing the state space.

7.1. Markovian Failure Process

We first study the special case where T_{12} , T_{13} , and T_{23} are all exponential, under which the underlying system dynamics is a CTMC. Its optimal mission abort decision making is a POMDP, and our POMDP analysis above applies to this problem directly with $m_1 = m_2 = 1$. This simple setting lends itself to a straightforward structure for the optimal policy. Let $\Pi_n = \mathbb{P}(X_n = 2 \mid Y_{1:n})$ be the conditional probability that the system is at the defective state given $Y_{1:n}$. After observing the values of $Y_{1:n}$, the system state at time $n\delta$ is realized as a scalar $\pi_n \in [0, 1]$. The probability of the system being at the healthy state is then $1 - \pi_n$.

The general result in Theorem 3 applies to this simple setting. That is, there exists \hat{n} such that, for all $n \geq \hat{n}$, continuation is optimal regardless of the system state Π_n . Similarly, the threshold \tilde{n} in Lemma 6 becomes $\tilde{n} = \max\{n = 0, \dots, N : V_{ab}(n, 1) < V_c(n, 1)\}$. The univariate belief state Π_n obviates the need for introducing the spherical coordinate system to depict the optimal policy when $n < \hat{n}$. The optimal policy can be shown to be a control-limit policy with respect to π_n .

COROLLARY 2. Suppose $X(t)$ is a CTMC. Under Assumptions 1–3, the optimal mission abort policy has the following structure.

- For $n = 0, \dots, \tilde{n}$, there exists a threshold $\underline{\pi}_n$ such that it is optimal to abort the mission at time $n\delta$ if and only if the system belief state π_n satisfies $\pi_n > \underline{\pi}_n$ and to continue the mission otherwise.
- For $n = \tilde{n} + 1, \dots, \hat{n} - 1$, there exists an interval $[\underline{\pi}_n, \bar{\pi}_n] \subseteq [0, 1]$ such that it is optimal to abort the mission if and only if $\underline{\pi}_n \leq \pi_n \leq \bar{\pi}_n$, where the interval is allowed to be empty.
- For $n \geq \hat{n}$, the optimal policy is to continue the mission.

Compared with optimal CBM for a system with three states (e.g., Kim et al. 2010), the fundamental difference comes from the middle stage where continuation of the mission is optimal upon confirmation of the defective state and the last stage where abort is never optimal. From Corollary 2, it is interesting to see that a POMDP based on a three-state CTMC makes mission abort decisions only using the defective probability π_n . For a non-Markovian system, the sojourn time on the defective state is informative for decision-making. Theorem 4 implicitly considers this information using a spherical coordinate system. As shown by our numerical experiments in Section 9, loss of such critical information can lead to a significant cost increase if we approximate a semi-Markov system by a simple three-state CTMC.

Since the belief state space can be represented by a one-dimensional interval $[0, 1]$, it is unnecessary to use the PBVI algorithm in Section 6 to approximately solve the POMDP. Instead, we can discretize the interval $[0, 1]$ and use standard backward induction to exactly solve the stochastic dynamic program (see Algorithm EC.2 in Appendix B).

7.2. One-Phase Transition

Next, consider the surrogate POMDP with $m_1 > 1$ and $m_2 = 1$. Motivated by Wang and Lee (2015), we can derive a dimension reduction property in this case that facilitates solving the POMDP. Specifically, let

$$\varphi_j(\Phi) \triangleq (p_{2j}(\delta) - p_{1j}(\delta)) \cos \phi_1 + \sum_{i=3}^{m_1+1} (p_{ij}(\delta) - p_{1j}(\delta)) \cos \phi_{i-1} \prod_{k=1}^{i-2} \sin \phi_k$$

for $j \in [m_1 + 1]$. We arrive at the following proposition.

PROPOSITION 5. Consider $m_1 > 1$ and $m_2 = 1$. Suppose that given Y_1, \dots, Y_{n-1} , we have computed the system belief state (r_{n-1}, Φ_{n-1}) under the spherical coordinate system defined in Table 1. Then after observing Y_n at time $n\delta$, $\Phi_n = (\phi_{ni})_{i \in [m_1]}$ can be updated as

$$\begin{aligned} \phi_{ni} &= \arccos \frac{\varphi_{i+1}(\Phi_{n-1})}{\sqrt{\varphi_1^2(\Phi_{n-1}) + \sum_{j=i+1}^{m_1} \varphi_j^2(\Phi_{n-1}) + (\sum_{j=1}^{m_1} \varphi_j(\Phi_{n-1}))^2}}, \quad i \in [m_1 - 1]; \\ \phi_{n,m_1} &= \arccos \frac{-\sum_{i=1}^{m_1} \varphi_i(\Phi_{n-1})}{\sqrt{\varphi_1^2(\Phi_{n-1}) + (\sum_{j=1}^{m_1} \varphi_j(\Phi_{n-1}))^2}}, \end{aligned} \quad (21)$$

while r_n can be updated as a function of r_{n-1} and the observed Y_n . This function is complicated and is provided in Appendix A.17.

Proposition 5 reveals that the angle vector Φ_n at each decision epoch is *irrelevant* to the signals Y_1, \dots, Y_n and can be deterministically computed by (21) at time 0. In contrast, the radius r_n depends on the realizations of Y_1, \dots, Y_n . This means that the signals affect the cost-to-go only through the scalar r_n . Instead of using PBVI, we can discretize the domain of r_n and then use standard backward induction to exactly solve the Bellman equation. Routine algebra shows that to meet the constraint $\pi(r_n, \Phi_n) \in \mathcal{S}$, r_n should be within $[0, -(\cos \phi_{n,m_1} \prod_{k=1}^{m_1-1} \sin \phi_{nk})^{-1}]$. With this range for r_n , the detailed optimization procedure is similar to that in Section 7.1 and is relegated to Appendix B.

8. Extension to Multiple Tasks

In applications, a thorough system inspection may only be scheduled once the system has completed several scheduled tasks. Examples include a delivery drone tasked with multiple deliveries in a single day, and a UAV performing day-long line inspections in a power grid where the UAV may need to return for charging between flights. Another scenario is that a big task can be divided into a few phases and each phase can be treated as a mission. For example, a mission of tracking, telemetry, and command systems typically consists of two phases: data transformation and telecommand (Yu et al. 2020). As such, there is no assurance that the system is in a perfectly healthy state at the start of a mission.

Consider a system that completes missions $1, \dots, L$ in sequence, and each mission needs N_l periods to complete. A system failure incurs a cost C_s . To prevent failures, we can abort the mission any time during the operation, upon which the current and subsequent missions fail, and failure to complete mission $l \in [L]$ incurs a loss $C_m^{(l)}$. Upon completion of all L missions or rescue procedure, a comprehensive inspection is carried out to ensure that the system is at the healthy state. If the inspection reveals system defects, a repair cost C_r is incurred. After inspection, the system starts the next set of L missions with a healthy state. In this context, it would be advantageous to maximize the abort decision for all L missions jointly. Then the total number of decision periods is $N \triangleq \sum_{l=1}^L N_l$.

In practice, L is usually a small number, and thus the assumptions on the sojourn times of the underlying semi-Markov system dynamics are still valid. As such, we adhere to the model setting in Section 3 for the system failure process, observed signals, and rescue procedures. However, Assumption 3 may not hold. For example, consider a UAV that consecutively executes $L = 3$ tasks by departing from a depot, visiting three sites in sequence, and returning to the depot. If site 3 is closer to the depot than site 2, the rescue time is not necessarily monotone nondecreasing in

$n \in [N]$. Nevertheless, the solution methodology is largely the same as before. We first use two Erlang mixtures to approximate the non-exponential sojourn times T_{12} and T_{23} in the original semi-Markov process and formulate a CTMC. The surrogate POMDP is then constructed by closely following that outlined in Section 4 with two minor changes. First, the terminal cost needs to consider the possible repair cost after thorough inspection. Second, the mission failure cost now depends on the number of unfinished missions. Accordingly, the Bellman recursion in Eqs. (11)–(14) is changed to

$$V_{ab}(n, \boldsymbol{\pi}_n) = \sum_{l=1}^L C_m^{(l)} \mathbb{1} \left\{ n < \sum_{l'=1}^l N_{l'} \right\} + C_s \kappa(w_n, \boldsymbol{\pi}_n) + C_r \boldsymbol{\pi}'_n \tilde{\mathbf{P}}(w_n) \cdot (\mathbf{0}'_{m_1}, \mathbf{1}'_{m_2})'; \quad (22)$$

$$V_c(n, \boldsymbol{\pi}_n) = \left(C_s + \sum_{l=1}^L C_m^{(l)} \mathbb{1} \left\{ n < \sum_{l'=1}^l N_{l'} \right\} \right) \kappa(\delta, \boldsymbol{\pi}_n) + \mathbb{E}^{(\lambda)} [V^{(\lambda)}(n+1, \boldsymbol{\Pi}_{n+1}) | \boldsymbol{\Pi}_n = \boldsymbol{\pi}_n] \quad (23)$$

for $n = 0, \dots, N-1$, where $\mathbf{0}_r$ is the r -dimensional column vector of zeros. The terminal cost is

$$V^{(\lambda)}(N, \boldsymbol{\pi}_N) \triangleq V_c(N, \boldsymbol{\pi}_N) = (C_s + C_m^{(L)}) \kappa(w_N, \boldsymbol{\pi}_N) + C_r \boldsymbol{\pi}'_N \tilde{\mathbf{P}}(w_N) \cdot (\mathbf{0}'_{m_1}, \mathbf{1}'_{m_2})'. \quad (24)$$

The last terms on the right hand side of (22) and (24) represent the expected repair cost when system defects are revealed during the thorough inspection. Because this cost is linear in the belief state, it is readily shown that $\boldsymbol{\pi} \mapsto V^{(\lambda)}(n, \boldsymbol{\pi})$ remains concave for all $n \in [N]$. Then the optimal mission abort policy in the multi-task setting shares a similar structure to those in Theorem 4. Using Table 1 to transform a belief vector $\boldsymbol{\pi}_n$ at period n to $(r_n, \boldsymbol{\Phi}_n)$ in the spherical coordinate system, the optimal mission abort policy can be characterized as below.

THEOREM 5. *The optimal mission abort policy in the multi-task setting has the following structure.*

(i) *The optimal action is always to continue the mission if*

$$C_m^{(L)} \frac{\exp(-\lambda(T + w_N))}{1 - \exp(-\lambda(T + w_N))} \geq C_s + \sum_{l=1}^{L-1} C_m^{(l)} \frac{1 - \exp(-\lambda \delta \sum_{l'=1}^l N_{l'})}{1 - \exp(-\lambda(T + w_N))}. \quad (25)$$

Otherwise, the set of states $\{\boldsymbol{\pi} \in \mathcal{S} : V_{ab}(n, \boldsymbol{\pi}) \leq V_c(n, \boldsymbol{\pi})\}$ is convex for all $n = 0, \dots, N-1$. Moreover, aborting the missions is never optimal after completion of mission $l \in [L-1]$ if (EC.4) in Appendix A.18 is satisfied.

(ii) *If $V_{ab}(n, \mathbf{e}_{m_1+m_2}) \leq V_c(n, \mathbf{e}_{m_1+m_2})$, then there exists a function $\bar{r}_n(\boldsymbol{\Phi}_n) : [0, \pi/2]^{m_1+m_2-2} \times (\pi/2, \pi] \mapsto \mathbb{R}_+$ such that it is optimal to abort the mission if and only if $r_n < \bar{r}_n(\boldsymbol{\Phi}_n)$.*

(iii) *If $V_{ab}(n, \mathbf{e}_{m_1+m_2}) > V_c(n, \mathbf{e}_{m_1+m_2})$, then there exist two functions $\underline{r}_n, \bar{r}_n : [0, \pi/2]^{m_1+m_2-2} \times (\pi/2, \pi] \mapsto \mathbb{R}_+$ such that the mission abort is optimal if and only if $r_n \in [\underline{r}_n(\boldsymbol{\Phi}_n), \bar{r}_n(\boldsymbol{\Phi}_n)]$, where the interval is allowed to be empty.*

Characterizing the optimal mission abort policy needs to compare $V_{ab}(n, \mathbf{e}_{m_1+m_2})$ and $V_c(n, \mathbf{e}_{m_1+m_2})$ as stated in Theorem 5(ii) and (iii). Computing these functions for comparison is easy and does not require solving the Bellman equations in (22)–(24). This is because the system can only transition to a worse state. As such, we can obtain values of $V_{ab}(n, \mathbf{e}_{m_1+m_2})$ and $V_c(n, \mathbf{e}_{m_1+m_2})$ in a backward induction way by only using the values of $\{V(i, \mathbf{e}_{m_1+m_2})\}_{i=n+1}^N$.

9. Case Study

We consider a fixed-wing UAV that executes an inspection task on high-voltage power grids located at a mountainous area. This UAV application is widely adopted for line inspection of power and electronic industry in recent years, due to its advantage of low cost and high effectiveness. Our application aligns with the growing utilization of Internet-of-Things technologies to enhance operational safety (Olsen and Tomlin 2020, Li and Tomlin 2022). The UAV line inspection mission consists of three phases, i.e., (i) the UAV leaves its base to the predetermined inspection task location; (ii) the UAV executes the inspection task; (iii) the UAV flies back to the base. When the mission is aborted, the UAV halts the inspection task and directly heads back to the base. Hence, we only need to focus on the optimal mission abort policy for the first two phases of the mission. We conduct comprehensive simulations to assess the performance of our method.

9.1. Parameter Setting

In the simulation, the distance between the UAV base and power grid is 8 km. During the mission, the UAV departs from the base and flies to the power grid at a constant speed 19.2 km/h (Liu and Sun 2022). Upon arrival at the power grid, it executes the inspection task for 135 min. Hence, the total duration for the first two phases of the mission is $H = 60 \times 8/19.2 + 135 = 160$ min, which is typical for a power-grid inspection task (Qiu and Cui 2019). We set the inspection interval as $\delta = 1$ min, so the number of decision epochs is $N = H/\delta = 160$. Based on this setting, we obtain the time duration (in min) of a rescue procedure after aborting a mission at the n th decision epoch:

$$w_n = \begin{cases} n, & n \leq 25, \\ 25, & 25 < n \leq 160. \end{cases}$$

The system failure cost is set as $C_s = 2,000$ as with Yang et al. (2020). The mission failure cost is more subjective. We set $C_m = 2,000$ and conduct sensitivity analysis on C_m in Appendix C.2.

In practice, the UAV failure during a mission is a rare event because the times T_{12} and T_{13} from healthy to defective state and to failure state are expected to be long. If we directly use their distributions in simulations, the majority of missions would have no failure record, making it difficult to compare our method with benchmarks. Hence, we modify the distributions of T_{12}

Table 2 Five key physical states of a UAV under condition monitoring (Wang et al. 2019).

Description	Units
X-axis velocity	m/s
Y-axis velocity	m/s
Z-axis velocity	m/s
Pitch rate	degree/s
Yaw rate	degree/s

and T_{13} to render more failures during simulations. Following Khaleghei and Kim (2021), we use an Erlang distribution for T_{12} . Since an Erlang distribution corresponds to a CTMC, we do not need an Erlang mixture distribution for approximation. This leads to a CTMC with a similar structure to our constructed CTMC in Section 4.1, and the structural results hold for this CTMC; see Appendix C.1 for details. Next, we set $\zeta = 10^{-3}$ for T_{13} such that $\mathbb{E}[T_{13}]/\mathbb{E}[T_{12}]$ is around three to four according to Panagiotidou and Tagaras (2010). We consider two different distributions of T_{23} . In the first setting, we use a Weibull distribution for T_{23} with the following PDF:

$$f(t) = \frac{2.3}{108.8} \left(\frac{t}{108.8} \right)^{1.3} \exp(-(t/108.8)^{2.3}), \quad t \geq 0. \quad (26)$$

In the second setting, we assume F follows a mixture distribution, which is commonly used in reliability (Krivtsov 2007, Yao et al. 2017) and is given by

$$f(t) = \frac{1.3}{180.8} \left(\frac{t}{180.8} \right)^{1.6} \exp\left(-\left(\frac{t}{180.8}\right)^{2.6}\right) + \frac{1.15}{36.3} \left(\frac{t}{36.3} \right)^{1.3} \exp\left(-\left(\frac{t}{36.3}\right)^{2.3}\right). \quad (27)$$

for $t \geq 0$. Last, we determine the state-observation matrix \mathbf{D} . According to Wang et al. (2019), the UAV flight control system typically monitors five physical states as shown in Table 2. During flight, sensors on the UAV measure the in-situ values of these physical states, and an alarm system computes the differences between the measured and desired values. The differences for all the five physical states should be close to zero when the UAV is at the healthy state and deviate from zero at the defective state. We obtain a dataset about the differences of these physical states when the UAV is in a healthy and defective state, respectively. The differences of the five physical states lead to a five-dimensional signal. To use our proposed model, we fit a logistic regression model by treating the five-dimensional signal as predictors and the system state (healthy or defective) as label. A green (red) light condition-monitoring signal is observed when the predicted probability of being defective is smaller (larger) than 0.5, as commonly adopted in practice. The state-observation matrix \mathbf{D} is then estimated as the empirical probability of observing green and red light signals under each latent state, given by

$$\mathbf{D} = \begin{pmatrix} 0.737 & 0.263 \\ 0.101 & 0.899 \end{pmatrix}.$$

9.2. Performance of the Model

We simulate the system dynamics $\{X(t), t \geq 0\}$ and $Y_{1:n}$ based on the parameter setting in Section 9.1 and then use our method for abort decision-making. To approximate the distribution $F(\cdot)$ by an Erlang mixture in (2), we first fix m_2 and use the commonly used moment-matching method to determine λ such that the resulting Erlang mixture distribution has the same mean as the original distributions. We enumerate m_2 and compute the approximation error defined by $\max_{0 \leq t \leq H+w_N} |F(t) - F^{(\lambda)}(t)|$. By the elbow method that seeks the point where the rate of decrease sharply changes, $m_2 = 20$ with corresponding $\lambda = 0.134$ is chosen when T_{23} is Weibull in (26), and $m_2 = 50$ is chosen when T_{23} follows the mixture distribution in (27) with corresponding $\lambda = 0.209$. Figure 2 displays a comparison between the CDFs of T_{23} and $T_{23}^{(\lambda)}$ in the two settings, where we see $F^{(\lambda)}(\cdot)$ well approximates $F(\cdot)$. For the Weibull distribution, we verify that the constructed CTMC satisfies the monotone property in Lemma 1, supporting our choice of m_2 . Appendix C.2 further examines the sensitivity of the optimal policy with respect to (m_2, λ) and demonstrates how to select (m_2, λ) . The abort policy is optimized offline by Algorithm 1, with hyper-parameters $Z_1 = 10^5$, $Z_2 = 5 \times 10^5$, $L_1 = 10^4$, $\varepsilon = 10^{-3}$, and $W = 5,000$.

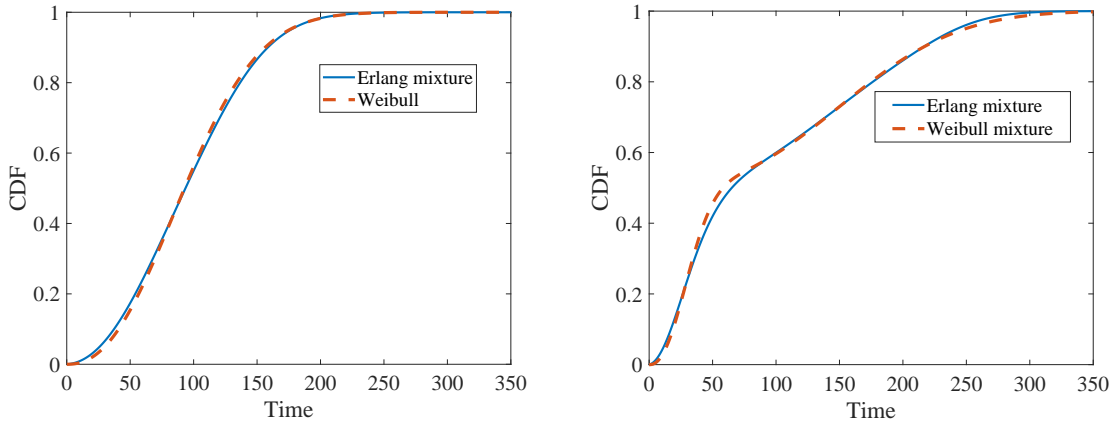


Figure 2 Approximating the distribution of T_{23} by the Erlang mixture distribution $F^{(\lambda)}(\cdot)$: The left panel uses $m_2 = 20$ and $\lambda = 0.134$ to approximate the Weibull distribution in (26). The right panel uses $m_2 = 50$ and $\lambda = 0.209$ to approximate the mixture distribution in (27).

For comparison, we consider four benchmarks for mission abort decision-making. The first two are rule-based heuristics. The first heuristic (referenced as “ \mathcal{C} -policy”) uses a control-chart scheme that deems the system as defective when receiving \tilde{m} warning signals in \tilde{N} consecutive periods. The mission is aborted once the system is deemed defective. We optimize both \tilde{m} and \tilde{N} by minimizing the expected operational cost. This rule-based heuristic generalizes the method in Yang et al. (2020). The second heuristic (referenced as “ \mathcal{R} -policy”) uses the system RUL to make decisions, and

the mission is aborted when the p th percentile of the predicted RUL is smaller than the remaining time to complete the mission. We optimize $p \in (0, 100)$ for minimizing the expected operational cost. The third benchmark (referenced as “ \mathcal{M} -policy”) uses a three-state CTMC to approximate the failure process. The transition rate matrix of this CTMC is determined such that the transition times between healthy, defective, and failure states have the same mean values as the original semi-Markov failure process. A similar approximation is used in [Iravani and Duenyas \(2002\)](#) for maintenance optimization. Since this approximation uses a three-state CTMC, Corollary 2 implies that the optimal \mathcal{M} -policy has a simple control-limit structure. The fourth benchmark keeps T_{12} as m_1 -phase Erlang distributed but sets $m_2 = 1$ for approximating T_{23} . This benchmark degenerates to \mathcal{M} -policy when we enforce $m_1 = 1$. Our dimension reduction result in Proposition 5 can be used to exactly solve the POMDP for the one-phase approximation. Details on optimizing these benchmarks are relegated to Appendix B.

We first compare the model performance when F is Weibull. Table 3 summarizes results for our model and the four benchmarks under 10,000 simulation replications. We can see that our method is consistently better than the benchmarks in term of smaller costs, larger mission success probability, and smaller system failure probability. Compared with the proposed method, the relative increase of the operational cost for the optimal \mathcal{C} -policy, \mathcal{R} -policy, \mathcal{M} -policy, and one-phase approximation is 4.89%, 7.52%, 4.93%, and 4.74%, respectively. We additionally conduct a sensitivity analysis in Appendix C.2 by varying C_m , \mathbf{D} , and m_2 . It reveals that our method consistently outperforms the benchmarks, and the benchmarks incur a cost increase by around 2%–13% compared to our model. We shall highlight that since the optimal policy of our model is solved offline, it can be implemented online in real time.

We next consider the mixture distribution in (27). The results averaged across 10,000 simulation replications are summarized in Table 4. Our method again outperforms the benchmarks in terms of costs, mission success probability, and system survival probability. The relative increase of the operational cost for the \mathcal{C} -policy, \mathcal{R} -policy, \mathcal{M} -policy, and one-phase approximation is 15.83%, 11.84%, 16.02%, and 15.96%, respectively. Compared with the results when F is Weibull, the gaps between the benchmarks and our method are significantly larger. This outcome is unsurprising since exponential approximation to a bimodal density typically lacks accuracy. In contrast, a mixture of Erlang distribution offers the flexibility to approximate any F , resulting in significantly enhanced policies through subsequent POMDP approximation. The sensitivity analysis in Appendix C.2 further shows that cost increases of the benchmarks generally range from 5% to 18% compared to our method under various C_m and \mathbf{D} .

We see an interesting and intuitive result by comparing Tables 3 and 4. When F is Weibull, an exponential distribution provides a relatively accurate approximation of F . Hence, the one-phase

Table 3 A comparison of the cost, the mission success probability and the system failure probability between the proposed model and the four benchmarks when T_{23} is Weibull in (26). The results are computed based on 10,000 Monte Carlo replications.

Policy	Cost per mission	Mission success prob.	System failure prob.
\mathcal{C} -policy	1063.0	0.668	0.198
\mathcal{R} -policy	1089.6	0.662	0.207
\mathcal{M} -policy	1063.4	0.666	0.198
One-phase approximation	1061.4	0.670	0.201
Proposed model	1013.4	0.681	0.188

Table 4 A comparison of the cost, the mission success probability and the system failure probability between the proposed model and the four benchmarks when T_{23} is a mixture distribution in (27). The results are computed based on 10,000 Monte Carlo replications.

Policy	Cost per mission	Mission success prob.	System failure prob.
\mathcal{C} -policy	1293.1	0.621	0.2675
\mathcal{R} -policy	1248.6	0.6697	0.294
\mathcal{M} -policy	1295.2	0.6242	0.2718
One-phase approximation	1294.6	0.6241	0.2714
Proposed model	1116.4	0.6881	0.2463

approximation outperforms all other benchmarks. However, when T_{23} is a mixture distribution, both the \mathcal{M} -policy and one-phase approximation exhibit significant deterioration in performance, as an exponential approximation to a bimodal density is inaccurate. In this scenario, the \mathcal{R} -policy excels among all benchmarks, as it effectively captures the bimodality of T_{23} in the RUL prediction. There is no benchmark that consistently outperforms others under the two distributions in (26) and (27). In contrast, our model uses the mixture of Erlang distribution to enhance advantages of both rule-based methods and POMDPs. It performs well even when the optimal mission abort policy is highly unstructured due to the bimodality of time from the defective to failure state.

9.3. Performance of the Modified PBVI

We compare our modified PBVI algorithm with the classical PBVI algorithm. Due to the curse of dimensionality, the value function for the problem instance in Section 9.1 cannot be solved exactly. For comparison, we first run the classical PBVI algorithm until hitting its termination condition. We then run our modified PBVI algorithm until the corresponding approximate value function is close to that obtained from the classical PBVI algorithm (see Appendix C.1 for the detailed rule to terminate the modified PBVI algorithm). We replicate the above procedure 10 times and compare the running times. The mean times to finish the modified and classical PBVI algorithms are 5.75 and 63.45 hours, respectively. The runtime of our modified PBVI algorithm is less than 10% of that for the classical PBVI algorithm.

To get a comprehensive insight into the runtime and accuracy of both algorithms, we create a small problem instance with $m_1 = 1$ and $m_2 = 2$, leading to a belief state $\{\boldsymbol{\pi} \in \mathbb{R}_+^3 : \pi_1 + \pi_2 + \pi_3 = 1\}$ before system failure. Other parameters are kept the same as those in Section 9.1. This instance represents possibly the maximum size that can be solved through belief space discretization and backward induction within a reasonable timeframe. The detailed parameter setting is given in Appendix C.1. The availability of the exact value function allows us to compute the optimality gaps of the two PBVI algorithms. The running times (averaged by 20 simulations) for the two PBVI algorithms to achieve solutions with different optimality gaps are summarized in Table 5. The two PBVI algorithms implement the same procedures at early stages, so their performances in this stage are comparable. In contrast, the modified PBVI algorithm becomes much faster in the presence of a small optimality gap. When the optimality gap is 0.3%, the running time of the modified PBVI algorithm is only around 3.5% of that for the classical PBVI algorithm.

Table 5 Runtime comparison (in minutes) for the classical PBVI and the proposed modified PBVI algorithms to achieve solutions with different optimality gaps.

Optimality gap	15%	10%	5%	1%	0.5%	0.3%
Classical PBVI	0.37	0.66	0.86	161.86	1712.08	9803.31
Modified PBVI	0.34	0.62	0.81	92.28	229.30	344.00

9.4. Mission Abort in a Multi-Task Setting

We conduct numerical experiments in a multi-task setting as described in Section 8. We set $L = 3$, and the $L = 3$ tasks need $N_1 = 35$, $N_2 = 50$, and $N_3 = 50$ periods to complete, respectively. The mission failure costs for each task are $(C_m^{(1)}, C_m^{(2)}, C_m^{(3)}) = (500, 300, 200)$. The repair cost is $C_r = 1,000$. The rescue times $(w_n)_{n \in [N]}$ are specified in Appendix C.1. For illustration, we only conduct experiments when the distribution F follows (27). Other settings such as the inter-sampling interval, system failure cost, and observation matrix are the same as those in Section 9.1. Using 1,000 simulation replications, the operational costs of the proposed method, \mathcal{C} -policy, \mathcal{R} -policy, \mathcal{M} -policy, and one-phase approximation are 893.6, 1002.5, 960.2, 1028.7, and 1026.7, respectively. Comparing these numbers with our model, we find that the \mathcal{C} -policy, \mathcal{R} -policy, \mathcal{M} -policy, and one-phase approximation increase the operational cost by 12.19%, 7.45%, 15.12%, and 14.89%, respectively. This reaffirms the cost-effectiveness of our method.

10. Conclusions

This study has developed a general surrogate POMDP framework for mission abort decisions of a three-state mission-critical system with imperfect condition-monitoring signals. Although the

original problem (1) is intractable and the optimal mission abort policy is expected to be highly unstructured, the optimal solution of the surrogate POMDP, with proper design in Figure 1, enjoys nice structural properties under a spherical coordinate system. In particular, mission abort is never optimal at the late stage of the mission; before this stage and given the belief state (r_n, Φ_n) under the spherical coordinate system at the n th decision epoch, the optimal abort policy has a simple upper-lower control-limit structure with respect to the radius r_n , but the control limits depend on the angle Φ_n . These properties enabled us to design a customized algorithm that first finds a cut-point for the late stage and then develop a modified PBVI algorithm to deal with the curse of dimensionality. When $w_n = 0$ for all $n \in [N]$, mission abort resembles the CBM setting (Zhu et al. 2021, Sun et al. 2023), which implies that our framework is applicable to CBM. The case study on a UAV reveals around 5%–20% reduction in the operational cost of the proposed method compared with rule-based policies and simple CTMC approximations under various parameter settings.

Beyond mission abort, the proposed surrogate POMDP framework applies to other discrete-time optimal stopping problems with bounded costs and . For example, it can be used to handle non-Markovian transition of the patient health state in treatment planning (Skandari and Shechter 2021). The framework is also applicable to some sequential decision-making problems, such as inventory control with inter-restocking intervals following a phase-type distribution (Wang et al. 2023). Some natural extensions are of interest for further investigation. If we specialize in mission abort scenarios for UAVs, range constraints due to battery capacity can be a potential issue. Consequently, location designs for rescue sites, where a UAV can safely land for rescue missions, becomes crucial. In a general mission abort problem, uncertainty in the transition and state-observation matrices can be considered. Promising approaches include Bayesian methods and robust POMDPs. Structural properties of our problem may be leveraged to speed up computation in these more complex cases. When historical data are available to infer these parameters, a prominent focus in recent literature has been the development of an end-to-end data-driven methodology that directly maps the available data to a control policy. Our approximation scheme provides a viable framework for this purpose with the Erlang mixture distribution as a key intermediary. Our Theorem 1 has shown that given the best approximating Erlang mixture distribution with a given phase, the optimal solution closely approximates the true optimal policy. The next step is to devise a statistical procedure to estimate this best approximating Erlang mixture distribution. This estimation is closely related to the method of sieve in statistics (Chen 2007). With a proper data-driven choice of the sieve, the estimated Erlang mixture distribution and the estimated policy are expected to be asymptotically consistent, which deserve future research.

Acknowledgment

This work was supported in part by the National Science Foundation of China (72071071, 72171037, 72371161, 72471144), Singapore MOE AcRF Tier 2 grant (A-8001052-00-00, A-8002472-00-00), and the Future Resilient Systems project supported by the National Research Foundation Singapore under its CREATE programme. The authors would like to thank the editor, an associate editor, and two anonymous referees for their valuable comments and constructive suggestions, which have led to a significant improvement in the quality and presentation of this work.

Author Biographies

- Qiuzhuang Sun is a Lecturer in the School of Mathematics and Statistics at the University of Sydney. His research focuses on data-driven decision-making, applied data science, and system reliability.
- Jiawen Hu is an Associate Professor with the School of Aeronautics and Astronautics, University of Electronic Science and Technology of China. His current research interests include maintenance optimization and degradation modeling.
- Zhi-Sheng Ye is an Associate Professor and the Dean's Chair in the Department of Industrial Systems Engineering & Management at the National University of Singapore. His research focuses on data-driven operations management, mathematical and industrial statistics, and system resilience.

References

- Abbou A, Makis V (2019) Group maintenance: A restless bandits approach. *INFORMS Journal on Computing* 31(4):719–731.
- Bertsekas D (2012) *Dynamic Programming and Optimal Control: Volume I* (Athena scientific).
- Bryan CG (2014) An analysis of helicopter EMS accidents using HFACS: 2000–2012 .
- Buchholz P, Kriege J, Felko I (2014) *Input Modeling with Phase-Type Distributions and Markov Models: Theory and Applications* (Springer).
- Cha JH, Finkelstein M, Levitin G (2018) Optimal mission abort policy for partially repairable heterogeneous systems. *European Journal of Operational Research* 271(3):818–825.
- Chen N, Ye ZS, Xiang Y, Zhang L (2015) Condition-based maintenance using the inverse gaussian degradation model. *European Journal of Operational Research* 243(1):190–199.
- Chen X (2007) Large sample sieve estimation of semi-nonparametric models. *Handbook of Econometrics* 6:5549–5632.
- Drent C, Drent M, Arts J, Kapodistria S (2023) Real-time integrated learning and decision making for cumulative shock degradation. *Manufacturing & Service Operations Management* 25(1):235–253.

- Durukan AB, Gurbuz HA, Ozcelik G, Yorgancioglu C (2016) Electrical failure during cardiopulmonary bypass: a critical moment. *Polish Journal of Thoracic and Cardiovascular Surgery* 13(2):143–144.
- Elwany AH, Gebraeel NZ, Maillart LM (2011) Structured replacement policies for components with complex degradation processes and dedicated sensors. *Operations Research* 59(3):684–695.
- Hong Y, Zhang M, Meeker WQ (2018) Big data and reliability applications: The complexity dimension. *Journal of Quality Technology* 50(2):135–149.
- Iravani SM, Duenyas I (2002) Integrated maintenance and production control of a deteriorating production system. *IIE Transactions* 34(5):423–435.
- Khaleghi A, Kim MJ (2021) Optimal control of partially observable semi-Markovian failing systems: An analysis using a phase methodology. *Operations Research* 69:1282–1304.
- Khojandi A, Maillart LM, Prokopyev OA, Roberts MS, Saba SF (2018) Dynamic abandon/extract decisions for failed cardiac leads. *Management Science* 64(2):633–651.
- Kim MJ (2016) Robust control of partially observable failing systems. *Operations Research* 64(4):999–1014.
- Kim MJ, Makis V (2013) Joint optimization of sampling and control of partially observable failing systems. *Operations Research* 61(3):777–790.
- Kim SH, Cohen MA, Netessine S, Veeraraghavan S (2010) Contracting for infrequent restoration and recovery of mission-critical systems. *Management Science* 56(9):1551–1567.
- Krishnamurthy V (2011) Bayesian sequential detection with phase-distributed change time and nonlinear penalty—A POMDP lattice programming approach. *IEEE Transactions on Information Theory* 57(10):7096–7124.
- Krivtsov VV (2007) Practical extensions to NHPP application in repairable system reliability analysis. *Reliability Engineering & System Safety* 92(5):560–562.
- Levitin G, Finkelstein M, Xiang Y (2021) Optimal mission abort policies for repairable multistate systems performing multi-attempt mission. *Reliability Engineering & System Safety* 209:107497.
- Li C, Tomlin B (2022) After-sales service contracting: Condition monitoring and data ownership. *Manufacturing & Service Operations Management* 24(3):1494–1510.
- Liu W, Sun X (2022) Energy-aware and delay-sensitive management of a drone delivery system. *Manufacturing & Service Operations Management* 24(3):1294–1310.
- Liu X, Sun Q, Ye ZS, Yildirim M (2021) Optimal multi-type inspection policy for systems with imperfect online monitoring. *Reliability Engineering & System Safety* 207:107335.
- Liu Z, Khojandi A, Li X, Mohammed A, Davis RL, Kamaleswaran R (2022) A machine learning-enabled partially observable Markov decision process framework for early sepsis prediction. *INFORMS Journal on Computing* 34(4):2039–2057.

- Makis V, Wu J, Gao Y (2006) An application of DPCA to oil data for CBM modeling. *European Journal of Operational Research* 174(1):112–123.
- Meeker WQ, Escobar LA, Pascual FG (2022) *Statistical Methods for Reliability Data* (John Wiley & Sons).
- Mittman E, Lewis-Beck C, Meeker WQ (2019) A hierarchical model for heterogenous reliability field data. *Technometrics* 61(3):354–368.
- Myers A (2009) Probability of loss assessment of critical k -out-of- n : G systems having a mission abort policy. *IEEE Transactions on Reliability* 58(4):694–701.
- Olsen TL, Tomlin B (2020) Industry 4.0: Opportunities and challenges for operations management. *Manufacturing & Service Operations Management* 22(1):113–122.
- Panagiotidou S, Tagaras G (2010) Statistical process control and condition-based maintenance: A meaningful relationship through data sharing. *Production and Operations Management* 19(2):156–171.
- Pineau J, Gordon G, Thrun S (2003) Point-based value iteration: An anytime algorithm for POMDPs. *International Joint Conference on Artificial Intelligence*, 1025–1032.
- Piri H, Huh WT, Shechter SM, Hudson D (2022) Individualized dynamic patient monitoring under alarm fatigue. *Operations Research* 70(5):2749–2766.
- Qiu Q, Cui L (2019) Gamma process based optimal mission abort policy. *Reliability Engineering & System Safety* 190:106496.
- Ranjan C, Reddy M, Mustonen M, Paynabar K, Pourak K (2018) Dataset: Rare event classification in multivariate time series. *arXiv preprint arXiv:1809.10717* .
- Sandıkçı B, Maillart LM, Schaefer AJ, Roberts MS (2013) Alleviating the patient’s price of privacy through a partially observable waiting list. *Management Science* 59(8):1836–1854.
- Shaked M, Shanthikumar JG (2007) *Stochastic Orders* (Springer).
- Silver D, Veness J (2010) Monte-Carlo planning in large POMDPs. *Advances in Neural Information Processing Systems*, 1–9.
- Skandari MR, Shechter SM (2021) Patient-type Bayes-adaptive treatment plans. *Operations Research* 69(2):574–598.
- Smallwood RD, Sondik EJ (1973) The optimal control of partially observable Markov processes over a finite horizon. *Operations Research* 21(5):1071–1088.
- Sun Q, Chen P, Wang X, Ye ZS (2023) Robust condition-based production and maintenance planning for degradation management. *Production and Operations Management* 32(12):3951–3967.
- Tian F, Sun P, Duenyas I (2021) Optimal contract for machine repair and maintenance. *Operations Research* 69(3):916–949.
- Tian Z, Han W, Powell WB (2022) Adaptive learning of drug quality and optimization of patient recruitment for clinical trials with dropouts. *Manufacturing & Service Operations Management* 24(1):580–599.

- Wang B, Liu D, Peng Y, Peng X (2019) Multivariate regression-based fault detection and recovery of UAV flight data. *IEEE Transactions on Instrumentation and Measurement* 69(6):3527–3537.
- Wang J (2022) Optimal sequential multiclass diagnosis. *Operations Research* 70(1):201–222.
- Wang J, Lee CG (2015) Multistate Bayesian control chart over a finite horizon. *Operations Research* 63(4):949–964.
- Wang L, Kulkarni V, Zhang H (2023) Inventory dispensation and restocking in multiclass inventory systems: A decoupling approach. *Production and Operations Management* 32(2):469–484.
- Whitlock C (2016) More Air Force drones are crashing than ever as mysterious new problems emerge. <https://www.washingtonpost.com/news/checkpoint/wp/2016/01/19/more-u-s-military-drones-are-crashing/>
- Wiens DP (1979) *Distributions for a two-unit repairable system*. Ph.D. thesis, University of Calgary.
- Yang L, Sun Q, Ye ZS (2020) Designing mission abort strategies based on early-warning information: Application to UAV. *IEEE Transactions on Industrial Informatics* 16(1):277–287.
- Yao YC, Tseng ST, Wong DSH (2017) Shelf-life prediction of nano-sol via pH acceleration. *Journal of Quality Technology* 49(1):46–63.
- Yu H, Wu X, Wu X (2020) An extended object-oriented petri net model for mission reliability evaluation of phased-mission system with time redundancy. *Reliability Engineering & System Safety* 197:106786.
- Zhang H (2010) Partially observable Markov decision processes: A geometric technique and analysis. *Operations Research* 58(1):214–228.
- Zhang H, Zhang W (2023) Analytical solution to a partially observable machine maintenance problem with obvious failures. *Management Science* 69(7):3993–4015.
- Zhao X, Fan Y, Qiu Q, Chen K (2021) Multi-criteria mission abort policy for systems subject to two-stage degradation process. *European Journal of Operational Research* 295(1):233–245.
- Zhu Z, Xiang Y, Zeng B (2021) Multicomponent maintenance optimization: A stochastic programming approach. *INFORMS Journal on Computing* 33(3):898–914.
- Zhu Z, Xiang Y, Zhao M, Shi Y (2023) Data-driven remanufacturing planning with parameter uncertainty. *European Journal of Operational Research* 309(1):102–116.

Electronic Companion to “Optimal Abort Policy for Mission-Critical Systems under Imperfect Condition Monitoring”

Qiuzhuang Sun,¹ Jiawen Hu,² and Zhi-Sheng Ye³

¹School of Mathematics and Statistics, University of Sydney, Australia

²School of Aeronautics and Astronautics, University of Electronic Science and Technology of China, China

³Department of Industrial Systems Engineering and Management, National University of Singapore, Singapore

Emails: qiuzhuang.sun@sydney.edu.au; hdl@sjtu.edu.cn; yez@nus.edu.sg

Appendix A: Technical Proofs

A.1. Proof of Proposition 1

Consider the continuous-time Markov chain (CTMC) $\{X^{(\lambda)}(t) : t \geq 0\}$ with initial probabilities in (4) and transition rate matrix \mathbf{Q} in (5). If $X^{(\lambda)}$ starts from state i , $i \in [m_1]$, the transition time $T_{12}^{(\lambda)}$ from this state to state $m_1 + 1$ follows an Erlang distribution with rate $\lambda - \zeta$ and shape $m_1 - i + 1$. Since $X^{(\lambda)}$ starts from m_1 with probability $\pi_{01}^{(\lambda)} = 1 - G((m_1 - 1)/(\lambda - \zeta))$ and from $i \in \{2, \dots, m_1\}$ with probability $\pi_{0i}^{(\lambda)} = G((m_1 + 1 - i)/(\lambda - \zeta)) - G((m_1 - i)/(\lambda - \zeta))$, $T_{12}^{(\lambda)}$ is a mixed Erlang random variable unconditionally. Its distribution can be specified from the initial probability $\pi_{0i}^{(\lambda)}$ and the Erlang distributions above, which is exactly $G^{(\lambda)}$ in (3).

A careful inspection of q_{ij} shows that for any state $i \in \mathcal{X}_1$, there is a transition rate $q_{i, m_1 + m_2 + 1} = \zeta$ to the absorbing state $m_1 + m_2 + 1$. Since $q_{i, m_1 + m_2 + 1}$ are identical for all $i \in \mathcal{X}_1$, the (potential) transition time, denoted as $T_{13}^{(\lambda)}$, follows an exponential distribution with rate ζ , same as T_{13} . By the memoryless property of exponential distributions, we see that the failure time of $X^{(\lambda)}$ has the same distribution as $T_{13}^{(\lambda)}$ when $T_{13}^{(\lambda)} \leq T_{12}^{(\lambda)}$. On the other hand, we derive the system failure time when $T_{13}^{(\lambda)} > T_{12}^{(\lambda)}$ as follows. When $T_{13}^{(\lambda)} > T_{12}^{(\lambda)}$, the system is at state $m_1 + 1$ at time $T_{12}^{(\lambda)}$. From this time on, the probability that $X^{(\lambda)}(t)$ enters the absorbing state $m_1 + m_2 + 1$ with additional l transitions is

$$p_l(\lambda) \prod_{i=1}^{l-1} (1 - p_i(\lambda)) = \frac{F(l/\lambda) - F((l-1)/\lambda)}{1 - F((l-1)/\lambda)} \prod_{i=1}^{l-1} \frac{1 - F(i/\lambda)}{1 - F((i-1)/\lambda)} = F\left(\frac{l}{\lambda}\right) - F\left(\frac{l-1}{\lambda}\right)$$

for $l \in [m_2 - 1]$, and

$$\prod_{i=1}^{m_2-1} (1 - p_i(\lambda)) = \prod_{i=1}^{m_2-1} \frac{1 - F(i/\lambda)}{1 - F((i-1)/\lambda)} = 1 - F\left(\frac{m_2-1}{\lambda}\right)$$

for $l = m_2$, where we use the fact that $F(0) = 0$. When $X^{(\lambda)}$ uses l steps to transition from state $m_1 + 1$ to state $m_1 + m_2 + 1$, the elapsed time follows an Erlang distribution with shape l and rate $\lambda > 0$ by our construction. This fact, in conjunction with the probability of l transitions to the absorbing state specified above, shows that the duration from time $T_{12}^{(\lambda)}$ to the absorbing state

follows a mixed Erlang distribution. It is easy to check that this mixed Erlang distribution is exactly the one specified in Equation (2) for $T_{23}^{(\lambda)}$. Combining the above analysis to see that the absorption time of $X^{(\lambda)}$ has the same distribution as $T_{13}^{(\lambda)} \mathbb{1}\{T_{13}^{(\lambda)} \leq T_{12}^{(\lambda)}\} + (T_{12}^{(\lambda)} + T_{23}^{(\lambda)}) \mathbb{1}\{T_{13}^{(\lambda)} > T_{12}^{(\lambda)}\}$, whence the proposition holds. \square

A.2. Proof of Theorem 1

Given that the realization of the condition-monitoring signals $Y_{1:n} = y_{1:n} \in \{0, \dots, K\}^n$, we let $\mathbb{C}_{\text{ab}}(n, y_{1:n})$ and $\mathbb{C}_{\text{c}}(n, y_{1:n})$ denote the minimum costs-to-go for $X(t)$ when the mission is aborted or continued at time $n\delta$, respectively. Similarly, given the same information, let $\mathbb{C}_{\text{ab},\lambda}(n, y_{1:n}) \triangleq V_{\text{ab}}^{(\lambda)}(n, \pi_n^{(\lambda)})$ and $\mathbb{C}_{\text{c},\lambda}(n, y_{1:n}) \triangleq V_{\text{c}}^{(\lambda)}(n, \pi_n^{(\lambda)})$ be the minimum costs-to-go for $X^{(\lambda)}(t)$, where V_{ab} and V_{c} are defined in Section 4.2, and here we explicitly indicate their dependence on λ . The optimal decision rules a_n^* and $a_{\lambda,n}^*$ can be determined by comparing the two costs-to-go, i.e., $a_n^*(y_{1:n}) = \mathbb{1}\{\mathbb{C}_{\text{ab}}(n, y_{1:n}) < \mathbb{C}_{\text{c}}(n, y_{1:n})\}$ and $a_{\lambda,n}^*(y_{1:n}) = \mathbb{1}\{\mathbb{C}_{\text{ab},\lambda}(n, y_{1:n}) < \mathbb{C}_{\text{c},\lambda}(n, y_{1:n})\}$. To show $a_{\lambda,n}^* \rightarrow a_n^*$ \mathbb{P} -almost surely as $\lambda \rightarrow \infty$, it suffices to show $\lim_{\lambda \rightarrow \infty} \mathbb{C}_{\text{ab},\lambda}(n, y_{1:n}) = \mathbb{C}_{\text{ab}}(n, y_{1:n})$ and $\lim_{\lambda \rightarrow \infty} \mathbb{C}_{\text{c},\lambda}(n, y_{1:n}) = \mathbb{C}_{\text{c}}(n, y_{1:n})$ for all $y_{1:n} \in \{0, \dots, K\}^n$ and $n \in [N]$.

Recall that $T_{12}^{(\lambda)}, T_{23}^{(\lambda)}, T_{13}^{(\lambda)}$ are the independent (potential) transition times from state clusters \mathcal{X}_1 to \mathcal{X}_2 , from \mathcal{X}_2 to \mathcal{X}_3 , and from \mathcal{X}_1 to \mathcal{X}_3 , respectively. We then show $(T_{12}^{(\lambda)}, T_{13}^{(\lambda)}, T_{23}^{(\lambda)}, Y_{1:N}^{(\lambda)})$ jointly converges to $(T_{12}, T_{13}, T_{23}, Y_{1:N})$ in distribution as $\lambda \rightarrow \infty$. Let $\mathbf{T}^{(\lambda)} = (T_{12}^{(\lambda)}, T_{13}^{(\lambda)}, T_{23}^{(\lambda)})$, $\mathbf{t} = (t_{12}, t_{13}, t_{23})$, $\mathbf{u} = (u_{12}, u_{13}, u_{23})$, and $\mathbf{F}^{(\lambda)}(\mathbf{t}) = P^{(\lambda)}(T_{12}^{(\lambda)} \leq t_{12}, T_{13}^{(\lambda)} \leq t_{13}, T_{23}^{(\lambda)} \leq t_{23})$. By the independence of $Y_1^{(\lambda)}, \dots, Y_n^{(\lambda)}$ conditional on the failure process $X^{(\lambda)}(t)$, we have

$$\begin{aligned} P^{(\lambda)}(\mathbf{T}^{(\lambda)} \leq \mathbf{t}, Y_{1:N}^{(\lambda)} = y_{1:N}) &= \int_{\mathbf{u} \leq \mathbf{t}} P^{(\lambda)}(Y_{1:N}^{(\lambda)} = y_{1:N} \mid \mathbf{T}^{(\lambda)} = \mathbf{u}) d\mathbf{F}^{(\lambda)}(\mathbf{u}) \\ &= \int_{\mathbf{u} \leq \mathbf{t}} \prod_{n=1}^N P^{(\lambda)}(Y_n^{(\lambda)} = y_n \mid \mathbf{T}^{(\lambda)} = \mathbf{u}) d\mathbf{F}^{(\lambda)}(\mathbf{u}). \end{aligned}$$

Similarly,

$$\mathbb{P}(\mathbf{T} \leq \mathbf{t}, Y_{1:N} = y_{1:N}) = \int_{\mathbf{u} \leq \mathbf{t}} \prod_{n=1}^N \mathbb{P}(Y_n = y_n \mid \mathbf{T} = \mathbf{u}) d\mathbf{F}(\mathbf{u}),$$

where $\mathbf{T} = (T_{12}, T_{13}, T_{23})$ and $\mathbf{F}(\mathbf{t}) = \mathbb{P}(T_{12} \leq t_{12}, T_{13} \leq t_{13}, T_{23} \leq t_{23})$. By our construction of the surrogate signals $Y_{1:N}^{(\lambda)}$, $P^{(\lambda)}(Y_n^{(\lambda)} = y_n \mid \mathbf{T}^{(\lambda)} = \mathbf{u})$ is equal to $\mathbb{P}(Y_n = y_n \mid \mathbf{T} = \mathbf{u})$. If we can show that $g_n(\mathbf{u}) \triangleq \mathbb{P}(Y_n = y_n \mid \mathbf{T} = \mathbf{u})$ is continuous almost everywhere with respect to the distribution of $\mathbf{T} = (T_{12}, T_{13}, T_{23})$, then we can use the fact that $\mathbf{F}^{(\lambda)} \rightsquigarrow \mathbf{F}$ and apply Portmanteau's theorem to the function $g(\mathbf{u}) \triangleq \prod_{n=1}^N g_n(\mathbf{u}) \mathbb{1}\{\mathbf{u} \leq \mathbf{t}\}$ to conclude that $P^{(\lambda)}(\mathbf{T}^{(\lambda)} \leq \mathbf{t}, Y_{1:N}^{(\lambda)} = y_{1:N}) \rightarrow \mathbb{P}(\mathbf{T} \leq \mathbf{t}, Y_{1:N} = y_{1:N})$ as $\lambda \rightarrow \infty$. Note that

$$\begin{aligned} \mathbb{P}(Y_n = y_n \mid \mathbf{T} = \mathbf{u}) &= d_{1,y_n} \mathbb{1}\{n\delta < \min\{u_1, u_2\}\} + d_{2,y_n} \mathbb{1}\{u_1 < n\delta \leq u_1 + u_3, u_1 < u_2\} \\ &\quad + \mathbb{1}\{y_n = 0, n\delta \geq u_2 \mathbb{1}\{u_1 \geq u_2\} + (u_1 + u_3) \mathbb{1}\{u_1 < u_2\}\}. \end{aligned}$$

This function has finite number of discontinuous points. It is continuous almost everywhere by the continuity assumption on T_{12}, T_{13}, T_{23} , whence Portmanteau's theorem applies. This implies that $P^{(\lambda)}(\mathbf{T}^{(\lambda)} \leq \mathbf{t}, Y_{1:N}^{(\lambda)} \leq y_{1:N}) \rightarrow P(\mathbf{T} \leq \mathbf{t}, Y_{1:N} \leq y_{1:N})$ as $\lambda \rightarrow \infty$. That is, $(T_{12}^{(\lambda)}, T_{13}^{(\lambda)}, T_{23}^{(\lambda)}, Y_{1:N}^{(\lambda)})$ converges to $(T_{12}, T_{13}, T_{23}, Y_{1:N})$ in distribution as $\lambda \rightarrow \infty$.

With the weak convergence established above, we now show $\lim_{\lambda \rightarrow \infty} \mathbb{C}_{\text{ab},\lambda}(n, y_{1:n}) = \mathbb{C}_{\text{ab}}(n, y_{1:n})$ and $\lim_{\lambda \rightarrow \infty} \mathbb{C}_{\text{c},\lambda}(n, y_{1:n}) = \mathbb{C}_{\text{c}}(n, y_{1:n})$ for all $n \in [N]$ by induction. For $n = N - 1$, assume the system is working and the realization of conditioning monitoring signals is $Y_{1:N-1} = Y_{1:N-1}^{(\lambda)} = y_{1:N-1}$. For the failure process $X^{(\lambda)}(t)$, the cost-to-go of aborting the mission is

$$\mathbb{C}_{\text{ab},\lambda}(N - 1, y_{1:N-1}) = C_{\text{m}} + C_{\text{s}} P^{(\lambda)}(\xi^{(\lambda)} \leq (N - 1)\delta + w_{N-1} \mid Y_{1:N-1}^{(\lambda)} = y_{1:N-1}).$$

For the failure process $X(t)$, the cost-to-go of aborting the mission is

$$\mathbb{C}_{\text{ab}}(N - 1, y_{1:N-1}) = C_{\text{m}} + C_{\text{s}} \mathbb{P}(\xi \leq (N - 1)\delta + w_{N-1} \mid Y_{1:N-1} = y_{1:N-1}).$$

Since $(T_{12}^{(\lambda)}, T_{13}^{(\lambda)}, T_{23}^{(\lambda)}, Y_{1:N}^{(\lambda)}) \rightsquigarrow (T_{12}, T_{13}, T_{23}, Y_{1:N})$ as $\lambda \rightarrow \infty$ and all transition times in the same probability space are independent, we have

$$\begin{aligned} & P^{(\lambda)}(\xi^{(\lambda)} \leq t \mid Y_{1:N-1}^{(\lambda)} = y_{1:N-1}) \\ &= P^{(\lambda)}(T_{13}^{(\lambda)} \mathbb{1}\{T_{13}^{(\lambda)} \leq T_{12}^{(\lambda)}\} + (T_{12}^{(\lambda)} + T_{23}^{(\lambda)}) \mathbb{1}\{T_{13}^{(\lambda)} > T_{12}^{(\lambda)}\} \leq t \mid Y_{1:N-1}^{(\lambda)} = y_{1:N-1}) \\ &= \frac{P^{(\lambda)}(T_{13}^{(\lambda)} \mathbb{1}\{T_{13}^{(\lambda)} \leq T_{12}^{(\lambda)}\} + (T_{12}^{(\lambda)} + T_{23}^{(\lambda)}) \mathbb{1}\{T_{13}^{(\lambda)} > T_{12}^{(\lambda)}\} \leq t, Y_{1:N-1}^{(\lambda)} = y_{1:N-1})}{P^{(\lambda)}(Y_{1:N-1}^{(\lambda)} = y_{1:N-1})} \\ &\rightarrow \frac{\mathbb{P}(T_{13} \mathbb{1}\{T_{13} \leq T_{12}\} + (T_{12} + T_{23}) \mathbb{1}\{T_{13} > T_{12}\} \leq t, Y_{1:N-1} = y_{1:N-1})}{\mathbb{P}(Y_{1:N-1} = y_{1:N-1})} \\ &= \mathbb{P}(\xi \leq t \mid Y_{1:N-1} = y_{1:N-1}) \end{aligned}$$

as $\lambda \rightarrow \infty$ for all $t > 0$ by the continuous mapping theorem. Hence, the cost-to-go $\mathbb{C}_{\text{ab},\lambda}(N - 1, y_{1:N-1})$ of aborting the mission using the stochastic process $X^{(\lambda)}(\cdot)$ converges to $\mathbb{C}_{\text{ab}}(N - 1, y_{1:N-1})$ based on $X(t)$ as $\lambda \rightarrow \infty$. By the same reasoning, the costs-to-go $\mathbb{C}_{\text{c},\lambda}(N - 1, y_{1:N-1})$ of continuing the mission under $X^{(\lambda)}(\cdot)$ also converges to $\mathbb{C}_{\text{c}}(N - 1, y_{1:N-1})$. By the assumption of unique set of optimal solutions of the original problem in (1), $\mathbb{C}_{\text{ab}}(N - 1, y_{1:N-1}) \neq \mathbb{C}_{\text{c}}(N - 1, y_{1:N-1})$. The uniqueness, in conjunction with the convergence above, implies that when λ is large enough, the sign of $\mathbb{C}_{\text{ab},\lambda}(N - 1, y_{1:N-1}) - \mathbb{C}_{\text{c},\lambda}(N - 1, y_{1:N-1})$ is the same as that of $\mathbb{C}_{\text{ab}}(N - 1, y_{1:N-1}) - \mathbb{C}_{\text{c}}(N - 1, y_{1:N-1})$. Consequently, $\lim_{\lambda \rightarrow \infty} \mathbb{C}_{\lambda}(N - 1, y_{1:N-1}) = \mathbb{C}(N - 1, y_{1:N-1})$, where $\mathbb{C}_{\lambda,n-1}(y_{1:n-1}) \triangleq \min\{\mathbb{C}_{\text{ab},\lambda}(n - 1, y_{1:n-1}), \mathbb{C}_{\text{c},\lambda}(n - 1, y_{1:n-1})\}$ and $\mathbb{C}(n - 1, y_{1:n-1}) \triangleq \min\{\mathbb{C}_{\text{ab}}(n - 1, y_{1:n-1}), \mathbb{C}_{\text{c}}(n - 1, y_{1:n-1})\}$ for all $n \in [N]$.

Now assume $a_{\lambda,n}^*(Y_{1:n}) \rightarrow a_n^*(Y_{1:n})$ \mathbb{P} -almost surely and $\mathbb{C}_{\lambda}(n, y_{1:n}) \rightarrow \mathbb{C}(n, y_{1:n})$ as $\lambda \rightarrow \infty$ for all $y_{1:n} \in [K]^n$ and $n = m, \dots, N - 1$. Then for $n = m - 1$, we can repeat the above argument for $n = N - 1$ to show that the costs-to-go for aborting the mission are the asymptotically same for the

two stochastic processes $X(t)$ and $X^{(\lambda)}(t)$ as $\lambda \rightarrow \infty$. Moreover, given $Y_{1:m-1} = y_{1:m-1} \in [K]^{m-1}$, the cost-to-go of continuing the mission for $X(t)$ is

$$\begin{aligned} \mathbb{C}_c(m-1, y_{1:m-1}) &= \mathbb{E}[(C_m + C_s) \mathbb{1}\{\xi \leq m\delta\} + \mathbb{C}_{ab}(m, Y_{1:m}) \mathbb{1}\{\xi > m\delta, a_m^*(Y_{1:m}) = 1\} \\ &\quad + \mathbb{C}_c(m, Y_{1:m}) \mathbb{1}\{\xi > m\delta, a_m^*(Y_{1:m}) = 0\} \mid Y_{1:m-1} = y_{1:m-1}]. \end{aligned}$$

Similarly, the cost-to-go of continuing the mission for $X^{(\lambda)}(t)$ is

$$\begin{aligned} \mathbb{C}_{c,\lambda}(m-1, y_{1:m-1}) &= \mathbb{E}^{(\lambda)}[(C_m + C_s) \mathbb{1}\{\xi^{(\lambda)} \leq m\delta\} + \mathbb{C}_{ab,\lambda}(m, Y_{1:m}^{(\lambda)}) \mathbb{1}\{\xi^{(\lambda)} > m\delta, a_{\lambda,m}^*(Y_{1:m}^{(\lambda)}) = 1\} \\ &\quad + \mathbb{C}_{c,\lambda}(m, Y_{1:m}^{(\lambda)}) \mathbb{1}\{\xi^{(\lambda)} > m\delta, a_{\lambda,m}^*(Y_{1:m}^{(\lambda)}) = 0\} \mid Y_{1:m-1}^{(\lambda)} = y_{1:m-1}]. \end{aligned}$$

The induction hypothesis implies that $\lim_{\lambda \rightarrow \infty} a_{\lambda,m}^*(y_{1:m}) = a_m^*(y_{1:m})$. By the weak convergence of $(T_{12}^{(\lambda)}, T_{13}^{(\lambda)}, T_{23}^{(\lambda)}, Y_{1:N}^{(\lambda)})$ to $(T_{12}, T_{13}, T_{23}, Y_{1:N})$, it can be routinely verified that the conditional distributions of $\xi^{(\lambda)}$ and $Y_m^{(\lambda)}$ given $Y_{1:m-1}^{(\lambda)} = y_{1:m-1}$ converge to those of ξ and Y_m given $Y_{1:m-1} = y_{1:m-1}$, as $\lambda \rightarrow \infty$. The random variables within the conditional expectations of $\mathbb{C}_{c,\lambda}(m-1, y_{1:m-1})$ above are bounded by $C_m + C_s$, and hence are uniformly integrable. As such, weak convergence implies convergence of moments, and $\mathbb{C}_{c,\lambda}(m-1, y_{1:m-1})$ converges to $\mathbb{C}_c(m-1, y_{1:m-1})$ as $\lambda \rightarrow \infty$. Again, by the assumption of unique set of optimal solutions of the original problem in (1), $\mathbb{C}_{ab}(m-1, y_{1:m-1}) \neq \mathbb{C}_c(m-1, y_{1:m-1})$. Therefore, the sign of $\mathbb{C}_{ab,\lambda}(m-1, y_{1:m-1}) - \mathbb{C}_{c,\lambda}(m-1, y_{1:m-1})$ will eventually be the same as that of $\mathbb{C}_{ab}(m-1, y_{1:m-1}) - \mathbb{C}_c(m-1, y_{1:m-1})$, implying a_{m-1}^* and $a_{\lambda,m-1}^*$ are asymptotically the same as $\lambda \rightarrow \infty$. Consequently, $\lim_{\lambda \rightarrow \infty} \mathbb{C}_\lambda(m-1, y_{1:m-1}) = \mathbb{C}(m-1, y_{1:m-1})$. Whence, if the induction hypothesis holds for $n = m, \dots, N-1$, we have shown that it also holds for $n = m-1$. Therefore, the induction hypothesis is true for all $n \in [N-1]$.

Moreover, given $Y_n = Y_n^{(\lambda)} = 0$, the corresponding actions are also the same by the last set of constraints in Problems (1) and (7), i.e., $a_{\lambda,n}^*(y_{1:n}) = a_n^*(y_{1:n}) = 1$ when $y_n = 0$ for all $n \in [N-1]$. Combining all the above arguments shows the almost sure convergence of $a_{\lambda,n}^*(Y_{1:n})$ to $a_n^*(Y_{1:n})$.

Since for any realization of the condition-monitoring signals $Y_{1:N}$, the actions corresponding to $(a_n^*)_{n \in [N-1]}$ and $(a_{\lambda,n}^*)_{n \in [N-1]}$ are the same as $\lambda \rightarrow \infty$, it means that $\mathfrak{T}^{(\lambda)} \rightarrow \mathfrak{T}^*$ \mathbb{P} -almost surely as $\lambda \rightarrow \infty$. Because $\mathfrak{T}^{(\lambda)}$ and \mathfrak{T}^* have a finite support $\{n\delta : n \in [N]\}$, we have $X(\mathfrak{T}^{(\lambda)} + w_{\mathfrak{T}^{(\lambda)}/\delta}) \rightarrow X(\mathfrak{T}^* + w_{\mathfrak{T}^*/\delta})$ \mathbb{P} -almost surely as $\lambda \rightarrow \infty$. Since $X(\mathfrak{T}^{(\lambda)} + w_{\mathfrak{T}^{(\lambda)}/\delta})$ and $X(\mathfrak{T}^* + w_{\mathfrak{T}^*/\delta})$ also only have a finite support $\mathbb{S} = \{1, 2, 3\}$, we have the corresponding cost $C(X(\mathfrak{T}^{(\lambda)} + w_{\mathfrak{T}^{(\lambda)}/\delta}), \mathfrak{T}^{(\lambda)}) \rightarrow C(X(\mathfrak{T}^* + w_{\mathfrak{T}^*/\delta}), \mathfrak{T}^*)$ \mathbb{P} -almost surely as $\lambda \rightarrow \infty$. Then, because the cost during a mission is bounded from above by $C_m + C_s$, it follows from the dominated convergence theorem to conclude $\lim_{\lambda \rightarrow \infty} \mathbb{E}[C(X(\mathfrak{T}^{(\lambda)} + w_{\mathfrak{T}^{(\lambda)}/\delta}), \mathfrak{T}^{(\lambda)})] = \mathbb{E}[C(X(\mathfrak{T}^* + w_{\mathfrak{T}^*/\delta}), \mathfrak{T}^*)]$. \square

A.3. Proof of Lemma 1

We prove the monotonicity of $h^{(\lambda)}(t)$ by first showing that q_{i,m_1+m_2+1} is nondecreasing in $i \in \mathcal{X}_2$. With a slight abuse of notation, let $\{X^{(\lambda)}(t) : t > 0\}$ be the same CTMC defined in Section 4 but starting from state $m_1 + 1$ with probability one at time $t = 0$. Then the absorption time of $X^{(\lambda)}$ is $T_{23}^{(\lambda)}$, so that the system failure rate at time $t = 0$ is

$$\begin{aligned} h^{(\lambda)}(0) &\triangleq \lim_{\Delta t \downarrow 0} \frac{P^{(\lambda)}(X^{(\lambda)}(\Delta t) = m_1 + m_2 + 1 \mid X^{(\lambda)}(0) = m_1 + 1)}{\Delta t} \\ &= q_{m_1+1, m_1+m_2+1} = \lambda p_1(\lambda) = \lambda F(1/\lambda), \end{aligned}$$

where the second equality follows from the definition of transition rates of CTMCs. By definition of $F(\cdot)$, we have $\lim_{\lambda \rightarrow \infty} \lambda F(1/\lambda) = h(0)$, which is larger than ζ by Assumption 1. When the system is at state $i = m_1 + 1, \dots, m_1 + m_2 - 1$, the transition rate to the failure state $m_1 + m_2 + 1$ is $q_{i, m_1+m_2+1} = \lambda p_{i-m_1}(\lambda)$. By Khaleghei and Kim (2021, Lemma 1), there exists $\bar{\lambda}$ such that $p_{i-m_1}(\lambda)$ is nondecreasing in i for all $\lambda > \bar{\lambda}$, so is q_{i, m_1+m_2+1} . Moreover, we have $q_{m_1+m_2, m_1+m_2+1} = \lambda \geq q_{i, m_1+m_2+1}$ for all $i \in \mathcal{X}_2$ because $p_j(\lambda) \leq 1$ for all $j \in [m_2 - 1]$ by definition.

Let $\tilde{\mathbf{p}}(t) \triangleq \left(\frac{p_{m_1+1, j}(t)}{1 - p_{m_1+1, m_1+m_2+1}(t)} \right)_{j \in \mathcal{X}_2}$ be the vector of probabilities that $X^{(\lambda)}(t) = j \in \mathcal{X}_2$, given that $X^{(\lambda)}(0) = m_1 + 1$ and $X^{(\lambda)}(t) < m_1 + m_2 + 1$. We then show $\tilde{\mathbf{p}}(t_1) \succeq_{\text{LR}} \tilde{\mathbf{p}}(t_2)$ for any $t_1 \geq t_2 > 0$. Indeed, since our CTMC has a finite number of states, the transition between states follows Kolmogorov's forward equations, i.e., for any $t > 0$,

$$p'_{ii}(t) = -\lambda p_{ii}(t) \quad \text{and} \quad p'_{ij}(t) = \lambda[1 - p_{j-m_1-1}(\lambda)]p_{i, j-1}(t) - \lambda p_{ij}(t),$$

with $i, j \in \mathcal{X}_2$ and $i < j$. Solving these equations yields

$$p_{ii}(t) = \exp(-\lambda t) \quad \text{and} \quad p_{ij}(t) = \lambda[1 - p_{j-m_1-1}(\lambda)]e^{-\lambda t} \int_0^t e^{\lambda s} p_{i, j-1}(s) ds.$$

Fixing $i = m_1 + 1$ and recursively using the above identities for $j = m_1 + 2, \dots, m_1 + m_2$ give

$$p_{m_1+1, j}(t) = \frac{\prod_{k=m_1+1}^{j-1} [1 - p_{k-m_1}(\lambda)]}{(j - m_1 - 1)!} (\lambda t)^{j-m_1-1} \exp(-\lambda t), \quad t > 0,$$

for all $j \in \mathcal{X}_2$. We then have $p_{m_1+1, j+1}(t)/p_{m_1+1, j}(t) = [1 - p_{j-m_1}(\lambda)]\lambda t/(j - m_1)$, which increases in $t > 0$. By definition of the likelihood ratio order, $\tilde{\mathbf{p}}(t_1) \succeq_{\text{LR}} \tilde{\mathbf{p}}(t_2)$ for any $t_1 \geq t_2 > 0$ is equivalent to

$$\begin{aligned} \frac{p_{m_1+1, j+1}(t_1)}{1 - p_{m_1+1, m_1+m_2+1}(t_1)} \cdot \frac{1 - p_{m_1+1, m_1+m_2+1}(t_2)}{p_{m_1+1, j+1}(t_2)} &\geq \frac{p_{m_1+1, j}(t_1)}{1 - p_{m_1+1, m_1+m_2+1}(t_1)} \cdot \frac{1 - p_{m_1+1, m_1+m_2+1}(t_2)}{p_{m_1+1, j}(t_2)} \\ &\Leftrightarrow \frac{p_{m_1+1, j+1}(t_1)}{p_{m_1+1, j}(t_1)} \geq \frac{p_{m_1+1, j+1}(t_2)}{p_{m_1+1, j}(t_2)} \end{aligned}$$

for all $j \in \{m_1 + 1, \dots, m_1 + m_2 - 1\}$, which is true based on the above monotone property of $t \mapsto p_{m_1+1, j+1}(t)/p_{m_1+1, j}(t)$.

The failure rate at time $t > 0$ is then given by

$$\begin{aligned} h^{(\lambda)}(t) &= \lim_{\Delta t \downarrow 0} \frac{P^{(\lambda)}(X^{(\lambda)}(t + \Delta t) = m_1 + m_2 + 1 | X^{(\lambda)}(0) = m_1 + 1, X^{(\lambda)}(t) \neq m_1 + m_2 + 1)}{\Delta t} \\ &= \lim_{\Delta t \downarrow 0} \sum_{j=m_1+1}^{m_1+m_2} \frac{P^{(\lambda)}(X^{(\lambda)}(t + \Delta t) = m_1 + m_2 + 1 | X^{(\lambda)}(t) = j) P^{(\lambda)}(X^{(\lambda)}(t) = j | X^{(\lambda)}(0) = m_1 + 1)}{\Delta t P^{(\lambda)}(X^{(\lambda)}(t) \neq m_1 + m_2 + 1 | X^{(\lambda)}(0) = m_1 + 1)} \\ &= \frac{\sum_{j=m_1+1}^{m_1+m_2} p_{m_1+1,j}(t) q_{j,m_1+m_2+1}}{1 - p_{m_1+1,m_1+m_2+1}(t)} = \mathbf{q}' \tilde{\mathbf{p}}(t), \end{aligned}$$

where $\mathbf{q} \triangleq (q_{j,m_1+m_2+1})_{j=m_1+1}^{m_1+m_2+1}$. Since \mathbf{q} is a nondecreasing sequence and $\tilde{\mathbf{p}}(t_1) \succeq_{\text{LR}} \tilde{\mathbf{p}}(t_2)$ for any $t_1 \geq t_2 \geq 0$, it then follows from Shaked and Shanthikumar (2007, (1.A.7)) that their inner product satisfies $h^{(\lambda)}(t_1) = \mathbf{q}' \tilde{\mathbf{p}}(t_1) \geq \mathbf{q}' \tilde{\mathbf{p}}(t_2) = h^{(\lambda)}(t_2)$ for any $0 \leq t_2 \leq t_1 \leq T$. \square

Remark. Based on the above proof, it suffices to ensure q_{i,m_1+m_2+1} is nondecreasing in $i \in [m_1 + m_2]$ to guarantee the monotonicity of $h^{(\lambda)}(t)$. To select a finite value of λ for optimization under Assumption 1, we can compute q_{i,m_1+m_2+1} for all $i \in \{m_1 + 1, \dots, m_1 + m_2 + 1\}$ by Equations (5) and (6), and check if q_{i,m_1+m_2+1} is nondecreasing in i .

A.4. Proof of Lemma 2

We prove the lemma by induction. By Equation (10), $\kappa(w_n, \boldsymbol{\pi})$ is a linear function of $\boldsymbol{\pi}$ for all $n = 0, \dots, N$. When $n = N$, the value function $V(N, \boldsymbol{\pi})$ is also a linear function in $\boldsymbol{\pi}$ by (14) and hence is concave in $\boldsymbol{\pi}$.

We then assume $V(n, \boldsymbol{\pi}) = \min\{V_{\text{ab}}(n, \boldsymbol{\pi}), V_{\text{c}}(n, \boldsymbol{\pi})\}$ is concave in $\boldsymbol{\pi}$ for all $n = l + 1, l + 2, \dots, N$. We show that both $V_{\text{ab}}(n, \boldsymbol{\pi})$ and $V_{\text{c}}(n, \boldsymbol{\pi})$ are concave in $\boldsymbol{\pi}$ when $n = l$. We first consider $V_{\text{ab}}(n, \boldsymbol{\pi})$. By linearity of $\kappa(w_n, \boldsymbol{\pi})$ in $\boldsymbol{\pi}$ and Equation (11), $V_{\text{ab}}(n, \boldsymbol{\pi})$ is linear and hence concave in $\boldsymbol{\pi}$ for all $n = 0, \dots, N - 1$.

We next consider $V_{\text{c}}(n, \boldsymbol{\pi})$. By Equation (12) and linearity of $\kappa(w_n, \boldsymbol{\pi})$ in $\boldsymbol{\pi}$, it suffices to show that $U(n, \boldsymbol{\pi}) = \mathbb{E}^{(\lambda)}[V(n + 1, \boldsymbol{\Pi}_{n+1}) | \boldsymbol{\Pi}_n = \boldsymbol{\pi}]$ is concave in $\boldsymbol{\pi}$ when $n = l$. Let $\boldsymbol{\pi} = \alpha \boldsymbol{\pi}^{(1)} + (1 - \alpha) \boldsymbol{\pi}^{(2)}$, for some $\boldsymbol{\pi}^{(1)}, \boldsymbol{\pi}^{(2)} \in \mathcal{S}$ and $\alpha \in (0, 1)$. Then by (13), we can write

$$\pi_n(\boldsymbol{\pi}, k) = \frac{\boldsymbol{\pi}' \tilde{\mathbf{P}}(\delta) \text{diag}(\tilde{\mathbf{d}}_k)}{\boldsymbol{\pi}' \tilde{\mathbf{P}}(\delta) \tilde{\mathbf{d}}_k} \triangleq \frac{\boldsymbol{\pi}' \mathbf{A}(k)}{\boldsymbol{\pi}' \mathbf{b}(k)}, \quad \forall n = 0, \dots, N - 1,$$

where $\mathbf{A}(k) \in \mathbb{R}^{(m_1+m_2) \times (m_1+m_2)}$ with the $(i-j)$ th entry being $\mathbf{A}(k)_{ij} \triangleq p_{ij}(\delta) \tilde{d}_{jk}$, and $\mathbf{b}(k) \in \mathbb{R}^{m_1+m_2}$ with the i th component being $\mathbf{b}(k)_i \triangleq \sum_{j=1}^{m_1+m_2} p_{ij}(\delta) \tilde{d}_{jk}$. Let $\tilde{\alpha} \triangleq \alpha \frac{(\boldsymbol{\pi}^{(1)})' \mathbf{b}(k)}{\boldsymbol{\pi}' \mathbf{b}(k)}$. Routine algebra then shows that

$$\pi_n(\boldsymbol{\pi}, k) = \tilde{\alpha} \frac{(\boldsymbol{\pi}^{(1)})' \mathbf{A}(k)}{(\boldsymbol{\pi}^{(1)})' \mathbf{b}(k)} + (1 - \tilde{\alpha}) \frac{(\boldsymbol{\pi}^{(2)})' \mathbf{A}(k)}{(\boldsymbol{\pi}^{(2)})' \mathbf{b}(k)}, \quad \forall n = 1, \dots, N - 1.$$

Note that the map from α to $\tilde{\alpha}$ is one-to-one from $[0, 1]$ to $[0, 1]$. Therefore, we see that

$$\begin{aligned} V(l + 1, \boldsymbol{\pi}_{l+1}(\boldsymbol{\pi}, k)) &= V\left(l + 1, \frac{\boldsymbol{\pi}' \mathbf{A}(k)}{\boldsymbol{\pi}' \mathbf{b}(k)}\right) = V\left(l + 1, \tilde{\alpha} \frac{(\boldsymbol{\pi}^{(1)})' \mathbf{A}(k)}{(\boldsymbol{\pi}^{(1)})' \mathbf{b}(k)} + (1 - \tilde{\alpha}) \frac{(\boldsymbol{\pi}^{(2)})' \mathbf{A}(k)}{(\boldsymbol{\pi}^{(2)})' \mathbf{b}(k)}\right) \\ &\geq \tilde{\alpha} V\left(l + 1, \frac{(\boldsymbol{\pi}^{(1)})' \mathbf{A}(k)}{(\boldsymbol{\pi}^{(1)})' \mathbf{b}(k)}\right) + (1 - \tilde{\alpha}) V\left(l + 1, \frac{(\boldsymbol{\pi}^{(2)})' \mathbf{A}(k)}{(\boldsymbol{\pi}^{(2)})' \mathbf{b}(k)}\right), \end{aligned}$$

where the inequality follows from the induction hypothesis that $V(l+1, \boldsymbol{\pi})$ is concave in $\boldsymbol{\pi}$.

Plugging the above inequality in (13) gives

$$\begin{aligned} U(l, \boldsymbol{\pi}) &= \sum_{k=1}^K \boldsymbol{\pi}' \mathbf{b}(k) V\left(l+1, \frac{\boldsymbol{\pi}' \mathbf{A}(k)}{\boldsymbol{\pi}' \mathbf{b}(k)}\right) \\ &\geq \sum_{k=1}^K \boldsymbol{\pi}' \mathbf{b}(k) \left[\tilde{\alpha} V\left(l+1, \frac{(\boldsymbol{\pi}^{(1)})' \mathbf{A}(k)}{(\boldsymbol{\pi}^{(1)})' \mathbf{b}(k)}\right) + (1-\tilde{\alpha}) V\left(l+1, \frac{(\boldsymbol{\pi}^{(2)})' \mathbf{A}(k)}{(\boldsymbol{\pi}^{(2)})' \mathbf{b}(k)}\right) \right] \\ &= \sum_{k=1}^K \left[\alpha (\boldsymbol{\pi}^{(1)})' \mathbf{b}(k) V\left(l+1, \frac{(\boldsymbol{\pi}^{(1)})' \mathbf{A}(k)}{(\boldsymbol{\pi}^{(1)})' \mathbf{b}(k)}\right) + (1-\alpha) (\boldsymbol{\pi}^{(2)})' \mathbf{b}(k) V\left(l+1, \frac{(\boldsymbol{\pi}^{(2)})' \mathbf{A}(k)}{(\boldsymbol{\pi}^{(2)})' \mathbf{b}(k)}\right) \right] \\ &= \alpha U(l, \boldsymbol{\pi}^{(1)}) + (1-\alpha) U(l, \boldsymbol{\pi}^{(2)}), \end{aligned}$$

which shows $U(l, \boldsymbol{\pi})$ is concave in $\boldsymbol{\pi}$.

Since the minimum operator preserves concavity, $V(n, \boldsymbol{\pi})$ is also concave in $\boldsymbol{\pi}$ when $n = l$. This completes the induction.

We then show that $V(n, \boldsymbol{\pi})$ is piecewise linear for all $n = 0, \dots, N$. Assume that the value function is piecewise linear in $\boldsymbol{\pi}$ for all $n = l+1, \dots, N$, so $V(n, \boldsymbol{\pi}) = \max_{\boldsymbol{\alpha} \in \mathcal{A}} \boldsymbol{\alpha}' \boldsymbol{\pi}$ for some finite set \mathcal{A} , where $\boldsymbol{\alpha} = (\alpha_j)_{j=1}^{m_1+m_2}$. Then for $n = l$, we already show that $V_{\text{ab}}(l, \boldsymbol{\pi})$ is linear in $\boldsymbol{\pi}$. Moreover, routine algebra shows that

$$V_c(l, \boldsymbol{\pi}) = \kappa(w_l, \boldsymbol{\pi}) + \sum_{k=1}^K \max_{\boldsymbol{\alpha} \in \mathcal{A}} \sum_{i=1}^{m_1+m_2} \sum_{j=1}^{m_1+m_2} \pi_i p_{ij}(\delta) d_{jk} \alpha_j.$$

Since $\kappa(w_n, \boldsymbol{\pi})$ is linear in $\boldsymbol{\pi}$, the above display is clearly piecewise linear in $\boldsymbol{\pi}$ as well. Since $V(n, \boldsymbol{\pi})$ is a pointwise minimum of a linear function and a piecewise linear function, we have $V(n, \boldsymbol{\pi})$ is also piecewise linear in $\boldsymbol{\pi}$ for any fixed n . \square

A.5. Proof of Lemma 3

We first show the monotonicity of $p_{i, m_1+m_2+1}(t)$ in i by induction. First, $p_{m_1+m_2+1, m_1+m_2+1}(t) = 1$, and by solving the Kolmogorov backward equation, $p_{m_1+m_2, m_1+m_2+1}(t) = 1 - \exp(-\lambda t) < 1$. For induction, assume $p_{i, m_1+m_2+1}(t) \leq p_{i+1, m_1+m_2+1}(t) \leq \dots \leq p_{m_1+m_2+1, m_1+m_2+1}(t)$ for some $i = 2, \dots, m_1+m_2$. We consider three cases to show $p_{i-1, m_1+m_2+1}(t) \leq p_{i, m_1+m_2+1}(t)$.

Case 1: $i-1 > m_1$. By the Kolmogorov backward equation and noting $p_{m_1+m_2+1, m_1+m_2+1}(t) = 1$,

$$p'_{i-1, m_1+m_2+1}(t) = \lambda(1 - p_{i-m_1-1}(\lambda)) p_{i, m_1+m_2+1}(t) + \lambda p_{i-m_1-1}(\lambda) - \lambda p_{i-1, m_1+m_2+1}(t),$$

yielding

$$p_{i-1, m_1+m_2+1}(t) = \lambda \int_0^t \exp(\lambda(u-t)) [(1 - p_{i-m_1-1}(\lambda)) p_{i, m_1+m_2+1}(u) + p_{i-m_1-1}(\lambda)] du.$$

Similarly, we can solve

$$p_{i,m_1+m_2+1}(t) = \lambda \int_0^t \exp(\lambda(u-t))[(1-p_{i-m_1}(\lambda))p_{i+1,m_1+m_2+1}(u) + p_{i-m_1}(\lambda)]du.$$

Then it suffices to show $(1-p_{i-m_1}(\lambda))p_{i+1,m_1+m_2+1}(u) + p_{i-m_1}(\lambda) \geq (1-p_{i-m_1-1}(\lambda))p_{i,m_1+m_2+1}(u) + p_{i-m_1-1}(\lambda)$, which holds because

$$\begin{aligned} (1-p_{i-m_1}(\lambda))p_{i+1,m_1+m_2+1}(u) + p_{i-m_1}(\lambda) &\geq (1-p_{i-m_1}(\lambda))p_{i,m_1+m_2+1}(u) + p_{i-m_1}(\lambda) \\ &= p_{i,m_1+m_2+1}(u) + p_{i-m_1}(\lambda)(1-p_{i,m_1+m_2+1}(u)) \geq p_{i,m_1+m_2+1}(u) + p_{i-m_1-1}(\lambda)(1-p_{i,m_1+m_2+1}(u)). \end{aligned}$$

Here, the first inequality follows from the induction hypothesis, and the second inequality follows from Assumption 1.

Case 2: $i-1 = m_1$. Similarly, we can solve the Kolmogorov backward equations for $p_{m_1,m_1+m_2+1}(t)$ and $p_{m_1+1,m_1+m_2+1}(t)$, where

$$p_{m_1,m_1+m_2+1}(t) = \int_0^t \exp(\lambda(u-t))[\zeta + (\lambda - \zeta)p_{m_1+1,m_1+m_2+1}(u)]du,$$

and $p_{m_1+1,m_1+m_2+1}(t)$ is given in Case 1 by letting $i = m_1 + 1$. Then it suffices to show $\zeta + (\lambda - \zeta)p_{m_1+1,m_1+m_2+1}(u) \leq \lambda[p_1(\lambda)(1-p_{m_1+2,m_1+m_2+1}(u)) + p_{m_1+2,m_1+m_2+1}(u)]$, which is true as

$$\begin{aligned} \zeta + (\lambda - \zeta)p_{m_1+1,m_1+m_2+1}(u) &\leq \zeta + (\lambda - \zeta)p_{m_1+2,m_1+m_2+1}(u) \\ &= \zeta(1-p_{m_1+2,m_1+m_2+1}(u)) + \lambda p_{m_1+2,m_1+m_2+1}(u) \\ &\leq \lambda[p_1(\lambda)(1-p_{m_1+2,m_1+m_2+1}(u)) + p_{m_1+2,m_1+m_2+1}(u)]. \end{aligned}$$

Here, the first inequality follows from the induction hypothesis. The second inequality follows from Assumption 1 and Lemma 1 where for $\lambda > \bar{\lambda}$, we have $\zeta \leq \lambda F(1/\lambda) = \lambda p_1(\lambda)$.

Case 3: $i-1 < m_1$. We can again solve the Kolmogorov backward equation to obtain

$$\begin{aligned} p_{i-1,m_1+m_2+1}(t) &= \int_0^t \exp(\lambda(u-t))[\zeta + (\lambda - \zeta)p_{i,m_1+m_2+1}(u)]du; \\ p_{i,m_1+m_2+1}(t) &= \int_0^t \exp(\lambda(u-t))[\zeta + (\lambda - \zeta)p_{i+1,m_1+m_2+1}(u)]du. \end{aligned}$$

It is then easy to see $p_{i-1,m_1+m_2+1}(t) \leq p_{i,m_1+m_2+1}(t)$ due to the induction hypothesis.

We then show the monotonicity of $V_{ab}(n, \boldsymbol{\pi})$ and $V_c(n, \boldsymbol{\pi})$. The value function for abort is $V_{ab}(n, \boldsymbol{\pi}) = C_m + C_s \kappa(w_n, \boldsymbol{\pi})$. We show that $\kappa(w_n, \boldsymbol{\pi})$ is monotone likelihood ratio (MLR) increasing in $\boldsymbol{\pi}$ for all $n = 1, \dots, N-1$. Indeed, recall $\kappa(w_n, \boldsymbol{\pi}) = \sum_{i=1}^{m_1+m_2} \pi_i p_{i,m_1+m_2+1}(w_n)$. By Lemma 3, $p_{i,m_1+m_2+1}(\delta)$ is nondecreasing in i . The MLR monotonicity of $\kappa(w_n, \boldsymbol{\pi})$ in $\boldsymbol{\pi}$ then follows from the fact that $\sum_j \pi_j^{(1)} f(j) \geq \sum_j \pi_j^{(2)} f(j)$ for any nondecreasing function f and $\boldsymbol{\pi}^{(1)}, \boldsymbol{\pi}^{(2)} \in \mathcal{S}$ such that $\boldsymbol{\pi}^{(1)} \succeq_{LR} \boldsymbol{\pi}^{(2)}$ (Shaked and Shanthikumar 2007). To show the monotone property of

$V_{\text{ab}}(n, \boldsymbol{\pi})$ in n , we note that w_n is nondecreasing in n by Assumption 3. Hence, $\kappa(w_n, \boldsymbol{\pi}) = \sum_{i=1}^{m_1+m_2} \pi_i p_{i, m_1+m_2+1}(w_n)$ is nondecreasing with n for any fixed $\boldsymbol{\pi} \in \mathcal{S}$, whence $V_{\text{ab}}(n, \boldsymbol{\pi})$ is also nondecreasing with n .

For the function $\bar{V}_c(n, \boldsymbol{\pi})$, we have

$$\begin{aligned} \bar{V}_c(n, \boldsymbol{\pi}) &= (C_m + C_s) \kappa((N-n)\delta + w_N, \boldsymbol{\pi}) \\ &= (C_m + C_s) \sum_{i=1}^{m_1+m_2} \pi_i p_{i, m_1+m_2+1}((N-n)\delta + w_N). \end{aligned}$$

Note that the term $(N-n)\delta + w_N$ is nonincreasing with n . By the same way, we can prove $\bar{V}_c(n, \boldsymbol{\pi})$ is MLR increasing with $\boldsymbol{\pi}$ and nonincreasing with n . \square

Remark. We remark that the construction of $G^{(\lambda)}$ using $\lambda - \zeta$ in (3) leads to identical transition rates out of any transient state, facilitating the analysis in Case 2 in the above proof.

A.6. Proof of Theorem 2

Based on Lemma 3, if

$$V_{\text{ab}}(n, \boldsymbol{\pi}) \geq \bar{V}_c(n, \boldsymbol{\pi}) \geq V_c(n, \boldsymbol{\pi}), \quad \forall n = 1, \dots, N-1, \boldsymbol{\pi} \in \mathcal{S}, \quad (\text{EC.1})$$

then the mission is never aborted during the mission time $[0, H]$. Note that $V_{\text{ab}}(0, \mathbf{e}_1) < V_{\text{ab}}(n, \boldsymbol{\pi})$ for all $n > 1$ and $\boldsymbol{\pi} \in \mathcal{S}$, where the inequality follows from Lemma 3. Similarly, we have $\bar{V}_c(0, \mathbf{e}_{m_1+m_2}) > \bar{V}_c(n, \boldsymbol{\pi})$ for all $n > 1$ and $\boldsymbol{\pi} \in \mathcal{S}$ by monotonicity of $\bar{V}_c(\cdot)$. Then a sufficient condition for (EC.1) to hold is $V_{\text{ab}}(0, \mathbf{e}_1) \geq \bar{V}_c(0, \mathbf{e}_{m_1+m_2})$, i.e., $C_m \geq (C_s + C_m)(1 - \exp[-\lambda(T + w_N)])$, where we use the property $w_0 = 0$. Routine algebra yields Eq. (16). \square

A.7. Proof of Theorem 3

By Lemma 3, $V_{\text{ab}}(n, \boldsymbol{\pi})$ and $\bar{V}_c(n, \boldsymbol{\pi})$ are, respectively, nondecreasing and nonincreasing in n for any given $\boldsymbol{\pi}$. Hence, for any given $\boldsymbol{\pi} \in \mathcal{S}$, there may exist a threshold $\hat{n}(\boldsymbol{\pi})$ dependent on $\boldsymbol{\pi}$ such that $V_{\text{ab}}(n, \boldsymbol{\pi}) \geq \bar{V}_c(n, \boldsymbol{\pi})$ for all $n \geq \hat{n}(\boldsymbol{\pi})$ and $V_{\text{ab}}(n, \boldsymbol{\pi}) < \bar{V}_c(n, \boldsymbol{\pi})$ for all $n < \hat{n}(\boldsymbol{\pi})$. Let $\hat{n} \triangleq \max_{\boldsymbol{\pi} \in \mathcal{S}} \hat{n}(\boldsymbol{\pi})$. Then we see $V_{\text{ab}}(n, \boldsymbol{\pi}) \geq \bar{V}_c(n, \boldsymbol{\pi}) \geq V_c(n, \boldsymbol{\pi})$ for all $n \geq \hat{n}$ and $\boldsymbol{\pi} \in \mathcal{S}$. This tallies with the theorem statement that the optimal action is to continue the mission when $n \geq \hat{n}$, no matter of the observed signals. As such, it is easy to see $V(n, \boldsymbol{\pi}) = \bar{V}_c(n, \boldsymbol{\pi})$ for all $\boldsymbol{\pi} \in \mathcal{S}$, $n = \hat{n}, \dots, N-1$, by the definition of $\bar{V}_c(n, \boldsymbol{\pi})$. \square

A.8. Proof of Lemma 4

We first show the following lemma for the transition probability matrix $\tilde{\mathbf{P}}(\delta)$ defined in Section 4.2.

LEMMA EC.1. *The matrix $\tilde{\mathbf{P}}(t)$ is totally positive of order 2 (TP2) for all $t > 0$.*

Proof of Lemma EC.1: Let $\Delta_{ij}(t) \triangleq p_{ik}(t)p_{jl}(t) - p_{il}(t)p_{jk}(t)$ for $i, j \in [m_1 + m_2]$ and some fixed $k, l \in [m_1 + m_2]$. Note $\Delta_{ii}(t) = 0$ for all $i \in [m_1 + m_2]$ and $t > 0$. Without loss of generality, it suffices to show $\Delta_{ij}(t) \geq 0$ for all $t > 0$ when $i < j$ and $k < l$. If $k < j$, then $\Delta_{ij}(t) = p_{ik}(t)p_{jl}(t) \geq 0$. Thus it suffices to prove $\Delta_{ij}(t) \geq 0$ for $i < j \leq k < l$. We show this by following an exhaustive list of cases.

Case 1: $i < j = k < l \leq m_1$. We can use the Kolmogorov backward equation to show $\Delta'_{ij}(t) = -2\lambda\Delta_{ij}(t) + (\lambda - \zeta)[\Delta_{i+1,j}(t) + p_{j+1,l}(t)p_{ik}(t)]$, which yields $\Delta_{ij}(t) = (\lambda - \zeta) \int_0^t \exp(2\lambda(u - t))(\Delta_{i+1,j}(u) + p_{j+1,l}(u)p_{ik}(u))du$. Due to the recursive formula, it suffices to show $\Delta_{ij}(t) \geq 0$ when $i = k - 1$ and $j = k$ for any fixed k and l . This holds as $\Delta_{k-1,k}(t) = (\lambda - \zeta) \int_0^t \exp(2\lambda(u - t))(\Delta_{kk}(u) + p_{k+1,l}(u)p_{k-1,k}(u))du \geq 0$.

Case 2: $i < j < k < l \leq m_1$. We can use the Kolmogorov backward equation to show $\Delta'_{ij}(t) = -2\lambda\Delta_{ij}(t) + (\lambda - \zeta)[\Delta_{i+1,j}(t) + \Delta_{i,j+1}(t)]$, which yields $\Delta_{ij}(t) = (\lambda - \zeta) \int_0^t \exp(2\lambda(u - t))(\Delta_{i+1,j}(u) + \Delta_{i,j+1}(u))du$. Based on the recursive formula and $\Delta_{ii} = 0$, it suffices to show $\Delta_{i,k-1}(t) \geq 0$ for all $i < k - 1$. As $\Delta_{k-1,k-1}(t) = 0$ and we show $\Delta_{k-2,k}(t) \geq 0$ in Case 1, we can use the recursive formula to show $\Delta_{k-2,k-1}(t) \geq 0$. We then use the recursive formula again to show $\Delta_{i,k-1}(t) \geq 0$ for $i < k - 2$.

Case 3: $i < j \leq k \leq m_1 < l$. When $j = k$, the proof follows the same procedure as in Case 1. When $j < k$, the proof follows the same procedure as in Case 2.

Case 4: $m_1 < i < j \leq k < l$. We can first use nearly the same proof as in Cases 1 for $j = k$ and then follow nearly the same proof for Case 2 to show $\Delta_{ij}(t) \geq 0$ for $j < k$.

Case 5: $i \leq m_1 < j \leq k < l$. We can solve the Kolmogorov backward equation to obtain $\Delta_{ij}(t) = \int_0^t \exp(2\lambda(u - t))[(\lambda - \zeta)\Delta_{i+1,j}(u) + \lambda(1 - p_{j-m_1}(\lambda))p_{ik}(u)p_{j+1,l}(u)]du$ when $j = k$ and $\Delta_{ij}(t) = \int_0^t \exp(2\lambda(u - t))[(\lambda - \zeta)\Delta_{i+1,j}(u) + \lambda(1 - p_{j-m_1}(\lambda))\Delta_{i,j+1}(u)]du$ when $j < k$. Using the recursive formula, it suffices to show $\Delta_{m_1,k}(t) \geq 0$. We can show this by using the recursive formula again and noting $\Delta_{m_1+1,k}(t) \geq 0$ as shown in Case 4.

Case 6: $i < j \leq m_1 < k < l$. Similar to Case 2, we have $\Delta_{ij}(t) = (\lambda - \zeta) \int_0^t \exp(2\lambda(u - t))(\Delta_{i+1,j}(u) + \Delta_{i,j+1}(u))du$. Based on this recursion, $\Delta_{ij}(t) \geq 0$ if $\Delta_{i,m_1}(t) \geq 0$ for all $i < m_1$. We can use the recursive formula to show $\Delta_{m_1-1,m_1}(t) \geq 0$, as $\Delta_{m_1,m_1}(t) = 0$ and $\Delta_{m_1-1,m_1+1}(t) \geq 0$ as shown in Case 5. Again using the recursive formula shows $\Delta_{ij}(t) \geq 0$ for all i, j in this case.

Since the above proof is for all possible values of k, l , we conclude that $\tilde{\mathbf{P}}(\delta)$ is TP2. We remark that the CTMC construction in Figure 1 significantly simplifies the Kolmogorov backward equations, hence facilitating the proof of the TP2 property for $\tilde{\mathbf{P}}(t)$. \square

We now show the first statement of Lemma 4 on the MLR ordering of $\pi_n(\pi, k)$ with respect to π . We have $\pi_n(\pi, k) \propto \pi' \tilde{\mathbf{P}}(\delta) \text{diag}(\tilde{\mathbf{d}}_k)$ based on (13). By Lemma EC.1, $\tilde{\mathbf{P}}(\delta)$ is TP2. Moreover, $\text{diag}(\tilde{\mathbf{d}}_k)$ is TP2 as any diagonal matrix is TP2 by definition. By Karlin and Rinott (1980, Theorem 1.2), the product of two TP2 matrices is TP2. Since the MLR ordering is preserved by right multiplying a TP2 matrix, we see $\pi_n(\pi^{(1)}, k) \succeq_{\text{LR}} \pi_n(\pi^{(2)}, k)$ for any $\pi^{(1)} \succeq_{\text{LR}} \pi^{(2)}$.

We then show the second statement on the MLR ordering of $\pi_n(\pi, k)$ with respect to k . By definition of MLR ordering, it suffices to show for any $k_1 \geq k_2$,

$$\frac{\pi_{ni}(\pi, k_1)}{\pi_{ni}(\pi, k_2)} \geq \frac{\pi_{nj}(\pi, k_1)}{\pi_{nj}(\pi, k_2)}, \quad \forall i > j.$$

Based on Equation (13), the above inequality is equivalent to

$$\frac{\tilde{d}_{ik_1}}{\tilde{d}_{ik_2}} \geq \frac{\tilde{d}_{jk_1}}{\tilde{d}_{jk_2}}, \quad \forall i > j.$$

This is satisfied by Assumption 2 that the state-observation matrix \mathbf{D} is TP2. \square

Remark. An alternative proof of Lemma EC.1 is to use the fact that a tridiagonal matrix \mathbf{P} is TP2 if and only if $\mathbf{P}_{ii}\mathbf{P}_{i+1,i+1} \geq \mathbf{P}_{i,i+1}\mathbf{P}_{i+1,i}$ for all i (Krishnamurthy 2011). By our construction of the CTMC in Figure 1, $\tilde{\mathbf{P}}(t)$ trivially satisfies the above inequality. This underscores the benefit of constructing the CTMC as in Figure 1.

A.9. Proof of Lemma 5

We first prove the MLR monotonicity of $V_c(n, \pi)$ in $\pi \in \mathcal{S}$ by induction. When $n = N - 1$, $V_c(N - 1, \pi) = (C_s + C_m)\kappa(\delta + w_N, \pi)$, and the MLR monotonicity holds since $\kappa(\delta + w_N, \pi)$ is MLR increasing in $\pi \in \mathcal{S}$. Next assume that $V_c(n, \pi)$ is MLR increasing in $\pi \in \mathcal{S}$ for all $n = l + 1, \dots, N - 1$, so $V(n, \pi)$ also has this MLR monotone property for $n = l + 1, \dots, N - 1$. Then for $n = l$, we have

$$V_c(l, \pi) = (C_m + C_s)\kappa(\delta, \pi) + \sum_{k=1}^K V(l + 1, \pi_{l+1}(\pi, k)) \sum_{i=1}^{m_1+m_2} \pi_i \sum_{j=1}^{m_1+m_2} p_{ij}(\delta) \tilde{d}_{jk},$$

where $\tilde{d}_{jk} \triangleq d_{1k}$ for $j \in \mathcal{X}_1$ and $\tilde{d}_{jk} \triangleq d_{2k}$ for $j \in \mathcal{X}_2$. Let $\tilde{h}(k, \pi) \triangleq \sum_{i=1}^{m_1+m_2} \pi_i \sum_{j=1}^{m_1+m_2} p_{ij}(\delta) \tilde{d}_{jk}$ be the conditional probability that the next observed signal is $k \in [K]$ given the current belief state π . Then we show that the likelihood ratio $\tilde{h}(k, \pi^{(1)})/\tilde{h}(k, \pi^{(2)})$ is increasing in k for any $\pi^{(1)} \succeq_{\text{LR}} \pi^{(2)}$. Indeed, the transition matrix $\tilde{\mathbf{P}}(\delta)$ are TP2 by Lemma EC.1. Let $\tilde{\pi}^{(i)} \triangleq \tilde{\mathbf{P}}(\delta)\pi^{(i)}$, $i = 1, 2$. Since $\pi^{(1)} \succeq_{\text{LR}} \pi^{(2)}$ and $\tilde{\mathbf{P}}(\delta)$ is TP2, we have $\tilde{\pi}^{(1)} \succeq_{\text{LR}} \tilde{\pi}^{(2)}$ by Lovejoy (1987, Lemma 1.3). For any $k_1 > k_2$, we have

$$\frac{\sum_{i=1}^{m_1+m_2} \tilde{\pi}_i^{(1)} \tilde{d}_{ik_1}}{\sum_{i=1}^{m_1+m_2} \tilde{\pi}_i^{(2)} \tilde{d}_{ik_1}} \geq \frac{\sum_{i=1}^{m_1+m_2} \tilde{\pi}_i^{(1)} \tilde{d}_{ik_2}}{\sum_{i=1}^{m_1+m_2} \tilde{\pi}_i^{(2)} \tilde{d}_{ik_2}} \Leftrightarrow \sum_{i=1}^{m_1+m_2} \sum_{j=1}^{i-1} (\tilde{\pi}_i^{(1)} \tilde{\pi}_j^{(2)} - \tilde{\pi}_j^{(1)} \tilde{\pi}_i^{(2)}) (\tilde{d}_{ik_1} \tilde{d}_{jk_2} - \tilde{d}_{ik_2} \tilde{d}_{jk_1}) \geq 0.$$

The last inequality holds because (i) $\tilde{\pi}_i^{(1)} \tilde{\pi}_j^{(2)} - \tilde{\pi}_j^{(1)} \tilde{\pi}_i^{(2)} \geq 0$ for all $i > j$ due to $\tilde{\pi}^{(1)} \succeq_{\text{LR}} \tilde{\pi}^{(2)}$ and (ii) $\tilde{d}_{ik_1} \tilde{d}_{jk_2} - \tilde{d}_{ik_2} \tilde{d}_{jk_1} \geq 0$ for all $k_1 > k_2$ due to the assumption that \mathcal{D} is TP2 so $\tilde{\mathbf{d}}_{k_1} \succeq_{\text{LR}} \tilde{\mathbf{d}}_{k_2}$.

For $\pi^{(1)} \succeq_{\text{LR}} \pi^{(2)}$, recall that $\pi_n(\pi, k)$ is MLR increasing in π and k for fixed n by Lemma 4. It then follows that

$$\begin{aligned} \sum_{k=1}^K V(l + 1, \pi_{l+1}(\pi^{(1)}, k)) \tilde{h}(k, \pi^{(1)}) &\geq \sum_{k=1}^K V(l + 1, \pi_{l+1}(\pi^{(1)}, k)) \tilde{h}(k, \pi^{(2)}) \\ &\geq \sum_{k=1}^K V(l + 1, \pi_{l+1}(\pi^{(2)}, k)) \tilde{h}(k, \pi^{(2)}), \end{aligned}$$

where the first inequality follows from $(\tilde{h}(k, \boldsymbol{\pi}^{(1)}))_{k=1}^K \succeq_{\text{LR}} (\tilde{h}(k, \boldsymbol{\pi}^{(2)}))_{k=1}^K$, the induction hypothesis, and the MLR monotonicity of $\boldsymbol{\pi}_n(\boldsymbol{\pi}, k)$ in k , and the second inequality follows from the induction hypothesis and the MLR monotonicity of $\boldsymbol{\pi}_n(\boldsymbol{\pi}, k)$ in $\boldsymbol{\pi}$. Together with the MLR monotonicity of $\kappa(\delta, \boldsymbol{\pi})$ in $\boldsymbol{\pi} \in \mathcal{S}$, we see that $V_c(l, \boldsymbol{\pi})$ is also MLR increasing in $\boldsymbol{\pi} \in \mathcal{S}$.

We have shown the MLR monotonicity of $V_{\text{ab}}(n, \boldsymbol{\pi})$ with $\boldsymbol{\pi} \in \mathcal{S}$ for all $n = 0, \dots, N-1$ in the proof of Lemma 3. Since $V(n, \boldsymbol{\pi}) = \min\{V_{\text{ab}}(n, \boldsymbol{\pi}), V_c(n, \boldsymbol{\pi})\}$, its MLR monotonicity in $\boldsymbol{\pi} \in \mathcal{S}$ follows directly from the monotone properties of $V_{\text{ab}}(n, \boldsymbol{\pi})$ and $V_c(n, \boldsymbol{\pi})$. \square

A.10. Proof of Lemma 6

Assume on the opposite that there exists n such that $V_c(n-1, \mathbf{e}_{m_1+m_2}) < V_{\text{ab}}(n-1, \mathbf{e}_{m_1+m_2})$ and $V_c(n, \mathbf{e}_{m_1+m_2}) > V_{\text{ab}}(n, \mathbf{e}_{m_1+m_2})$. We then have

$$\begin{aligned} V_c(n-1, \mathbf{e}_{m_1+m_2}) &= C_m \kappa(\delta, \mathbf{e}_{m_1+m_2}) + V(n, \mathbf{e}_{m_1+m_2})(1 - \kappa(\delta, \mathbf{e}_{m_1+m_2})) \\ &= C_m + C_s(p_{m_1+m_2, m_1+m_2+1}(\delta) + p_{m_1+m_2, m_1+m_2}(\delta)p_{m_1+m_2, m_1+m_2+1}(w_n)), \end{aligned}$$

where the second equality follows from $V(n, \mathbf{e}_{m_1+m_2}) = V_{\text{ab}}(n, \mathbf{e}_{m_1+m_2})$. Moreover, we have

$$V_{\text{ab}}(n-1, \mathbf{e}_{m_1+m_2}) = C_m + C_s p_{m_1+m_2, m_1+m_2+1}(w_{n-1}).$$

Then $V_c(n-1, \mathbf{e}_{m_1+m_2}) < V_{\text{ab}}(n-1, \mathbf{e}_{m_1+m_2})$ is equivalent to

$$p_{m_1+m_2, m_1+m_2+1}(\delta) + p_{m_1+m_2, m_1+m_2}(\delta)p_{m_1+m_2, m_1+m_2+1}(w_n) < p_{m_1+m_2, m_1+m_2+1}(w_{n-1}).$$

We note that left and right hand side of the above inequality are the system failure probabilities in the next $\delta + w_n$ and w_{n-1} time units, respectively. Since w_n is nondecreasing in n by Assumption 3, we have $\delta + w_n > w_{n-1}$, so that $p_{m_1+m_2, m_1+m_2+1}(\delta) + p_{m_1+m_2, m_1+m_2}(\delta)p_{m_1+m_2, m_1+m_2+1}(w_n) > p_{m_1+m_2, m_1+m_2+1}(w_{n-1})$. This leads to a contradiction. \square

A.11. Proof of Proposition 2

For any $1 \leq j < i < m_1 + m_2$, we have $\pi_{1i}/\pi_{1j} = \pi_{2i}/\pi_{2j}$ based on the inverse transform of the Cartesian belief vector in Table 1. For any $1 < j < i = m_1 + m_2$ and $l \in \{1, 2\}$, we have

$$\frac{\pi_{m_1+m_2}^{(l)}}{\pi_j^{(l)}} = \frac{1 + r_l \cos \phi_{m_1+m_2-1} \prod_{k=1}^{m_1+m_2-2} \sin \phi_k}{r_l \cos \phi_{j-1} \prod_{k=1}^{j-2} \sin \phi_k} = \frac{1/r_l + \cos \phi_{m_1+m_2-1} \prod_{k=1}^{m_1+m_2-2} \sin \phi_k}{\cos \phi_{j-1} \prod_{k=1}^{j-2} \sin \phi_k}.$$

We then have $\pi_{m_1+m_2}^{(1)}/\pi_j^{(1)} > \pi_{m_1+m_2}^{(2)}/\pi_j^{(2)}$ as $r_1 < r_2$. We can similarly prove such an inequality for $1 = j < i = m_1 + m_2$. Based on all the above cases, we can conclude $\boldsymbol{\pi}^{(1)} \succeq_{\text{LR}} \boldsymbol{\pi}^{(2)}$. \square

A.12. Proof of Theorem 4

We first consider the case $n \leq \tilde{n}$, where $V_{\text{ab}}(n, \mathbf{e}_{m_1+m_2}) \leq V_c(n, \mathbf{e}_{m_1+m_2})$. Recall that $r(\boldsymbol{\pi})$ and $\Phi(\boldsymbol{\pi})$ are the radius and spherical angle of $\boldsymbol{\pi}$ in the spherical coordinate system with origin $\mathbf{e}_{m_1+m_2}$, respectively. Define the subsimplex $\mathcal{S}_{-(m_1+m_2)} \triangleq \{\boldsymbol{\pi} \in \mathcal{S} : \pi_{m_1+m_2} = 0\}$. For any $\boldsymbol{\pi}_0 \in \mathcal{S}_{-(m_1+m_2)}$, we consider the line segment $\mathcal{S}(\boldsymbol{\pi}_0) = \{\boldsymbol{\pi} \in \mathcal{S} : \Phi(\boldsymbol{\pi}) = \Phi(\boldsymbol{\pi}_0), 0 \leq r(\boldsymbol{\pi}) \leq r(\boldsymbol{\pi}_0)\}$. We then consider the value function restricted on this line segment $\{V(n, \boldsymbol{\pi})\}_{\boldsymbol{\pi} \in \mathcal{S}(\boldsymbol{\pi}_0)}$ and write this function in the spherical coordinates as $\tilde{V}(n, r, \Phi(\boldsymbol{\pi}_0))$. Similarly, we write $\tilde{V}_{\text{ab}}(n, r, \Phi(\boldsymbol{\pi}_0))$ and $\tilde{V}_c(n, r, \Phi(\boldsymbol{\pi}_0))$ for $V_{\text{ab}}(n, \boldsymbol{\pi})$ and $V_c(n, \boldsymbol{\pi})$ on this line segment, respectively. For any fixed $\boldsymbol{\pi}_0$ and the spherical angle $\Phi(\boldsymbol{\pi}_0)$, the function $\tilde{V}_{\text{ab}}(n, r, \Phi(\boldsymbol{\pi}_0))$ is linear in r because $V_{\text{ab}}(n, \boldsymbol{\pi})$ is linear in $\boldsymbol{\pi}$ and π_i is linear in r for all $i \in [m_1 + m_2]$ as shown in Table 1. Moreover, $\tilde{V}_c(n, r, \Phi(\boldsymbol{\pi}_0))$ is concave in r given $\Phi(\boldsymbol{\pi}_0)$, because $V_c(n, \boldsymbol{\pi})$ is concave in $\boldsymbol{\pi}$ by Lemma 2 and π_i is linear in r for all $i \in [m_1 + m_2]$. In the spherical coordinate system, $V_{\text{ab}}(n, \mathbf{e}_{m_1+m_2}) \leq V_c(n, \mathbf{e}_{m_1+m_2})$ translates into $\tilde{V}_{\text{ab}}(n, 0, \Phi(\boldsymbol{\pi})) \leq \tilde{V}_c(n, 0, \Phi(\boldsymbol{\pi}))$ for all $\boldsymbol{\pi}$. Then by the concavity of $\tilde{V}_c(n, r, \Phi)$ and linearity of $\tilde{V}_{\text{ab}}(n, r, \Phi)$ in $r \geq 0$, we can conclude that $\tilde{V}_c(n, r, \Phi)$ and $\tilde{V}_{\text{ab}}(n, r, \Phi)$ have at most one intersection in the interval $0 \leq r(\boldsymbol{\pi}) < r(\boldsymbol{\pi}_0)$ for any $\boldsymbol{\pi}_0 \in \mathcal{S}_{-(m_1+m_2)}$ and fixed $\Phi \triangleq \Phi(\boldsymbol{\pi}_0)$. If such an intersection exists, it is the threshold \bar{r}_n so that it is optimal to abort the mission when $r < \bar{r}_n$ and to continue the mission otherwise. If such an intersection does not exist, the mission would never be successfully executed, and we may set $\bar{r}_n = \infty$ for any $\boldsymbol{\pi}_0 \in \mathcal{S}_{-(m_1+m_2)}$.

We then consider the case $\tilde{n} < n < \hat{n}$. As in the previous case, we consider $\tilde{V}_c(n, r, \Phi)$ and $\tilde{V}_{\text{ab}}(n, r, \Phi)$ restricted on the line segment $\mathcal{S}(\boldsymbol{\pi}_0)$ for $0 \leq r \leq r(\boldsymbol{\pi}_0)$ and $\boldsymbol{\pi}_0 \in \mathcal{S}_{-(m_1+m_2)}$. When $\tilde{n} < n < \hat{n}$, we have $V_{\text{ab}}(n, 0, \Phi(\boldsymbol{\pi}_0)) > \tilde{V}_c(n, 0, \Phi(\boldsymbol{\pi}_0))$ for all $\boldsymbol{\pi}_0 \in \mathcal{S}_{-(m_1+m_2)}$. By the linearity of $\tilde{V}_{\text{ab}}(n, r, \Phi)$ in r and concavity of $\tilde{V}_c(n, r, \Phi)$ in r , there could be two scenarios: (a) There is no intersection between $\tilde{V}_{\text{ab}}(n, r, \Phi)$ and $\tilde{V}_c(n, r, \Phi)$ for the fixed $\Phi \triangleq \Phi(\boldsymbol{\pi}_0)$, so the mission abort is never executed; (b) There are two intersections of $\tilde{V}_{\text{ab}}(n, r, \Phi)$ and $\tilde{V}_c(n, r, \Phi)$, and we denote the two intersections by \bar{r}_{n1} and \bar{r}_{n2} such that $0 \leq \bar{r}_{n1} \leq \bar{r}_{n2} \leq r(\boldsymbol{\pi}_0)$ and $\tilde{V}_{\text{ab}}(n, r, \Phi) \leq \tilde{V}_c(n, r, \Phi)$ only when $r \in [\bar{r}_{n1}, \bar{r}_{n2}]$ for fixed $\Phi \triangleq \Phi(\boldsymbol{\pi}_0)$, which is the region for abort.

We last show that the region $\{\boldsymbol{\pi} \in \mathcal{S} : V_{\text{ab}}(n, \boldsymbol{\pi}) \leq V_c(n, \boldsymbol{\pi})\}$ is convex for all $n = 0, \dots, N$. Let $\boldsymbol{\pi}^{(1)}, \boldsymbol{\pi}^{(2)} \in \mathcal{S}$ be two belief states such that the corresponding optimal action is to abort the mission. Then we have $V(n, \boldsymbol{\pi}^{(l)}) = V_{\text{ab}}(n, \boldsymbol{\pi}^{(l)}) = C_m + C_s \kappa(w_n, \boldsymbol{\pi}^{(l)})$ for $l = 1, 2$. For some $\alpha \in (0, 1)$, let $\boldsymbol{\pi}' = \alpha \boldsymbol{\pi}^{(1)} + (1 - \alpha) \boldsymbol{\pi}^{(2)}$. By concavity of $V(n, \boldsymbol{\pi})$ in $\boldsymbol{\pi}$, we have $V(n, \boldsymbol{\pi}') \geq \alpha V(n, \boldsymbol{\pi}^{(1)}) + (1 - \alpha) V(n, \boldsymbol{\pi}^{(2)}) = V_{\text{ab}}(n, \boldsymbol{\pi}')$. Moreover, since $V(n, \boldsymbol{\pi}') \leq V_{\text{ab}}(n, \boldsymbol{\pi}')$ by definition, we can conclude $V(n, \boldsymbol{\pi}') = V_{\text{ab}}(n, \boldsymbol{\pi}')$, so the region for abort is convex for all $n = 0, \dots, N - 1$. \square

A.13. Proof of Corollary 1

We can follow the same proof of Theorem 4 to show that the structural results in Theorem 4(i) and (iii) still hold. Since we cannot find a time threshold for no abort, we need to replace \hat{n} with N and then follow the same proof to show that Theorem 4(ii) holds for $n = \tilde{n} + 1, \dots, N - 1$. \square

A.14. Proof of Proposition 3

We first consider condition (i). By definition of \hat{n} , there exists $\boldsymbol{\pi} \in \mathcal{S}$ such that $\bar{V}_c(\hat{n} - 1, \boldsymbol{\pi}) > V_{ab}(\hat{n} - 1, \boldsymbol{\pi})$. This inequality is equivalent to

$$\begin{aligned}
& (C_s + C_m)\kappa((N - \hat{n} + 1)\delta + w_N, \boldsymbol{\pi}) > C_m + C_s\kappa(w_{\hat{n}-1}, \boldsymbol{\pi}), \exists \boldsymbol{\pi} \in \mathcal{S} \\
\Leftrightarrow & C_s \sum_{i=1}^{m_1+m_2} \pi_i [p_{i,m_1+m_2+1}((N - \hat{n} + 1)\delta + w_N) - p_{i,m_1+m_2+1}(w_{\hat{n}-1})] \\
& + C_m \sum_{i=1}^{m_1+m_2} \pi_i p_{i,m_1+m_2+1}((N - \hat{n} + 1)\delta + w_N) > C_m, \exists \boldsymbol{\pi} \in \mathcal{S} \\
\Leftrightarrow & \max_{\boldsymbol{\pi} \in \mathcal{S}} C_s \sum_{i=1}^{m_1+m_2} \pi_i [p_{i,m_1+m_2+1}((N - \hat{n} + 1)\delta + w_N) - p_{i,m_1+m_2+1}(w_{\hat{n}-1})] \\
& + C_m \sum_{i=1}^{m_1+m_2} \pi_i p_{i,m_1+m_2+1}((N - \hat{n} + 1)\delta + w_N) > C_m.
\end{aligned}$$

Since \mathcal{S} is a probability simplex, it is clear that the optimal solution to the linear program on the left side of the last inequality is $\boldsymbol{\pi} = \mathbf{e}_l$ with $l = \arg \max_{i \in [m_1+m_2]} (C_s + C_m)p_{i,m_1+m_2+1}((N - \hat{n} + 1)\delta + w_N) - C_s p_{i,m_1+m_2+1}(w_{\hat{n}-1})$. The condition in the proposition statement ensures $l = m_1 + m_2$. Since abort is not executed at periods $n = \hat{n}, \dots, N - 1$, we have $\bar{V}_c(\hat{n} - 1, \boldsymbol{\pi}) = V_c(\hat{n} - 1, \boldsymbol{\pi})$ for all $\boldsymbol{\pi} \in \mathcal{S}$; in particular $\bar{V}_c(\hat{n} - 1, \mathbf{e}_{m_1+m_2}) = V_c(\hat{n} - 1, \mathbf{e}_{m_1+m_2})$. Then $\tilde{n} = \hat{n} - 1$ by definition of \tilde{n} .

We then prove the statement for condition (ii) by showing that this condition implies condition (i). Indeed, $p_{i,m_1+m_2+1}(w_{\hat{n}-1}) = 0$ for all $i \in [m_1 + m_2]$ when $w_{\hat{n}-1} = 0$. Since $p_{i,m_1+m_2+1}(t)$ is increasing in $i \in [m_1 + m_2]$ for all $t \geq 0$ by Lemma 3, it is clear that Problem (18) attains the maximum at $i^* = m_1 + m_2$. Condition (i) hence holds, and we have $\tilde{n} = \hat{n} - 1$. \square

A.15. Proof of Proposition 4

At each iteration, the function $\hat{V}^{(\tau)}(n, \boldsymbol{\pi})$ is the pointwise minimum of linear functions in $\boldsymbol{\pi}$, so it is concave in $\boldsymbol{\pi} \in \mathcal{S}$. We then use induction to prove the MLR monotonicity of $\hat{V}^{(\tau)}(n, \boldsymbol{\pi})$ in $\boldsymbol{\pi} \in \mathcal{S}$. At the last stage $N - 1$, we have $\hat{V}_c^{(\tau)}(N - 1, \boldsymbol{\pi}) = \kappa(\boldsymbol{\pi}, \delta)(C_s + C_m) + \mathbb{E}^{(\lambda)} [\hat{V}^{(\tau)}(N, \boldsymbol{\Pi}_N) \mid \boldsymbol{\Pi}_{N-1} = \boldsymbol{\pi}]$. Because $V(N, \boldsymbol{\pi})$ is linear in $\boldsymbol{\pi}$, the point-based value iteration (PBVI) algorithm can give the exact estimate of the terminal cost, i.e., $\hat{V}^{(\tau)}(N, \boldsymbol{\pi}) = V(N, \boldsymbol{\pi})$ for all τ , which is MLR increasing in $\boldsymbol{\pi}$ by Lemma 5. Then following the proof of Lemma 5, we can conclude $\mathbb{E}^{(\lambda)} [\hat{V}^{(\tau)}(N, \boldsymbol{\Pi}_N) \mid \boldsymbol{\Pi}_{N-1} = \boldsymbol{\pi}]$ is MLR increasing in $\boldsymbol{\pi}$. This shows $\hat{V}_c^{(\tau)}(N - 1, \boldsymbol{\pi})$ is MLR increasing in $\boldsymbol{\pi}$ for all τ . We can then replace $V(n, \boldsymbol{\pi})$ with $\hat{V}^{(\tau)}(n, \boldsymbol{\pi})$ in the proof of Lemma 5 and follow the same induction procedure to conclude $\hat{V}^{(\tau)}(n, \boldsymbol{\pi})$ is MLR increasing in $\boldsymbol{\pi}$ for $n = 0, \dots, N - 2$. \square

A.16. Proof of Corollary 2

Following a similar procedure as in the proof of Lemma 2, we can show that $V_c(n, \boldsymbol{\pi})$ is concave in $\boldsymbol{\pi}$ for all $n = 0, \dots, N$. When $n \leq \tilde{n}$, we have $V_{ab}(n, 1) < V_c(n, 1)$. By linearity of $V_{ab}(n, \boldsymbol{\pi})$ and

concavity of $V_c(n, \pi)$, there is at most one intersection between $V_{ab}(n, \pi)$ and $V_c(n, \pi)$ for $\pi \in [0, 1]$, which is the control limit $\underline{\pi}_n$. When $n > \tilde{n}$, we have $V_{ab}(n, 1) \geq V_c(n, 1)$. Again by linearity of $V_{ab}(n, \pi)$ and concavity of $V_c(n, \pi)$, there could be two scenarios, i.e., (i) there are two intersections between $V_{ab}(n, \pi)$ and $V_c(n, \pi)$ for $\pi \in [0, 1]$, which are the thresholds $\underline{\pi}_n$ and $\bar{\pi}_n$, and (ii) there is no intersection between $V_{ab}(n, \pi)$ and $V_c(n, \pi)$, so abort is never optimal. \square

A.17. Proof of Proposition 5

Note that there are $m_1 + m_2 = m_1 + 1$ states for the CTMC when $m_2 = 1$. Let π_n^- be the realization of the system state before observing the signal Y_n at time $n\delta$. Given the belief vector $\Pi_{n-1} = \pi_{n-1} = (\pi_{n-1,i})_{i \in \mathcal{X}_1 \cup \mathcal{X}_2}$, the i th coordinate of π_n^- is then written as $\pi_{ni}^- = \sum_{j=1}^{m_1+1} \pi_{n-1,j} p_{ji}(\delta)$. By noting $p_{m_1+1,i}(\delta) = 0$ for all $i \in [m_1]$, we can derive $\pi_{ni}^- = r_{n-1} \varphi_i(\Phi_{n-1})$ for all $i \in [m_1]$, where $r_{n-1} = r_{n-1}(\pi_{n-1})$ and $\Phi_{n-1} = \Phi_{n-1}(\pi_{n-1})$. We note $\sum_{i=1}^{m_1+1} \pi_{ni}^- < 1$ because it is likely that the system directly fails between two consecutive inspections. Nevertheless, since it is impossible to observe the signal $Y_n \in [K]$ if the system has failed before $n\delta$, $\sum_{i=1}^{m_1+1} \pi_{ni}^- < 1$ does not affect the constraint $\pi_n' \mathbf{1}_{m_1+1} = 1$ after observing the realization of $Y_n = y_n \in [K]$.

Assume the realization of Y_n is $y_n \in [K]$. Then the angle vector Φ_n after observing $Y_n = y_n$ is

$$\phi_{ni} = \arccos \frac{\pi_{n,i+1}}{\sqrt{\pi_{n,i+1}^2 + \cdots + (\pi_{n,m_1+1} - 1)^2 + \pi_{n1}^2}} \quad (\text{EC.2})$$

$$\begin{aligned} &= \arccos \left[\frac{\pi_{n,i+1}^- \tilde{d}_{i+1,y_n}}{\sum_{j=1}^{m_1+1} \pi_{nj}^- \tilde{d}_{j,y_n}} \left(\left(\frac{\pi_{n,i+1}^- \tilde{d}_{i+1,y_n}}{\sum_{j=1}^{m_1+1} \pi_{nj}^- \tilde{d}_{j,y_n}} \right)^2 + \cdots \right. \right. \\ &\quad \left. \left. + \left(\frac{-\sum_{j=1}^{m_1} \pi_{nj}^- \tilde{d}_{j,y_n}}{\sum_{j=1}^{m_1+1} \pi_{nj}^- \tilde{d}_{j,y_n}} \right)^2 + \left(\frac{\pi_{n1}^- \tilde{d}_{1,y_n}}{\sum_{j=1}^{m_1+1} \pi_{nj}^- \tilde{d}_{j,y_n}} \right)^2 \right)^{-1/2} \right] \quad (\text{EC.3}) \\ &= \arccos \frac{\pi_{n,i+1}^-}{\sqrt{(\pi_{n,i+1}^-)^2 + \cdots + (\sum_{j=1}^{m_1} \pi_{nj}^-)^2 + (\pi_{n1}^-)^2}}, \quad i \in [m_1 - 1], \end{aligned}$$

which is irrelevant to y_n and is Equation (21) by routine algebra. The last equality follows from $\tilde{d}_{i1} = \cdots = \tilde{d}_{iK}$ for all $i \in [m_1]$. A similar procedure proves the case of ϕ_{n,m_1} .

Last, we show that r_n can be computed recursively by

$$\begin{aligned} r_n &= \sqrt{\sum_{i=1}^{m_1} \pi_{ni}^2 + (\pi_{n,m_1+1} - 1)^2} = \left[\sum_{i=1}^{m_1} \left(\frac{\pi_{ni}^- \tilde{d}_{i,y_n}}{\sum_{j=1}^{m_1+1} \pi_{nj}^- \tilde{d}_{j,y_n}} \right)^2 + \left(\frac{-\sum_{j=1}^{m_1} \pi_{nj}^- \tilde{d}_{j,y_n}}{\sum_{j=1}^{m_1+1} \pi_{nj}^- \tilde{d}_{j,y_n}} \right)^2 \right]^{\frac{1}{2}} \\ &= \left[\sum_{i=1}^{m_1} \left(\frac{\pi_{ni}^-}{\sum_{j=1}^{m_1} \pi_{nj}^- + \pi_{n,m_1+1}^- d_{2,y_n}/d_{1,y_n}} \right)^2 + \left(\frac{-\sum_{j=1}^{m_1} \pi_{nj}^-}{\sum_{j=1}^{m_1} \pi_{nj}^- + \pi_{n,m_1+1}^- d_{2,y_n}/d_{1,y_n}} \right)^2 \right]^{\frac{1}{2}} \\ &= \frac{\sqrt{\sum_{i=1}^{m_1} (\pi_{ni}^-)^2 + (\sum_{i=1}^{m_1} \pi_{ni}^-)^2}}{\sum_{i=1}^{m_1} \pi_{ni}^- + \pi_{n,m_1+1}^- d_{2,y_n}/d_{1,y_n}} \end{aligned}$$

$$\begin{aligned}
&= \frac{r_{n-1} \sqrt{\sum_{i=1}^{m_1} \varphi_i^2(\Phi_{n-1}) + (\sum_{i=1}^{m_1} \varphi_i(\Phi_{n-1}))^2}}{r_{n-1} \sum_{i=1}^{m_1} \varphi_i(\Phi_{n-1}) + (r_{n-1} \varphi_{m_1+1}(\Phi_{n-1}) + p_{m_1+1, m_1+1}(\delta)) d_{2, y_n} d_{1, y_n}^{-1}} \\
&= \frac{\sqrt{\sum_{i=1}^{m_1} \varphi_i^2(\Phi_{n-1}) + (\sum_{i=1}^{m_1} \varphi_i(\Phi_{n-1}))^2}}{\sum_{i=1}^{m_1} \varphi_i(\Phi_{n-1}) + (\varphi_{m_1+1}(\Phi_{n-1}) + p_{m_1+1, m_1+1}(\delta) r_{n-1}^{-1}) d_{2, y_n} d_{1, y_n}^{-1}}
\end{aligned}$$

given $Y_n = y_n \in [K]$. The equation follows from $\pi_{ni}^- = \sum_{j=1}^{m_1+1} \pi_{n-1, j} p_{ji}(\delta)$, the transform formula in Table 1, the relationship between π_n^- and π_n in (EC.2) and (EC.3), and $\pi_{n, m_1+1}^- = 1 + (\pi_{n, m_1+1}^- - 1) = 1 + \sum_{j=1}^{m_1+1} \pi_{n-1, j} (p_{j, m_1+1}(\delta) - 1) = 1 + r_{n-1} \varphi_{m_1+1}(\Phi_{n-1}) + p_{m_1+1, m_1+1}(\delta) - 1 = r_{n-1} \varphi_{m_1+1}(\Phi_{n-1}) + p_{m_1+1, m_1+1}(\delta)$. \square

A.18. Proof of Theorem 5

Similar to the single-mission case, we let $\bar{V}_c(n, \pi_n)$ be the cost-to-go if we continue the mission at time $n\delta$ with belief state π_n until the end of the mission. For any n , let $\tilde{l}(n) = \min\{l \in [L] : \sum_{l'=1}^l N_{l'} > n\}$. We can readily compute

$$\bar{V}_c(n, \pi_n) = C_s \kappa((N - n)\delta + w_N, \pi_n) + \sum_{l=\tilde{l}(n)}^L C_m^{(l)} \kappa\left(\left(\sum_{l'=1}^l N_{l'} - n\right)\delta + w_N \mathbb{1}\{l = L\}, \pi_n\right).$$

We know $n \geq \sum_{l'=1}^l N_{l'}$ if mission $l \in [L - 1]$ has been completed. Since $\kappa(t, \pi)$ is increasing in t and MLR increasing π , an upper bound of $\bar{V}_c(n, \pi)$ for $n \geq \sum_{l'=1}^l N_{l'}$ is

$$\begin{aligned}
\bar{V}_c\left(\sum_{l'=1}^l N_{l'}, \mathbf{e}_{m_1+m_2}\right) &= C_s \left[1 - e^{-\lambda(T - \delta \sum_{l'=1}^l N_{l'} + w_N)}\right] \\
&\quad + \sum_{l'=l+1}^L C_m^{(l')} \left\{1 - \exp\left[-\lambda\left(\sum_{l''=l+1}^{l'} N_{l''} \delta + w_N \mathbb{1}\{l' = L\}\right)\right]\right\}.
\end{aligned}$$

By the same way, a lower bound of $V_{ab}(n, \pi)$ with $n \geq \sum_{l'=1}^l N_{l'}$ is $C_s e_1' \exp(\mathbf{Q} w_{\sum_{l'=1}^l N_{l'}}) \mathbf{e}_{m_1+m_2+1} + C_m^{(L)}$. The mission is never aborted after completing mission l if $V_c(\sum_{l'=1}^l N_{l'}, \mathbf{e}_{m_1+m_2}) \leq C_m^{(L)} + C_s e_1' \exp(\mathbf{Q} w_{\sum_{l'=1}^l N_{l'}}) \mathbf{e}_{m_1+m_2+1}$, which is

$$\begin{aligned}
&\sum_{l'=l+1}^L C_m^{(l')} \left\{ \mathbb{1}\{l' < L\} - \exp\left[-\lambda\left(\sum_{l''=l+1}^{l'} N_{l''} \delta + w_N \mathbb{1}\{l' = L\}\right)\right] \right\} \\
&\leq C_s \left[e_1' \exp(\mathbf{Q} w_{\sum_{l'=1}^l N_{l'}}) \mathbf{e}_{m_1+m_2+1} + \exp\left(-\lambda\left(T - \delta \sum_{l'=1}^l N_{l'} + w_N\right)\right) - 1 \right]. \quad (\text{EC.4})
\end{aligned}$$

When $l = 0$, $\sum_{l'=1}^0 N_{l'} = 0$. The mission is never aborted in this case, and (EC.4) simplifies to (25).

Since the expected repair cost for aborting or stopping system at $n\delta$ is $C_r \pi' \tilde{\mathbf{P}}(w_n) \cdot (\mathbf{0}'_{m_1}, \mathbf{1}'_{m_2})'$, which is linear in π , we can use the same proof for Lemma 2 to show that $V^{(\lambda)}(n, \pi)$, $V_{ab}(n, \pi)$, and $V_c(n, \pi)$ are all concave in π for all n . However, since w_n may not be nondecreasing in n , we

cannot guarantee existence of the thresholds \hat{n} and \tilde{n} . Nevertheless, we can examine the values of $V_{\text{ab}}(n, \mathbf{e}_{m_1+m_2})$ and $V_c(n, \mathbf{e}_{m_1+m_2})$ for each n . If $V_{\text{ab}}(n, \mathbf{e}_{m_1+m_2}) > V_c(n, \mathbf{e}_{m_1+m_2})$, the optimal abort policy is of the form as in Theorem 4(i); otherwise, it is of the form as in Theorem 4(ii), both proved using the concavity of $V^{(\lambda)}(n, \boldsymbol{\pi})$, $V_{\text{ab}}(n, \boldsymbol{\pi})$, and $V_c(n, \boldsymbol{\pi})$. Again using the concavity of value functions, the region in which abort is optimal can be shown to be convex. \square

Appendix B: Implementation Details

We first illustrate the details of the PBVI algorithm. At the τ th iteration of the algorithm, the backup step first constructs $\hat{\mathcal{A}}_n^{(\tau)}$ based on $\{\boldsymbol{\pi}_n^{(l)}\}_{l \in [L_\tau]}$ in a backward induction way. Specifically, we have $V(n, \boldsymbol{\pi}) = \bar{V}_c(n, \boldsymbol{\pi})$ for $n = \hat{n}, \dots, N$ by Theorem 3, which is a linear function in $\boldsymbol{\pi}$. All the sets \mathcal{A}_n , $n = \hat{n}, \dots, N$, are hence a singleton, and the only element therein can be determined by Equation (15). We simply let $\hat{\mathcal{A}}_n^{(\tau)} = \mathcal{A}_n$ for all $n \geq \hat{n}$. When $n = \hat{n} - 1$, we have two choices, i.e., to abort or to continue the mission, and $V(n, \boldsymbol{\pi}) = \min\{V_{\text{ab}}(n, \boldsymbol{\pi}), V_c(n, \boldsymbol{\pi})\}$. The cost-to-go $V_{\text{ab}}(n, \boldsymbol{\pi})$ can be exactly computed since the map $\boldsymbol{\pi} \mapsto V_{\text{ab}}(\hat{n} - 1, \boldsymbol{\pi})$ in (11) is linear. On the other hand, exactly computing $V_c(\hat{n} - 1, \boldsymbol{\pi})$ needs to solve the Bellman equation in (12), which is computationally intensive. Hence, we approximately compute $V_c(\hat{n} - 1, \boldsymbol{\pi})$ by replacing $V(n, \boldsymbol{\pi})$ with $\hat{V}^{(\tau)}(n, \boldsymbol{\pi})$ in (12), yielding an approximation

$$\begin{aligned} \hat{V}_c^{(\tau)}(\hat{n} - 1, \boldsymbol{\pi}) &= \kappa(\boldsymbol{\pi}, \delta)(C_s + C_m) \\ &+ \sum_{k=1}^K \min_{\boldsymbol{\alpha}_{\hat{n}} \in \hat{\mathcal{A}}_{\hat{n}}^{(\tau)}} \sum_{i=1}^{m_1+m_2} \sum_{j=1}^{m_1+m_2} \alpha_{\hat{n}j} \pi_i p_{ij}(\delta) (d_{1k} \mathbb{1}\{j \leq m_1\} + d_{2k} \mathbb{1}\{j > m_1\}), \end{aligned} \quad (\text{EC.5})$$

where $\alpha_{\hat{n}j}$ is the j th coordinate of $\boldsymbol{\alpha}_{\hat{n}}$. Since $\boldsymbol{\pi} \mapsto \kappa(\boldsymbol{\pi}, \delta)$ is linear, Equation (EC.5) implies both $\hat{V}_c(n, \boldsymbol{\pi})$ and $\hat{V}^{(\tau)}(n, \boldsymbol{\pi}) \triangleq \min\{V_{\text{ab}}(n, \boldsymbol{\pi}), \hat{V}_c(n, \boldsymbol{\pi})\}$ are piecewise linear and concave in $\boldsymbol{\pi}$. Based on $V_{\text{ab}}(n, \boldsymbol{\pi})$ in (11) and $\hat{V}_c(n, \boldsymbol{\pi})$ in (EC.5), the set $\hat{\mathcal{A}}_{\hat{n}-1}$ can be readily obtained. This finishes the backward induction step for $n = \hat{n} - 1$. We keep repeating this procedure from $n = \hat{n} - 2$ to $n = 0$ to complete the backup step.

The expansion step then expands the sets $\{\boldsymbol{\pi}_n^{(l)}\}_{l \in [L_\tau]}$ by adding new elements $\boldsymbol{\pi}_n^{(l)}$, $l = L_\tau + 1, \dots, L_{\tau+1}$, for each $n \in [\hat{n} - 1]$. The expanded sets $\{\boldsymbol{\pi}_n^{(l)}\}_{l \in [L_{\tau+1}]}$ will then be used in the backup step at the $(\tau + 1)$ th iteration. To ensure a good approximation, we need to find states $\{\boldsymbol{\pi}_n^{(l)}\}_{l=L_\tau+1}^{L_{\tau+1}}$ that are more likely to reach for the partially observable Markov decision process (POMDP) (Pineau et al. 2003, Liu et al. 2022). Hence, we resort to the CTMC model in Section 4.1 to simulate system states. Specifically, for each $l \in [L_\tau]$ and $n = 0, \dots, \hat{n} - 2$, we run a batch of simulations starting from the state $\boldsymbol{\pi}_n^{(l)}$ and find the belief state at the next decision epoch. To this end, we first sample an underlying state from each belief state $\boldsymbol{\pi}_n^{(l)}$ and then sample the state at the next decision epoch and the associated observation. The belief state at the next decision epoch is computed

based on the Bayesian update. For all states simulated from $\pi_n^{(l)}$, we keep the one that is farthest away from $\mathcal{A}_{n+1}^{(\tau)}$ as with Pineau et al. (2003) and denote this state by $\pi_{n+1}^{(L_\tau+l)}$. We expand the set of belief states by adding all the above kept states. In this way, we double the size of $\{\pi_n^{(l)}\}_{l \in [L_\tau]}$, $n \in [\hat{n} - 1]$, after each iteration, i.e., $L_{\tau+1} = 2L_\tau$. When the iteration number τ is larger than Z_2 , we discard all the belief states following Algorithm 1. This completes the expansion step.

We next illustrate the binary search to find the time threshold \hat{n} . The detailed procedures are provided in Algorithm EC.1.

Algorithm EC.1 Binary search to find the threshold \hat{n} .

Input: The functions $\bar{V}_c(n, \pi)$ and $V_{ab}(n, \pi)$

Output: The time threshold \hat{n} for abort

```

1: Init  $\underline{n} \leftarrow 0$ ,  $\bar{n} \leftarrow N$ , and  $\hat{n} \leftarrow \lfloor (\bar{n} + \underline{n})/2 \rfloor$ 
2: while  $\bar{n} > \underline{n} + 1$  do
3:   Set  $\hat{n} \leftarrow \lfloor (\bar{n} + \underline{n})/2 \rfloor$ 
4:   for  $\pi = e_1, \dots, e_{m_1+m_2}$  do
5:     if  $\bar{V}_c(\hat{n}, \pi) - V_{ab}(\hat{n}, \pi) > 0$  then
6:       Set  $\underline{n} \leftarrow \hat{n}$  Break the for-loop
7:     end if
8:   end for
9:   Set  $\bar{n} \leftarrow \hat{n}$ 
10: end while
11: Set  $\hat{n} \leftarrow \underline{n}$ 
12: for  $\pi = e_1, \dots, e_{m_1+m_2}$  do
13:   if  $\bar{V}_c(\underline{n}, \pi) - V_{ab}(\underline{n}, \pi) > 0$  then
14:     Set  $\hat{n} \leftarrow \bar{n}$ 
15:     Break the for-loop
16:   end if
17: end for
```

We then illustrate the optimization for the special cases of our model. When $m_1 = m_2 = 1$, the failure process follows a CTMC. We discretize the belief space $[0, 1]$ into $\{0, \Delta, 2\Delta, \dots, 1 - \Delta, 1\}$, where Δ is the granularity parameter. We then obtain the control limits $\underline{\pi}_n, \bar{\pi}_n$ at each decision epoch $n\delta$, $n = 0, \dots, N - 1$ by the backward algorithm summarized in Algorithm EC.2. When $m_1 > 1$ and $m_2 = 1$, we need to first compute $(\Phi_n)_{n=0}^N$ by (21). We then discretize the interval $[0, -(\cos \phi_{n,m_1} \prod_{k=1}^{m_1-1} \sin \phi_{nk})^{-1}]$ with granularity Δ for each $n = 0, \dots, N$. Nearly the same as Algorithm EC.2, we can use standard backward induction to exactly solve the corresponding Bellman equation after discretization.

We last demonstrate the optimization of the benchmark methods used in Section 9. For the optimal \mathcal{C} -policy and \mathcal{R} -policy, two brute-force searches are used to separately optimize (\check{m}, \check{N}) and p . To obtain the optimal \mathcal{M} -policy, we can formulate a POMDP as in Section 7.1 under the

Algorithm EC.2 Backward induction algorithm to calculate the control limits $\underline{\pi}_n, \bar{\pi}_n$.

Input: $\mathbf{Q}, \mathbf{D}, C_m, C_s, \delta, N, \Delta$

Output: The control limits $\underline{\pi}_n, \bar{\pi}_n$ at each decision epoch $n\delta$, $n = 0, 1, \dots, N - 1$

```

1: for  $\pi_N \in \{0, \Delta, 2\Delta, \dots, 1 - \Delta, 1\}$  do
2:   Calculate  $V(N, \pi_N)$  based on (14)
3: end for
4: for  $n \leftarrow N - 1, \dots, 0$  do
5:   for  $\pi_n \in \{0, \Delta, 2\Delta, \dots, 1 - \Delta, 1\}$  do
6:     Calculate  $V(n, \pi_n)$  based on (9)
7:   end for
8:   Find the thresholds  $\underline{\pi}_n, \bar{\pi}_n$  based on the value function
9: end for

```

three-state CTMC approximation. As shown in Theorem 2, the optimal abort policy has a control-limit structure on the belief state $[0, 1]$. Specifically, we let the transition rates be $q_{01} = \nu/m_1 = 4.01 \times 10^{-3}$, $q_{02} = \lambda = 10^{-3}$, and $q_{12} = [\alpha\Gamma(1 + 1/\beta)]^{-1} = 1.04 \times 10^{-3}$, where $\Gamma(\cdot)$ is the gamma function, to match the mean time of transition between states for the original failure process. We then discretize the state space with granularity $\Delta = 0.01$ and use standard backward induction as shown in Algorithm EC.2 to solve the POMDP. The threshold to abort at each period can be readily obtained for the optimal \mathcal{M} -policy. The benchmark with the one-phase approximation uses similar procedures to the \mathcal{M} -policy while keeping the first m_1 phases unchanged.

Appendix C: Additional Numerical Settings and Results

C.1. Numerical Settings

When comparing our modified PBVI algorithm with the classical one in numerical experiments, we randomly sample 100 belief states at the end of each iteration of our modified PBVI algorithm. For each sampled belief state, we evaluate the approximate value function under the current iteration of the modified PBVI algorithm and compare it with that already obtained from the classical PBVI algorithm. The modified PBVI terminates if for all the 100 sampled belief states, the absolute differences between the two approximate values are smaller than one.

In Section 9.1, we assume T_{12} follows an Erlang distribution, with shape m_1 and rate ν . We set the shape parameter of T_{12} as $m_1 = 2$ (Khaleghei and Kim 2021), which is commonly used for machinery systems. Then we determine $\nu = 8.01 \times 10^{-3}$ to make $\mathbb{E}[T_{12}]$ the same as that in Yang et al. (2020). Since the Erlang distribution can capture the absorption time of a CTMC, we construct a CTMC with transition rate matrix $\mathbf{Q} = (q_{ij})_{i,j \in \mathcal{X}}$, where

$$q_{ij} = \begin{cases} \nu, & j = i + 1, i \in \mathcal{X}_1, \\ \zeta, & i \in \mathcal{X}_1, j = m_1 + m_2 + 1, \\ [1 - p_{i-m_1}(\lambda)]\lambda, & j = i + 1, i, j \in \mathcal{X}_2, \\ p_{i-m_1}(\lambda)\lambda, & i \in \mathcal{X}_2 \setminus \{m_1 + m_2\}, j = m_1 + m_2 + 1, \\ \lambda, & i = m_1 + m_2, j = m_1 + m_2 + 1, \end{cases}$$

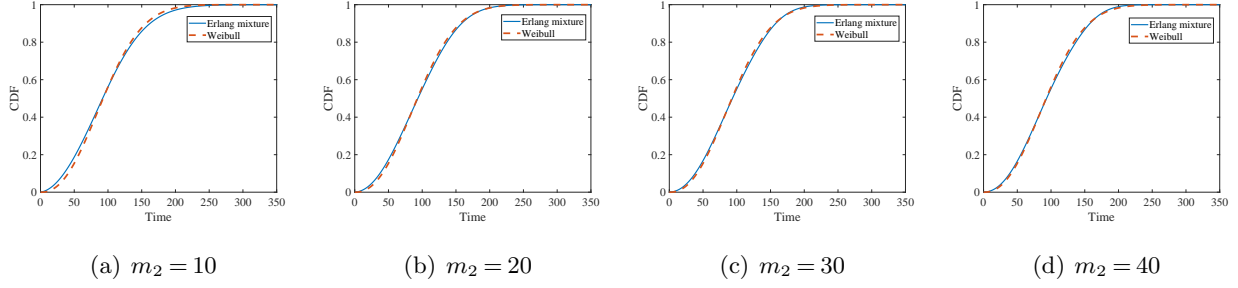


Figure EC.1 Approximating the distribution F of T_{23} in (26) by the Erlang mixture distribution $F^{(\lambda)}(\cdot)$ under various values of m_2 .

$q_{ij} = 0$ for other $i \neq j$, and $q_{ii} = -\sum_{j \in \mathcal{X}: j \neq i} q_{ij}$. The CTMC starts from the first state with probability one, i.e., $X^{(\lambda)}(0) = 1$. The optimal mission abort policy can be obtained by solving $V(0, \mathbf{e}_1)$ from the Bellman recursion. Lemmas 1 and 2 in Khaleghi and Kim (2021) suggest that all structural results in Section 5 still hold if we formulate a POMDP based on this CTMC.

Moreover, Assumption 1 fails when F is a mixture of two Weibull distributions. In a real application, if a mixture of Erlang distribution $F^{(\lambda)}$ is used to approximate a general positive distribution F , the values of both $\lambda > 0$ and $m_2 \in \mathbb{N}_+$ need to be determined. In our numerical experiment, for a fixed value of m_2 , we use the commonly used moment-matching method to determine λ such that $F^{(\lambda)}$ and F have the same mean value. As such, we only need to choose the value of m_2 for optimization. An intuitive way to choose a reasonable m_2 value is to plot the cumulative distribution functions (CDFs) of the true F and the mixture of Erlang for approximation in the same graph and visually compare the two curves. We do this comparison for both the Weibull distribution in (26) and the mixture distribution in (27). For the Weibull distribution, we examine $m_2 \in \{10, 20, 30, 40\}$ and the results are provided in Figure EC.1. For the mixture distribution, we examine $m_2 \in \{10, 30, 50, 70\}$, with the results provided in Figure EC.2. In the first case, $m_2 = 20$ has provided an accurate approximation to F , and further increasing m_2 only leads to marginal improvement. In the second case, the lack of fit mainly comes from the CDF at the neighborhood of time $t = 50$. The choice of $m_2 = 50$ seems to provide a big improvement on the fit in this area compared to $m_2 = 30$, while increasing m_2 to 70 improves the approximation marginally. The observations validate our argument of choosing m_2 by visually inspecting the true CDF and the approximating CDF.

To compare the two PBVI algorithms in terms of both running time and accuracy, we consider a problem instance with $m_1 = 1$ and $m_2 = 2$. Specifically, the transition from the healthy to defective state follows an exponential distribution, and that from the defective to failure state follows a two-

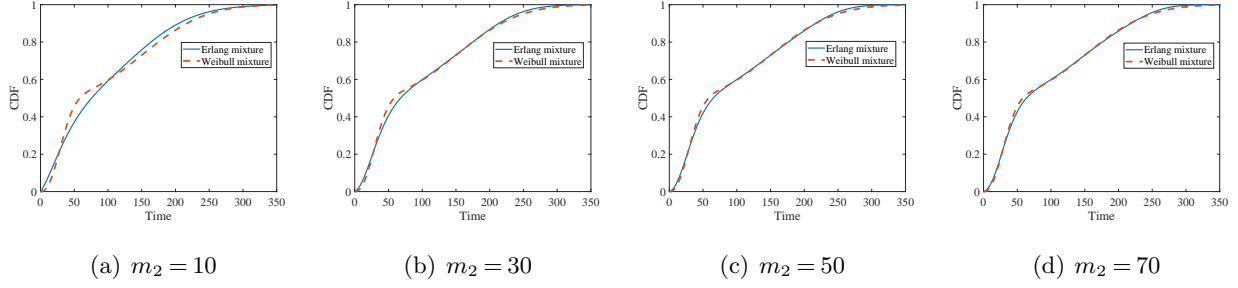


Figure EC.2 Approximating the distribution F of T_{23} in (27) by the Erlang mixture distribution $F^{(\lambda)}(\cdot)$ under various values of m_2 .

phase mixture of Erlang distribution. This stochastic process can be represented by a four-state CTMC with the transition rate matrix given by

$$\mathbf{Q} = \begin{bmatrix} -2.75 \times 10^{-3} & 2.29 \times 10^{-3} & 0 & 4.59 \times 10^{-4} \\ 0 & -1.04 \times 10^{-2} & 6.92 \times 10^{-3} & 3.46 \times 10^{-3} \\ 0 & 0 & -2.86 \times 10^{-2} & 2.86 \times 10^{-2} \\ 0 & 0 & 0 & 0 \end{bmatrix}.$$

The state-observation matrix is the same as that in Section 9.1. Since the failure state is observable, the belief state is three-dimensional, i.e., $\{\boldsymbol{\pi} \in \mathbb{R}_+^3 : \pi_1 + \pi_2 + \pi_3 = 1\}$. We discretize $[0, 1]$ for each dimension of $\boldsymbol{\pi}$ into 1,000 states, resulting in $1,000^3 = 10^9$ states in total. It takes around three days for a computing server to use backward induction to find the optimal solution for this problem instance. For our modified PBVI algorithm, we set $L_1 = 2$, $Z_1 = 30$, and $Z_2 = 10$.

Last, for the numerical study in Section 9.4, the rescue time w_n can be computed by the law of cosines based on the locations of the depot and sites 1 to 3. The rescue time is set to be

$$w_n = \begin{cases} n, & 0 \leq n < 25, \\ 25, & 25 \leq n < 60, \\ \sqrt{625 + (n - 60)(n - 85)}, & 60 \leq n < 85, \\ 25, & 85 \leq n < 110, \\ \sqrt{625 + (n - 110)(n - 135)}, & 110 \leq n < 135, \\ 25, & 135 \leq n \leq 185, \end{cases}$$

to assess the model performance in a multi-task setting.

C.2. Sensitivity Analysis

For a comprehensive comparison, we conduct sensitivity analysis on several model parameters. We first consider the case when F is Weibull. Since the mission failure cost is subjective, we fix C_s and examine different values of C_m for $C_m/C_s \in \{0.25, 0.5, 1, 2, 4\}$. Table EC.1 shows that our proposed model consistently achieves the smallest expected cost per mission under all the parameter settings. Among the benchmarks, the one-phase approximation performs the best when C_m is small, and the

Table EC.1 Comparison of the operational costs per mission when the mission failure cost C_m changes and F is Weibull. The results are averaged under 10,000 simulation replications.

Policy	$C_m = 500$	$C_m = 1,000$	$C_m = 2,000$	$C_m = 4,000$	$C_m = 8,000$
\mathcal{C} -policy	522.8	717.7	1063.0	1775.9	3063.6
\mathcal{R} -policy	547.6	753.5	1089.6	1724.0	2952.7
\mathcal{M} -policy	503.8	721.5	1063.4	1730.1	2968.9
One-phase approximation	500.5	717.3	1061.4	1741.2	3015.6
Proposed model	494.3	697.6	1013.4	1635.0	2783.3

Table EC.2 Comparison of the operational costs per mission on the false alarm probabilities d_{12} when F is Weibull. The results are averaged under 10,000 simulation replications.

Policy	$d_{12} = 0.05$	$d_{12} = 0.1$	$d_{12} = 0.15$	$d_{12} = 0.2$	$d_{12} = 0.25$	$d_{12} = 0.3$
\mathcal{C} -policy	1048.5	1053.3	1055.5	1056.8	1062.2	1065.3
\mathcal{R} -policy	1071.7	1075.1	1082.5	1087.9	1088.5	1092.2
\mathcal{M} -policy	1050.0	1055.8	1059.9	1058.8	1062.6	1067.4
One-phase approximation	1050.7	1053.9	1054.5	1059.6	1059.2	1061.4
Proposed model	996.5	1001.0	1005.3	1008.1	1011.2	1015.7

\mathcal{R} -policy performs the best when C_m is large. Nevertheless, all benchmarks lead to a cost increase by around 2%–13% compared with our method.

We then compare our model with the benchmarks under different values of the state-observation matrix \mathbf{D} . We let the false alarm probability d_{12} vary in $\{0.05, 0.1, \dots, 0.3\}$, compute $d_{11} = 1 - d_{12}$, while keeping other parameters the same as those in Section 9.1. Table EC.2 compares the expected cost per mission of the five policies. Although the \mathcal{M} -policy considers the noises in condition monitoring, the resulting cost is consistently more than 5% higher than that of our optimal policy, because it overlooks the non-Markovian nature of the failure process. We see that the operational cost per mission of our model and the \mathcal{M} -policy generally increases in d_{12} , because the signal-noise-ratio decreases in d_{12} . Moreover, the optimal \mathcal{C} -policy and one-phase approximation generally perform the best among all benchmarks. The cost increase of the benchmarks are around 5%–8% compared with our method.

Similar to the case examining d_{12} , we also conduct sensitivity analysis on the false negative rate d_{21} . Table EC.3 shows the comparison results, where the operational costs per mission as a function of d_{21} for the benchmarks exhibit similar patterns to that when d_{12} changes. The \mathcal{C} -policy performs the best when d_{21} is small, and the one-phase approximation performs the best when d_{21} increases. Moreover, we see around 5%–9% increases of the operational cost for the benchmarks compared with our model, validating the effectiveness of the proposed method again.

We then examine the sensitivity of the our model performance compared to the benchmarks when F follows a mixture of Weibull distributions. We again fix C_s and examine different values of C_m for $C_m/C_s \in \{0.25, 0.5, 1, 2, 4\}$. The results are summarized in Table EC.4. The \mathcal{R} -policy outperforms

Table EC.3 Comparison of the operational costs per mission on the false negative rate d_{21} when F is Weibull.

The results are averaged under 10,000 simulation replications.

Policy	$d_{21} = 0.05$	$d_{21} = 0.1$	$d_{21} = 0.15$	$d_{21} = 0.2$	$d_{21} = 0.25$	$d_{21} = 0.3$
\mathcal{C} -policy	1059.0	1063.0	1067.6	1071.2	1078.2	1086.6
\mathcal{R} -policy	1081.7	1089.4	1094.2	1102.2	1104.2	1107.0
\mathcal{M} -policy	1062.4	1063.1	1065.9	1071.8	1074.6	1084.1
One-phase approximation	1059.9	1061.3	1064.9	1070.8	1070.9	1080.3
Proposed model	1010.1	1013.4	1016.6	1020.1	1021.3	1024.8

Table EC.4 Comparison of the operational costs per mission when the mission failure cost C_m changes and F is a mixture distribution. The results are averaged under 10,000 simulation replications.

Policy	$C_m = 500$	$C_m = 1,000$	$C_m = 2,000$	$C_m = 4,000$	$C_m = 8,000$
\mathcal{C} -policy	530.7	906.6	1293.1	1968.2	3290.4
\mathcal{R} -policy	565.3	894.3	1248.6	1866.7	3099.3
\mathcal{M} -policy	506.8	908.2	1295.2	1970.7	3279.6
One-phase approximation	524.3	909.2	1294.6	1874.5	3291.3
Proposed model	502.1	814.1	1116.4	1693.9	2797.1

Table EC.5 The operational cost per mission when the parameter d_{12} changes and F is a mixture distribution.

The results are averaged under 10,000 simulation replications.

Policy	$d_{12} = 0.05$	$d_{12} = 0.1$	$d_{12} = 0.15$	$d_{12} = 0.2$	$d_{12} = 0.25$	$d_{12} = 0.3$
\mathcal{C} -policy	1275.1	1278.2	1284.5	1289.5	1290.1	1301.6
\mathcal{R} -policy	1235.2	1234.9	1242.6	1245.7	1247.5	1249.7
\mathcal{M} -policy	1273.6	1283.4	1283.5	1288.4	1290.0	1293.4
One-phase approximation	1272.3	1284.0	1282.0	1289.2	1293.3	1294.2
Proposed model	1096.2	1103.6	1104.1	1106.9	1110.2	1114.3

other benchmarks when $C_m \geq 1,000$. However, the cost gaps between the benchmarks and our method can be very large when F follows a mixture of Weibull distributions. Nearly all benchmarks lead to a cost increase larger than 10% in different parameter settings. When $C_m = 8,000$, the gaps between our method and the \mathcal{C} -policy, \mathcal{M} -policy, and one-phase approximation are all near 20%.

We then examine the sensitivity of our model performance to d_{12} and d_{21} . The results are summarized in Tables EC.5 and EC.6, respectively. We can again see that the optimal \mathcal{R} -policy outperforms other benchmarks in all parameter settings. Nevertheless, the optimal \mathcal{R} -policy still incurs a cost increase consistently around 12% in all parameter settings compared with our model. Similar to the base setting, all other benchmarks lead to a cost increase more than 15% under all parameter settings. This demonstrates the effectiveness of our model when the time from the defective to failure state is bimodal.

Finally, we examine the optimal operational cost under various values of λ and m_2 , the two parameters determining the Erlang mixture approximation. This numerical experiment reveals how fast our surrogate policy converges to the optimal policy in the non-asymptotic regime. For the Weibull distribution, we study the value of $m_2 \in \{5, 10, \dots, 35\}$ and compute the corresponding λ

Table EC.6 The operational cost per mission when the parameter d_{21} changes and F is a mixture distribution.
The results are averaged under 10,000 simulation replications.

Policy	$d_{21} = 0.05$	$d_{21} = 0.1$	$d_{21} = 0.15$	$d_{21} = 0.2$	$d_{21} = 0.25$	$d_{21} = 0.3$
\mathcal{C} -policy	1290.2	1293.0	1300.2	1307.4	1308.4	1314.0
\mathcal{R} -policy	1247.8	1248.6	1251.2	1252.0	1257.9	1260.9
\mathcal{M} -policy	1293.2	1294.9	1298.7	1302.3	1303.7	1309.7
One-phase approximation	1284.0	1294.5	1297.4	1301.9	1303.8	1311.6
Proposed model	1115.1	1116.4	1120.3	1122.1	1126.5	1131.1

Table EC.7 The operational cost per mission when the parameter m_2 changes and F is Weibull. The results are averaged under 10,000 simulation replications.

m_2	5	10	15	20	25	30	35
λ	0.041	0.074	0.105	0.134	0.163	0.191	0.218
Mean cost per mission	1061.4	1044.8	1027.8	1013.4	1013.4	1013.1	1013.1

Table EC.8 The operational cost per mission when the parameter m_2 changes and F is a mixture distribution.
The results are averaged under 10,000 simulation replications.

m_2	10	20	30	40	50	60	70
λ	0.054	0.095	0.134	0.172	0.209	0.245	0.281
Mean cost per mission	1256.6	1200.4	1155.2	1127.0	1116.4	1111.8	1110.8

by matching the mean with the Weibull distribution in Section 9.1. When F follows the mixture distribution, we set the value of $m_2 \in \{10, \dots, 70\}$ as it needs more phases for the mixture of Erlang distribution to accurately approximate F with a more irregular shape, as evidenced in Figure EC.2. The results are summarized in Tables EC.7 and EC.8. We can see that the λ value obtained from moment-matching increases with m_2 in both tables. This implies that λ chosen in this way satisfies the conditions in Corollary 4.1 of Wiens (1979), and it ensures that $F^{(\lambda)}$ approximates F well with a large enough m_2 . Moreover, when F is Weibull, the expected cost per mission decreases significantly as m_2 increases from 5 to 20, and almost remains stable when m_2 increases from 20 to 35. This implies that our surrogate policy converges quickly to the optimal policy for moderate m_2 values. On the other hand, when F is a mixture distribution, it is expected that the expected cost by adopting the surrogate policy converges to the optimal cost more slowly. In this case, the mean cost per mission nearly keeps constant if we increase m_2 from 50 and λ from 0.209, again validating our model performance in the non-asymptotic regime.

References

- Karlin S, Rinott Y (1980) Classes of orderings of measures and related correlation inequalities. I. Multivariate totally positive distributions. *Journal of Multivariate Analysis* 10(4):467–498.
- Khaleghei A, Kim MJ (2021) Optimal control of partially observable semi-Markovian failing systems: An analysis using a phase methodology. *Operations Research* 69:1282–1304.

- Krishnamurthy V (2011) Bayesian sequential detection with phase-distributed change time and nonlinear penalty—A POMDP lattice programming approach. *IEEE Transactions on Information Theory* 57(10):7096–7124.
- Liu Z, Khojandi A, Li X, Mohammed A, Davis RL, Kamaleswaran R (2022) A machine learning-enabled partially observable Markov decision process framework for early sepsis prediction. *INFORMS Journal on Computing* 34(4):2039–2057.
- Lovejoy WS (1987) Some monotonicity results for partially observed Markov decision processes. *Operations Research* 35(5):736–743.
- Pineau J, Gordon G, Thrun S (2003) Point-based value iteration: An anytime algorithm for POMDPs. *International Joint Conference on Artificial Intelligence*, 1025–1032.
- Shaked M, Shanthikumar JG (2007) *Stochastic Orders* (Springer).
- Yang L, Sun Q, Ye ZS (2020) Designing mission abort strategies based on early-warning information: Application to UAV. *IEEE Transactions on Industrial Informatics* 16(1):277–287.